TECHNISCHE UNIVERSITÄT MÜNCHEN

FAKULTÄT WISSENSCHAFTSZENTRUM WEIHENSTEPHAN
FÜR ERNÄHRUNG, LANDNUTZUNG UND UMWELT
LEHRSTUHL FÜR TIERZUCHT

Molecular Genetics of Phosphate Homeostasis

Susanne Beate Diener

Vollständiger Abdruck der von der Fakultät Wissenschaftszentrum Weihenstephan für Ernährung, Landnutzung und Umwelt der Technischen Universität München zur Erlangung des akademischen Grades eines

Doktors der Naturwissenschaften

genehmigten Dissertation.

Vorsitzender:	Univ.-Prof. Dr. Michael W. Pfaffl
Prüfer der Dissertation:	1. Univ.-Prof. Dr. Hans-Rudolf Fries
	2. apl. Prof. Dr. Walter Just (Universität Ulm)

Die Dissertation wurde am 12. März 2015 bei der Technischen Universität München eingereicht und durch die Fakultät Wissenschaftszentrum Weihenstephan für Ernährung, Landnutzung und Umwelt am 09. Juni 2015 angenommen.

To my parents.

SUMMARY

Phosphate homeostasis is crucial for manifold physiological processes ranging from cellular signalling to bone mineralisation. It is maintained by a complex network that involves several factors and organs. Within the so-called bone-kidney axis, bone-derived fibroblast growth factor 23 (FGF23) has emerged as the key regulator of systemic phosphate turnover. It controls, through activating FGF receptor (FGFR)/Klotho complexes in the kidney, renal phosphate handling and vitamin D metabolism. If the body's phosphate balance is disturbed, hypo- and hyperphosphatemic disorders can arise. Although several genes directly implicated in monogenic phosphate balance disorders have already been identified, the pathophysiology is still incompletely understood and many open questions remain to be elucidated.

The first part of this thesis focused on a next-generation sequencing (NGS)-based strategy to identify novel potential disease genes in human hypophosphatemia. 11 unrelated families with unknown genetic cause of phosphate wasting were analysed. However, no novel variants which seem to be of pathogenic relevance in at least two unrelated patients could be detected by exome sequencing. In the second part, a cohort of N-ethyl-N-nitrosourea (ENU)-derived mouse models with alterations in bone metabolism and skeletal development (n = 18) was screened for mutations by the use of exome sequencing to find new key regulators of phosphate homeostasis. The overall mutation detection rate was 78%, highlighting that exome sequencing provides a means for high-throughput genetic analysis of large mutant mouse collections like in the Munich ENU Mutagenesis Project. It comprises reliable information, which itself is sufficient to discover ENU-induced mutations even without any additional genetic mapping data. One mouse line of the cohort, *Fam46a*^{E157*Mhda}, which showed typical abnormalities in a bone turnover parameter (increased alkaline phosphatase (ALP) activity) as well as in bone content and structure, was chosen for further investigation and was identified as the first mouse model for a nonsense mutation within the *Fam46a* (family with sequence similarity 46, member A) gene. Homozygous *Fam46a*^{E157*Mhda} mice developed a severe skeletal phenotype with short stature and deformities of limbs, ribs, scapulae, pelvis and calvaria. Defects encompassed endochondral and intramembranous ossification suggesting a possible role of Fam46a in bone development and homeostasis. In the third part, a functional approach was utilised to examine the molecular mechanisms underlying FGF23 actions in

more detail. A cell model of FGF23-inducible human embryonic kidney cells stably transfected with the human *KLOTHO* gene (HEK293-KL cells) was established. Western blot analysis revealed that mitogen-activated protein kinase (MAPK) signalling pathway is activated and EGR1 (early growth response 1) expression is induced by FGF23 in HEK293-KL cells. These results were confirmed by comparative transcriptome analysis using RNA-Seq data, and *EGR1* was determined to be of central importance as an FGF23-responsive target gene. Subsequently, *in vitro* reporter assays on the basis of the established cell line were developed to discover small-molecule compounds which regulate FGF23 signalling in a high-throughput screening (HTS) approach. Robustness and appropriateness of the method could be verified, and four primary candidate compounds were nominated in a pilot screen of a library containing 1,280 approved drugs.

ZUSAMMENFASSUNG

Die Phosphathomöostase ist für vielfältige physiologische Prozesse, die von der zellulären Signalgebung bis hin zur Knochenmineralisierung reichen, von äußerster Wichtigkeit. Sie wird durch ein komplexes Netzwerk, das mehrere Faktoren und Organe involviert, aufrechterhalten. Innerhalb der sogenannten Knochen-Nieren-Achse hat sich der im Knochen gebildete Fibroblasten-Wachstumsfaktor FGF23 (fibroblast growth factor 23) als der Schlüsselregulator des systemischen Phosphatumsatzes erwiesen. Er kontrolliert über die Aktivierung von FGFR (fibroblast growth factor receptor)/Klotho-Komplexen in der Niere die renale Ausscheidung von Phosphat und den Vitamin D-Stoffwechsel. Wenn das Phosphatgleichgewicht im Körper gestört ist, können hypo- und hyperphosphatämische Erkrankungen auftreten. Obwohl bereits mehrere Gene identifiziert wurden, die in direkter Verbindung mit monogenen Störungen des Phosphathaushaltes stehen, ist die Pathophysiologie immer noch nicht vollständig verstanden und viele offene Fragen müssen geklärt werden.

Der erste Teil dieser Arbeit konzentrierte sich auf eine Next-Generation Sequencing (NGS)-basierte Strategie, um neue potenzielle Krankheitsgene in der humanen Hypophosphatämie zu identifizieren. 11 nicht miteinander verwandte Familien mit unbekannter genetischer Ursache für den Phosphatverlust wurden analysiert. Allerdings konnten keine neuen Varianten, die in mindestens zwei nicht verwandten Patienten von pathogener Bedeutung zu sein scheinen, durch Exom-Sequenzierung nachgewiesen werden. Im zweiten Teil wurde eine Kohorte von Mausmodellen, die durch N-Ethyl-N-nitrosoharnstoff (ENU) generiert wurden und Änderungen im Knochenstoffwechsel und in der Skelettentwicklung aufwiesen (n = 18), mittels Exom-Sequenzierung auf Mutationen geprüft, um neue Schlüsselregulatoren der Phosphathomöostase zu finden. Hierbei betrug die Mutationsdetektionsrate 78%. Dadurch konnte gezeigt werden, dass die Exom-Sequenzierung ein geeignetes Hilfsmittel ist für genetische Analysen großer Kollektive von Mausmutanten im Hochdurchsatzverfahren wie z. B. im Münchner ENU-Mutagenese-Projekt. Sie umfasst zuverlässige Informationen, die ausreichend sind, um ENU-induzierte Mutationen auch ohne zusätzliche genetische Kartierungsdaten zu ermitteln. Eine Mauslinie der Kohorte, *Fam46a*^{E157*Mhda}, die charakteristische Veränderungen sowohl in einem Parameter des Knochenumsatzes (erhöhte

Aktivität der alkalischen Phosphatase (ALP)) als auch im Knochengehalt und in der Knochenstruktur aufwies, wurde für weitere Untersuchungen ausgewählt. Sie wurde als das erste Mausmodell für eine Nonsense-Mutation im *Fam46a* (family with sequence similarity 46, member A)-Gen identifiziert. Homozygote *Fam46a*^{E157*Mhda} Mäuse entwickelten einen schweren skelettalen Phänotyp mit Kleinwuchs und Deformationen der Extremitäten, der Rippen, der Schulterblätter, des Beckens und der Schädeldecke. Die Defekte betrafen sowohl die enchondrale als auch die intramembranöse Verknöcherung. Dies deutet auf eine mögliche Rolle von Fam46a in der Knochenentwicklung und in der Knochenhomöostase hin. Im dritten Teil wurde ein funktionaler Ansatz genutzt, um die zugrundeliegenden molekularen Wirkmechanismen von FGF23 näher zu untersuchen. Hierfür wurde ein Zellmodell aus FGF23-induzierbaren humanen embryonalen Nierenzellen, die stabil mit dem humanen *KLOTHO*-Gen transfiziert wurden (HEK293-KL-Zellen), etabliert. Anhand von Western-Blot-Analysen konnte gezeigt werden, dass FGF23 in HEK293-KL-Zellen den MAPK (mitogen-activated protein kinase)-Signalweg aktiviert und die Expression von EGR1 (early growth response 1) induziert. Diese Ergebnisse wurden bestätigt durch vergleichende Transkriptom-Analyse unter Verwendung von RNA-Seq-Daten. Ebenso konnte die zentrale Bedeutung von *EGR1* als FGF23-responsives Zielgen festgestellt werden. Anschließend wurden *in vitro* Reporterassays basierend auf der etablierten Zelllinie entwickelt. Ziel war es, niedermolekulare Verbindungen, die die FGF23-vermittelte Signalgebung regulieren, in einem Hochdurchsatzverfahren zu entdecken. Die Robustheit und die Tauglichkeit des Verfahrens konnten verifiziert werden. Darüber hinaus wurden in einem Pilotscreen vier primäre Kandidaten aus einer Bibliothek mit 1.280 zugelassenen Medikamenten nominiert.

TABLE OF CONTENTS

LIST OF FIGURES

LIST OF TABLES

ABBREVIATIONS

°C	centigrade
$1,25(OH)_2D_3$	1α,25-dihydroxyvitamin D_3, calcitriol, active vitamin D
AA	amino acid
Ab	antibody
ad	autosomal dominant
ADAM10, 17	a disintegrin and metalloproteinase domain-containing protein 10, 17
ADHR	autosomal dominant hypophosphatemic rickets
ADSP	Assay Development and Screening Platform, Helmholtz Zentrum München
ALP	alkaline phosphatase
Alpha technology	amplified luminescent proximity homogenous assay technology
ar	autosomal recessive
ARHR1, 2	autosomal recessive hypophosphatemic rickets-1, -2
BAP014	Bone screen alkaline phosphatase #14
bFGF	basic fibroblast growth factor
bp	base pair
BPL010	Bone screen Pi low #10
BSA	bovine serum albumin
BWA	Burrows-Wheeler Aligner
c.	cDNA sequence position
Ca	calcium
cDNA	complementary DNA
chr	chromosome
cm^2	square centimetre

CO_2	carbon dioxide
COL24A1	collagen XXIV, α1
Col24a1	COL24A1 mouse orthologue
C-terminus	carboxy-terminus
CV	coefficient of variation
CYP24A1	24-hydroxylase
CYP27B1	1α-hydroxylase
d	day
Da	dalton
dbSNP	Single Nucleotide Polymorphism Database
dH_2O	deionised water
DHPLC-H_2O	denaturing high-performance liquid chromatography water
dl	decilitre
DMP1	dentin matrix protein 1
Dmp1	DMP1 mouse orthologue
DMSO	dimethyl sulfoxide
DNA	deoxyribonucleic acid
dNTP	deoxynucleotide
ds	double-stranded
DUF	domain of unknown function
dUTP	deoxyuridine triphosphate
EC_{50}	half maximal effective concentration
E. coli	*Escherichia coli*
EDTA	ethylenediaminetetraacetic acid
e.g.	exempli gratia
EGF	epidermal growth factor
EGR1	early growth response 1

ELISA	enzyme-linked immunosorbent assay
EMA	European Medicines Agency
ENPP1	ectonucleotide pyrophosphatase/phosphodiesterase 1
Enpp1	ENPP1 mouse orthologue
ENU	N-ethyl-N-nitrosourea
ERK1/2	extracellular signal-regulated kinases 1and 2
et al.	et alii
FAM20C	family with sequence similarity 20, member C
Fam20c	FAM20C mouse orthologue
FAM46A	family with sequence similarity 46, member A
Fam46a	FAM46A mouse orthologue
Fam46a$^{E157*/+}$	heterozygous *Fam46a*^{E157*} mutant
Fam46a$^{E157*/-}$	homozygous *Fam46a*^{E157*} mutant
FBS	foetal bovine serum
FDA	Food and Drug Administration
FGF	fibroblast growth factor
FGF23	fibroblast growth factor 23
Fgf23	FGF23 mouse orthologue
FGF23R179Q	fibroblast growth factor 23 (R179Q mutant)
FGFR	fibroblast growth factor receptor
FGFR1c	fibroblast growth factor receptor 1, isoform c
FRET	fluorescence resonance energy transfer
FTC	familial tumoural calcinosis
g	gram
GalNAc	N-acetylgalactosamine
GALNT3	polypeptide N-acetylgalactosaminyltransferase 3
Gb	gigabase

GFR	glomerular filtration rate
h	hour
HEK293	human embryonic kidney 293 cells
hERG	human ether-a-go-go-related gene
hg19	human genome assembly GRCh37 (February 2009), UCSC
HGMD	Human Gene Mutation Database
HHRH	hereditary hypophosphatemic rickets with hypercalciuria
HRP	horseradish peroxidase
HTRF	homogenous time-resolved fluorescence
HTS	high-throughput screening
i.a.	inter alia
IC_{50}	half maximal inhibitory concentration
i.e.	id est
IEG	Institute of Experimental Genetics, Helmholtz Zentrum München
IGV	Integrative Genomics Viewer
IHG	Institute of Human Genetics, Helmholtz Zentrum München
indel	small insertion and deletion variation
kb	kilobase
kDa	kilodalton
KTA041	Kinky tail alkaline phosphatase #41
l	litre
LDS	Loeys-Dietz syndrome
M	molar
µCT	micro computed tomography
µg	microgram
µl	microlitre
µM	micromolar

mA	milliampere
MAPK	mitogen-activated protein kinase
Mb	megabase
MEK1/2	mitogen-activated protein kinase kinases 1 and 2
MEPE	matrix extracellular phosphoglycoprotein
mg	milligram
$MgCl_2$	magnesium chloride
MGI	Mouse Genome Informatics
min	minute
ml	millilitre
mM	millimolar
mm9	mouse genome assembly NCBI37 (July 2007), UCSC
mRNA	messenger ribonucleic acid
NA	not available
NaPi-2a,-2c	sodium/phosphate co-transporter 2a, 2c
NCBI	National Center for Biotechnology Information
ng	nanogram
NGS	next-generation sequencing
NHERF1	sodium/hydrogen exchanger regulatory factor 1
nm	nanometer
nM	nanomolar
NM	RefSeq mRNA sequence
NP	RefSeq protein sequence
N-terminus	amino-terminus
OMIM	Online Mendelian Inheritance in Man
p.	protein sequence position
p-	phospho-

PAGE	polyacrylamide gel electrophoresis
PBS	phosphate buffer saline
PCR	polymerase chain reaction
PE	paired-end
p-ERK1/2	phosphorylated form of ERK1/2
PHEX	phosphate regulating gene with homologies to endopeptidases on the X-chromosome
Phex	PHEX mouse orthologue
Pi	inorganic phosphate
pmol	picomol
pQCT	peripheral quantitative computed tomography
PTH	parathyroid hormone
PVDF	polyvinylidene fluoride
RefSeq	NCBI Reference Sequence Database
RIN	RNA integrity number
RNA	ribonucleic acid
RT	room temperature
RT-PCR	reverse transcription polymerase chain reaction
s	second
SCUBE3	signal peptide CUB EGF domain-containing protein 3
Scube3	SCUBE3 mouse orthologue
SD	standard deviation
SDS	sodium dodecyl sulphate
sFRP4	secreted frizzled-related protein 4
SHFLD	split-hand/foot malformation with long-bone deficiency
SIBLING	small integrin-binding ligand N-linked glycoprotein
SLC34A1, 3	solute carrier family 34, subfamily A (type II sodium/phosphate co-transporter), member 1, 3

SLC9A3R1	solute carrier family 9, subfamily A (sodium/hydrogen exchanger), member 3, regulator 1
SNV	single nucleotide variant
SPC	subtilisin-like proprotein convertase
STAT5	signal transducer and activator of transcription 5
SW	signal window
TBE	Tris-borat-EDTA
TBST	Tris-buffered saline and Tween 20
TGF-β	transforming growth factor β
TIO	tumour-induced osteomalacia
TmP	maximal rate for tubular reabsorption of phosphate
TP63	transformation-related protein 63
Tris	2-amino-2(hydroxymethyl)-1,3-propandiol
Trp63	TP63 mouse orthologue
TTP	thymidine triphosphate
U	unit
UCSC	University of California, Santa Cruz
UTP	uridine triphosphate
UTR	untranslated region
UV	ultraviolet
V	volt
VNTR	variable number of tandem repeat
v/v	volume per volume
WNT	wingless-type MMTV integration site family
WT	wild-type
w/v	weight per volume
XLH	X-linked hypophosphatemic rickets

1. INTRODUCTION

Phosphorus in the form of phosphate is one of the body's most essential and abundant ions. It plays a critical role in numerous biological processes like cell structure (cell membrane integrity and nucleic acids), cellular energy metabolism (generation of ATP), regulation of subcellular processes (cell signalling through phosphorylation of proteins), maintenance of acid-base homeostasis (urinary buffering) and bone mineralisation (Penido and Alon, 2012). Therefore, maintaining serum phosphate levels within the physiological range is of critical importance.

1.1. PHOSPHATE HOMEOSTASIS

The average adult body contains about 700 g of phosphate, of which 85% is present in bones and teeth mainly complexed with calcium in the form of hydroxyapatite crystals ($Ca_5(PO_4)_3(OH)$), 14% in soft tissues and 1% in extracellular fluid. Of the 1% that is present in extracellular fluid, 10 - 20% is protein-bound and 5% is complexed with cations such as calcium, magnesium and sodium. The remainder exists as divalent HPO_4^{2-} or monovalent $H_2PO_4^-$ ions with a ratio of 4:1 at a physiological pH of 7.4 (Alizadeh Naderi and Reilly, 2010; Amanzadeh and Reilly, 2006; Gattineni and Baum, 2012). It is the extracellular phosphate that is measured by routine laboratory analysis, and consequently it does not always reflect the total body phosphate stores. The normal serum phosphate concentration varies as a function of age in humans: in the range of 3.8 - 5.5 mg/dl in children and 2.5 - 4.5 mg/dl in adults (Greenberg et al., 1960; Reilly, 2005). Moreover, serum phosphate concentration exhibits a circadian rhythm characterised by a rapid decrease in the early morning, reaching a nadir at 11:00 h, increasing to a plateau at 16:00 h and peaking between 1:00 h and 3:00 h. The variation from nadir to peak may be as much as 1 mg/dl, i.e. 25 - 30% change in concentration (Portale et al., 1987). The average adult phosphate intake is about 1.2 g per day, of which one-third is excreted in the stool and two-thirds in the urine to maintain phosphate balance. Due to continuous bone remodelling, 250 mg of phosphate is exchanged between the bone and the extracellular phosphate per day (Amanzadeh and Reilly, 2006; Gattineni and Baum, 2012) (Figure 1).

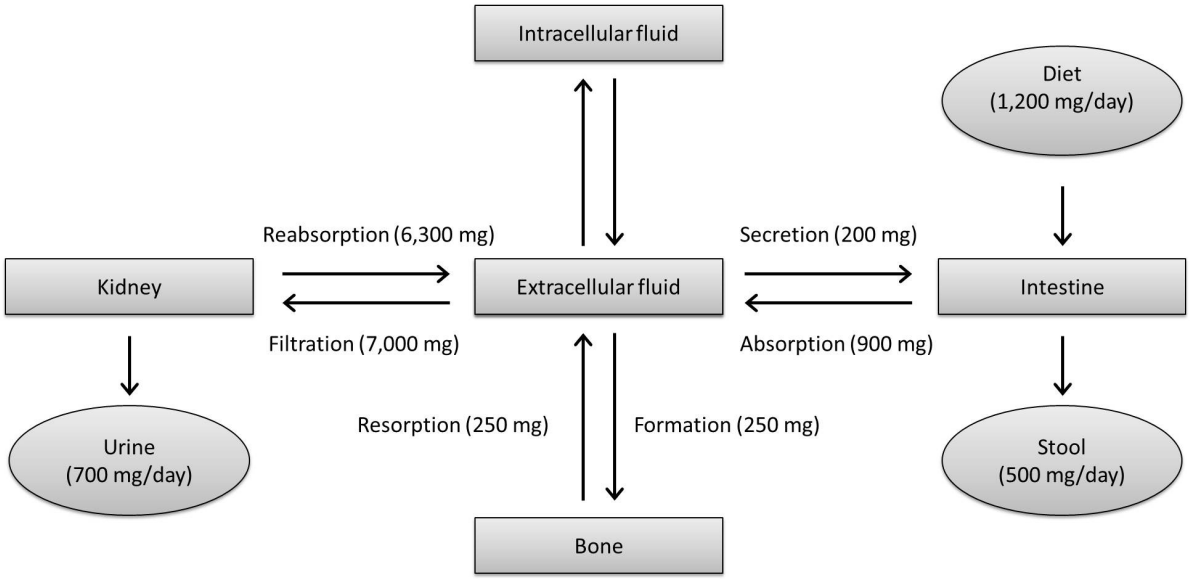

Figure 1: Phosphate fluxes between different compartments to keep extracellular serum phosphate levels. Figure adapted from (Amanzadeh and Reilly, 2006).

Both intestinal uptake and renal reabsorption are mediated by sodium/phosphate co-transporters, which belong to the *SLC34* gene family of solute carriers. There are three types of SLC34 transporters: NaPi-2a (SLC34A1), NaPi-2b (SLC34A2) and NaPi-2c (SLC34A3) (Biber et al., 2013; Wagner et al., 2014a). Ingested phosphate is absorbed from the gastrointestinal tract via passive (paracellular) and active (transcellular) transport processes. The paracellular pathway is diffusion-driven and non-saturable, i.e. phosphate transport increases with increasing dietary phosphate (Alizadeh Naderi and Reilly, 2010). Transcellular phosphate absorption is mediated by NaPi-2b, which is largely regulated by active vitamin D ($1,25(OH)_2D_3$, calcitriol), metabolic acidosis and dietary phosphate (Danisi et al., 1980; Hattenhauer et al., 1999).

Once phosphate enters the systemic circulation, free and complexed phosphate is filtered at the glomerulus. The kidney plays a major role in regulating phosphate homeostasis. Under basal conditions, 80 - 90% of the filtered phosphate load is reabsorbed by the kidney. The rest is excreted in the urine (Harris et al., 1977; Pastoriza-Munoz et al., 1978). This process represents the rate-limiting step and a maximal rate for tubular reabsorption of phosphate (TmP) can be determined. The balance between the rates of glomerular filtration (GFR) and maximal tubular reabsorption (TmP/GFR) defines the renal excretion of phosphate (Tenenhouse and Econs, 2001). Phosphate is primarily reabsorbed in the proximal tubule by the transporters NaPi-2a and NaPi-2c in the apical brush border membrane. The human

SLC34A1 gene, which encodes NaPi-2a, is located on chromosome 5q35.3, spans about 13 kb and consists of 13 exons. The human *SLC34A3* gene encodes NaPi-2c, is located on chromosome 9q34.3, spans approximately 5 kb and also contains 13 exons. Studies of the transport functions of SLC34A transporters and their structure-relationship revealed that NaPi-2a transports three sodium ions together with one divalent phosphate ion (HPO_4^{2-}) per transport cycle. This transport mode is electrogenic (Busch et al., 1995; Virkki et al., 2005). NaPi-2c only transports two sodium ions per phosphate and is electroneutral. So far, the putative proteins responsible for basolateral phosphate flux have not been identified. The phenotypes of mice deficient in NaPi-2a and NaPi-2c indicate that NaPi-2a is responsible for most phosphate renal reabsorption (Beck et al., 1998). In contrast, in the human kidney, NaPi-2c appears to have a comparatively greater role (Bergwitz et al., 2006; Lorenz-Depiereux et al., 2006b).

Additionally, a sodium/phosphate co-transporter from the *SLC20* gene family of solute carriers is expressed in the kidney. The physiological relevance of PiT-2 (SLC20A2) to phosphate reabsorption remains to be elucidated, but its contribution to overall phosphate reabsorption may be minor (Segawa et al., 2009).

1.2. REGULATION OF PHOSPHATE HOMEOSTASIS

The parathyroid hormone (PTH), whose chief role is the regulation of extracellular calcium concentration, also contributes to phosphate regulation (Bergwitz and Juppner, 2010). PTH mediates its action through a G protein-coupled receptor. The receptor is abundantly, though not exclusively, expressed in the bone and kidney. Especially in the proximal tubule, PTH acts via the PTH receptor 1 (PTHR1), whose activation leads to internalisation of the sodium/phosphate co-transporters NaPi-2a and NaPi-2c, and thus phosphaturia (Forster et al., 2006). However, the regulation of phosphate homeostasis cannot be explained by the phosphaturic action of PTH alone. Indeed, findings in two mouse models for hypophosphatemia (*Hyp* and *Gy*) (Eicher et al., 1976; Lyon et al., 1986) suggested that at least one additional factor must be involved in phosphate regulation. Moreover, transplantation of kidneys from *Hyp* mice into wild-type mice and vice versa (Nesbitt et al., 1992) as well as parabiosis experiments (Meyer et al., 1989) indicated that this putative factor is not intrinsic to the kidney. More likely, it is a phosphaturic humoral substance that is transported to the kidney via blood circulation. This hypothesis was further strengthened by studies of an

acquired condition, tumour-induced osteomalacia (TIO), which is caused by mostly benign, rare tumours leading to laboratory changes and clinical symptoms that are indistinguishable from those observed in hypophosphatemic disorders characterised by abnormally low serum levels of phosphate (Econs and Drezner, 1994). Based on early studies, it was postulated that this proposed phosphaturic factor is secreted from the bone, but its purification proved to be difficult.

In fact, most of the genes contributing to the regulation of phosphate homeostasis are expressed in the bone and were identified through genetic studies to define the molecular defects that cause different hypophosphatemic (*PHEX* (The HYP Consortium, 1995), *FGF23* (The ADHR Consortium, 2000), *DMP1* (Lorenz-Depiereux et al., 2006a), *ENPP1* (Lorenz-Depiereux et al., 2010) and *FAM20C* (Rafaelsen et al., 2013)) or hyperphosphatemic (*FGF23* (Benet-Pages et al., 2005) and *GALNT3* (Topaz et al., 2004)) disorders. Only the renal sodium/phosphate co-transporters NaPi-2a and NaPi-2c were isolated through expression cloning and homology searches, respectively (Magagnin et al., 1993). *Klotho* was discovered by serendipity in a mutant mouse line, when a transgene disrupted its promoter leading to a hypomorphic allele. Because these transgenic animals showed premature aging, Klotho was first thought to be a suppressor of aging (Kuro-o et al., 1997). The first disease-causing mutation in the human *KLOTHO* gene was reported in a patient with marked hyperphosphatemia a few years later (Ichikawa et al., 2007).

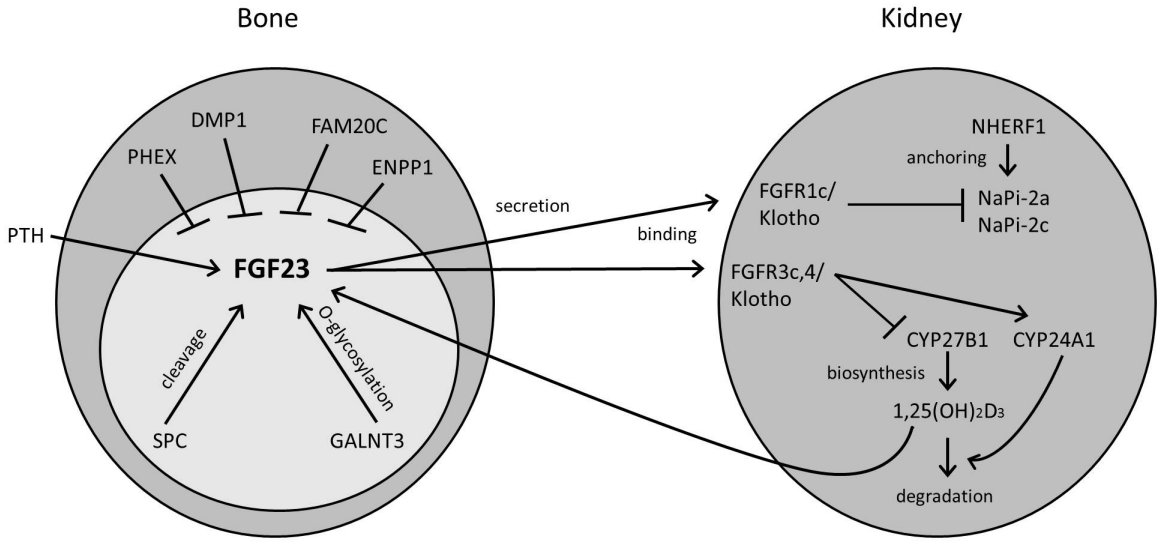

Figure 2: Schematic model of the bone-kidney axis involved in the regulation of phosphate homeostasis. The analysis of rare genetic disorders affecting phosphate metabolism in man and mouse led to the identification of several proteins that are critical for renal phosphate handling. Details can be found in the text. The circle filled by light grey colour displays intracellular interactions. Modified from (Strom and Juppner, 2008).

The corresponding proteins are now undoubtedly regarded to be members of a bone-kidney axis essential for the complex regulation of phosphate homeostasis in the body (Quarles, 2003; Strom and Juppner, 2008) (Figure 2).

1.2.1. FGF23 as a Key Regulator of Phosphate Homeostasis

Among the identified members of the bone-kidney axis, fibroblast growth factor 23 (FGF23) has materialised as the key regulator of phosphate homeostasis. FGF23 is part of the fibroblast growth factor (FGF) family comprising 22 FGFs in humans. Together with FGF19 and FGF21, FGF23 belongs to the subfamily of endocrine FGFs. FGFs have diverse roles in regulating cell proliferation, migration and differentiation (Ornitz and Itoh, 2001). The human *FGF23* gene on chromosome 12p13.3 is composed of three exons and encodes a protein of 251 amino acid residues with a hydrophobic leader sequence of 24 amino acids. The secreted protein $FGF23^{25\text{-}251}$ has a molecular weight of 32 kDa. The N-terminal domain of FGF23 shows homologies to the core barrel structure of other members of the FGF family, whereas the C-terminal domain is unique to FGF23 (Ornitz and Itoh, 2001) (Figure 3). Intracellularly during secretion, FGF23 is O-glycosylated at the C-terminal end between amino acids 179 and 180 by polypeptide N-acetylgalactosaminyltransferase 3 (GALNT3). O-glycosylation is critical for secretion of intact FGF23 and occurs at a subtilisin-like proprotein convertase (SPC) cleavage site (^{176}RXXR^{179} motif) (Benet-Pages et al., 2004; Kato et al., 2006) (Figure 3).

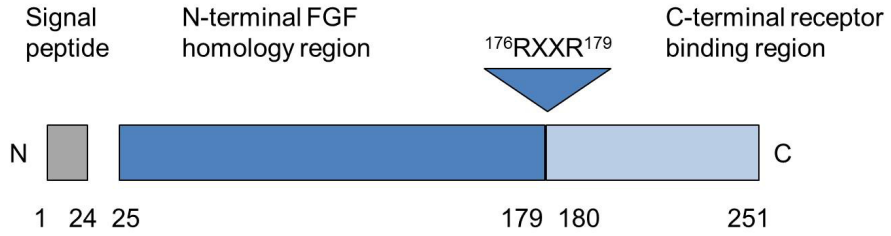

Figure 3: Fibroblast growth factor 23 (FGF23). Schematic structure of FGF23 including three main domains: The signal peptide (grey colour), the N-terminus that shares homology with other FGFs (dark blue colour) and the C-terminus that is unique and binds to its cognate receptor (light blue colour). FGF23 activity is regulated by a proteolytic cleavage at the ^{176}RXXR^{179} motif. FGF23 circulates in the blood as both intact (full-length) and cleaved fragments. Figure modified from (Hu et al., 2013b).

Proteolytic cleavage by SPCs controls the activity of FGF23 generating bioinactive N-terminal ($FGF23^{25\text{-}179}$) and C-terminal ($FGF23^{180\text{-}251}$) fragments (Goetz et al., 2007). Missense mutations at the cleavage site, which affect one of the two arginine residues at positions p.176

or p.179 leading to a glutamine or tryptophan substitution (R176Q, R179W and R179Q), render the protein resistant to proteolysis (The ADHR Consortium, 2000; White et al., 2001).

FGF23 is mainly produced by osteoblasts and osteocytes in the skeleton (Yoshiko et al., 2007), but it is also found, albeit at much lower concentrations, in other tissues including brain and heart. Together with the two other secreted FGFs (FGF19 and FGF21), FGF23 appears unique in that the topology of the heparin-binding region diverges from the typical structure seen in the canonical FGFs, which reduces the affinity to heparin sulphate (Mohammadi et al., 2005). This enables them to avoid capturing in the extracellular matrices, and hence confers their endocrine function (Goetz et al., 2007). After secretion from the bone, FGF23 circulates in the bloodstream to ultimately act on its principal target organ, the kidney. The major functions of FGF23 are (1) the inhibition of renal phosphate reabsorption by downregulating NaPi-2a and NaPi-2c abundance and activity and (2) the reduction of active vitamin D levels through lowering the expression of CYP27B1 (1α-hydroxylase) and increasing the expression of CYP24A1 (24-hydroxylase) (Baum et al., 2005; Saito et al., 2003; Segawa et al., 2003; Shimada et al., 2004a; Shimada et al., 2004b) (Figure 2, Figure 4).

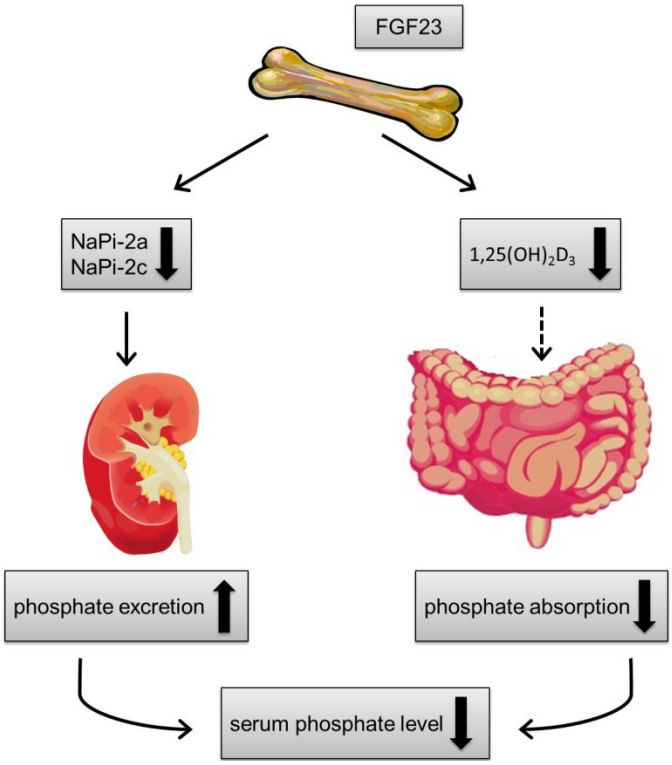

Figure 4: Phosphaturic effects of FGF23. FGF23 as a key regulator of phosphate homeostasis, which is mainly produced in the bone, suppresses NaPi-2a and NaPi-2c carriers in the brush border membrane of the proximal tubule in the kidney. Additionally, FGF23 reduces $1,25(OH)_2D_3$ levels, which in turn leads to decreased intestinal phosphate absorption and subsequently reduced serum levels of phosphate. Adapted from (Razzaque, 2009).

In sum, FGF23 as a phosphaturic factor promotes negative phosphate balance by increasing renal phosphate excretion and reducing intestinal phosphate absorption (Figure 4).

1.2.2. FGF23 Signalling

FGF23 directly acts on renal proximal tubules by binding to receptor complexes composed of FGF receptor (FGFR) and the co-receptor α-Klotho (hereinafter called "Klotho") (Andrukhova et al., 2012).

Ligands of the FGF family bind to FGFRs to mediate their actions. The four major FGFRs (FGFR1 - 4) are encoded by four genes, and alternative splicing (b and c isoforms of FGFR1 - 3) results in tissue- and ligand-binding specificity (Mohammadi et al., 2005; Ornitz and Itoh, 2001). A prototypical FGFR compasses three extracellular immunoglobulin-like domains (D1 - D3), a single-pass transmembrane domain and an intracellular domain (Mohammadi et al., 2005). This intracellular domain harbours an intrinsic tyrosine kinase activity and elicits tyrosine autophosphorylation of the receptors upon ligand binding (Szebenyi and Fallon, 1999). The proximal tubule, the site of most renal phosphate reabsorption (Baumann et al., 1975; Ullrich et al., 1977) and 1α-hydroxylase activity (Brunette et al., 1978), expresses FGFR1c, 3c and 4, but it does not express FGFR2c (Gattineni et al., 2009). While it is postulated that FGFR3c and FGFR4 are the main receptors involved in $1,25(OH)_2D_3$ regulation (Gattineni et al., 2011; Liu et al., 2008), there is strong support FGFR1c being the principal receptor mediating FGF23 phosphaturic effects (Gattineni et al., 2009). Thus, the focus will lie on this receptor isoform in the following.

To exert its phosphaturic activity, FGF23 requires Klotho as an obligate co-receptor that converts the canonical FGFR1c into a specific receptor complex for FGF23 (Urakawa et al., 2006). The dependence on Klotho compensates for the poor binding affinity of FGF23 to FGFR1c. Klotho constitutively binds FGFR1c, and the binary FGFR1c/Klotho complex shows enhanced binding affinity for FGF23 (Kurosu et al., 2006; Urakawa et al., 2006). It was demonstrated by Goetz et al. that the 72-residue long C-terminal tail of FGF23 (Figure 3) is critical for receptor binding. The C-terminal tail alone, however, does not transactivate the FGFR1c/Klotho complex and can potentially function as a competitive endogenous antagonist (Goetz et al., 2010).

Klotho, named after the ancient Greek goddess of fate, is a putative aging suppressor gene. In mice, a defect in its expression leads to a syndrome resembling human aging with phenotypes

like infertility, early thymic involution, skin and muscle atrophy, emphysema, osteoporosis, growth retardation, deranged mineral metabolism and a short lifespan (Kuro-o et al., 1997), while lifespan is prolonged by overexpression of Klotho (Kurosu et al., 2005). A lifespan-extending variant of the human *KLOTHO* gene was shown to be associated with enhanced cognition in heterozygous carriers (Arking et al., 2002; Dubal et al., 2014). In addition, Klotho is believed to have anti-inflammatory (Liu et al., 2011; Zhao et al., 2011) and tumour suppressor properties (Wolf et al., 2008). The Klotho protein consists of a large extracellular domain (approximately 130 kDa), a single-pass type I transmembrane domain and a very short intracellular domain of only ten amino acid residues. The extracellular domain consists of two internal repeat sequences, named KL1 and KL2, respectively. It exhibits homology to family 1 glycosidases, which are enzymes that hydrolyse terminal glycosidic linkages in sugars, glycoproteins and glycolipids (Tohyama et al., 2004). Moreover, the extracellular domain is subject to ectodomain shedding by disintegrin and metalloproteinases ADAM10 and ADAM17 and is released into the extracellular space (Chen et al., 2007). It can be detected in blood, urine and cerebrospinal fluid (Bloch et al., 2009; Chen et al., 2007; Imura et al., 2004). As a result, two forms exist: membrane Klotho and secreted Klotho. Secreted Klotho acts as a humoral factor with pleiotropic activities like suppression of insulin/IGF1 (insulin-like growth factor 1) and Wnt signalling (Liu et al., 2007) as well as regulation of ion channels and transporters (Chang et al., 2005; Huang, 2010). As aforementioned, membrane Klotho functions as a co-receptor for FGF23 and is expressed predominantly in the kidney. The phenotypes of $Klotho^{-/-}$ and $Fgf23^{-/-}$ mice are very similar involving premature aging and aberrant mineral metabolism (Kuro-o et al., 1997; Razzaque et al., 2006). These similarities point to the involvement of Klotho and Fgf23 in a common physiological pathway.

When FGF23 binds to FGFR1c/Klotho complexes, FGFR dimerisation is induced (Schlessinger et al., 2000), which juxtaposes the intracellular domains of the receptor so that one tyrosine kinase can phosphorylate, and hence activate, the other (Chen et al., 2008; Furdui et al., 2006). This activation enables cytoplasmic adapter proteins, chief among which is FGFR substrate 2α (FRS2α), to bind to it. The adaptor protein in turn promotes the attraction of so-called guanine-nucleotide exchange factors (GEFs) to the plasma membrane, where they activate small G proteins of the RAS subfamily. As a result, mitogen-activated protein kinase (MAPK) cascade is employed leading to phosphorylation and activation of mitogen-activated protein kinase kinase kinase (also known as RAF kinase), mitogen-activated protein kinase

kinases 1 and 2 (MEK1/2) and extracellular signal-regulated kinases 1 and 2 (ERK1/2) (Pearson et al., 2001; Yamashita et al., 2002). Many downstream targets of ERK1/2 have been identified including different kinases and transcription factors. Among others, FGF23 signalling finally results in an increased expression of one known downstream target gene, *EGR1* (early growth response 1) (Urakawa et al., 2006; Yamazaki et al., 2010), which encodes an 80-kDa zinc finger transcription factor (Gashler and Sukhatme, 1995). EGR1 belongs to a family of early response genes that also include EGR2, EGR3, EGR4 and the Wilm's tumour gene product.

1.3. DISODERS OF PHOSPHATE REGULATION

If phosphate balance becomes disrupted, phosphate balance disorders can arise. Disorders characterised by abnormally low serum phosphate levels are termed hypophosphatemic disorders. The mirror image, defined by abnormally high serum phosphate levels, comprises a group of hyperphosphatemic disorders.

1.3.1. Genetic Disorders

Causes of hypo- and hyperphosphatemic disorders are mostly caused by genetic defects in factors necessary for phosphate handling. They are summarised in Table 1.

Hereditary hypophosphatemic disorders can be divided into two different types. Firstly, phosphate wasting may be due to a primary renal tubular defect. While the importance of NaPi-2a in phosphate reabsorption remains controversial in humans (Lapointe et al., 2006; Magen et al., 2010; Prie et al., 2002; Virkki et al., 2003), the essential role of NaPi-2c has been very well described. Hereditary hypophosphatemic rickets with hypercalciuria (HHRH) is an autosomal recessive disorder due to mutations in the *SLC34A3* gene that cause a loss of function of the NaPi-2c at the brush border membrane of the proximal tubule (Bergwitz et al., 2006; Lorenz-Depiereux et al., 2006b). Additionally, loss-of-function mutations in *SLC9A3R1* are associated with phosphaturia in hypophosphatemic nephrolithiasis/osteoporosis-2 (NPHLOP2) (Courbebaisse et al., 2012; Karim et al., 2008). The sodium/hydrogen exchanger regulatory factor SLC9A3R1 (NHERF1) is a scaffolding protein that interacts with NaPi-2a and NaPi-2c transporters and may increase their stability in the brush border membrane (Andrukhova et al., 2012; Cunningham et al., 2010; Villa-Bellosta et al., 2008).

Table 1: Monogenic disorders of altered renal phosphate handling.

Disease	OMIM	Gene	Inheritance	Mutation	FGF23 levels	Pi levels
HHRH	#241530	*SLC34A3*	ar	loss of function	normal	low
NPHLOP2	#612287	*SLC9A3R1*	ad	loss of function	normal	low
ADHR	#193100	*FGF23*	ad	gain of function	high	low
XLH	#307800	*PHEX*	X-linked dominant	loss of function	high	low
ARHR1	#241520	*DMP1*	ar	loss of function	high	low
ARHR2	#613312	*ENPP1*	ar	loss of function	high	low
Raine syndrome	#259775	*FAM20C*	ar	loss of function	high	low
FD/MAS	#174800	*GNAS1*	ad, mosaicism	gain of function	high	low
Hypo-phosphatemic rickets	%612089	*KLOTHO*	translocation, dominant	overexpression	high	low
OD	#166250	*FGFR1*	ad?	gain of function	high	low
FTC	#211900	*GALNT3*	ar	loss of function	low	high
FTC	#211900	*FGF23*	ar	loss of function	low	high
FTC	#211900	*KLOTHO*	ar	loss of function	low	high

Red colour indicates increased serum levels of FGF23. Green colour indicates decreased serum levels of FGF23. OMIM = Online Mendelian Inheritance in Man; Pi = inorganic phosphate; HHRH = hereditary hypophosphatemic rickets with hypercalciuria; NPHLOP2 = hypophosphatemic nephrolithiasis/osteoporosis-2; ADHR = autosomal dominant hypophosphatemic rickets; XLH = X-linked hypophosphatemic rickets; ARHR1, 2 = autosomal recessive hypophosphatemic rickets-1, -2; FD = fibrous dysplasia; MAS = McCune-Albright syndrome; OD = osteoglophonic dysplasia; FTC = familial tumoural calcinosis; SLC34A3 = solute carrier family 34, subfamily A (type II sodium/phosphate co-transporter), member 3; SLC9A3R1 = solute carrier family 9, subfamily A (sodium/hydrogen exchanger), member 3, regulator 1; FGF23 = fibroblast growth factor 23; PHEX = phosphate regulating gene with homologies to endopeptidases on the X-chromosome; DMP1 = dentin matrix protein 1; ENPP1 = ectonucleotide pyrophosphatase/phosphodiesterase 1; FAM20C = family with sequence similarity 20, member C; GNAS1 = GNAS complex locus 1; FGFR1 = fibroblast growth factor receptor 1; GALNT3 = polypeptide N-acetylgalactosaminyltransferase 3; ad = autosomal dominant; ar = autosomal recessive

Secondly, phosphate wasting may be derivative to extrarenal inherited defects causing augmented FGF23 signalling (Table 1; marked in red). Increased FGF23 levels can be caused by inactivating mutations in genes encoding upstream inhibitory regulators of FGF23: *PHEX* (The HYP Consortium, 1995), *DMP1* (Lorenz-Depiereux et al., 2006a), *ENPP1* (Lorenz-Depiereux et al., 2010) or *FAM20C* (Rafaelsen et al., 2013). However, the underlying molecular mechanisms of the regulation of FGF23 synthesis and secretion are largely unknown. X-linked hypophosphatemic rickets (XLH) is caused by loss-of-function mutations in the *PHEX* gene (The HYP Consortium, 1995). It is the most common form of hereditary hypophosphatemia with an estimated incidence of 1:10,000 - 1:20,000 (Carpenter, 2014). XLH is transmitted as an X-linked dominant trait with complete penetrance but variable expressivity. Mutations in the mouse *Phex* gene were also identified in the *Hyp* and *Gy* mouse models of XLH (Eicher et al., 1976; Lyon et al., 1986; Strom et al., 1997). Furthermore, gain-of-function mutations in the *FGF23* gene render the encoded protein resistant to proteolysis by SPCs, and thus cause inappropriately high levels of circulating intact, biologically active FGF23 in autosomal dominant hypophosphatemic rickets (ADHR) (The ADHR Consortium, 2000). In fibrous dysplasia (FD), patients have activating mutations in *GNAS1* encoding the α-subunit of stimulatory G protein (G_s, α) (Weinstein et al., 1991). The mechanism behind how mutations in *GNAS1* result in elevated levels of FGF23 remains unknown. Abnormally high levels of FGF23 seem to be caused by an increase in FGF23-producing cells but not by an abnormal production of FGF23 per se (Riminucci et al., 2003). Additionally, activating mutations in *FGFR1* (White et al., 2005) as well as a translocation of *KLOTHO* that massively increases circulating Klotho levels (Brownstein et al., 2008) can cause hypophosphatemia due to higher FGF23 levels. So far, the causal mechanisms are unknown. It is suggested that circulating Klotho stimulates bone FGF23 production (Smith et al., 2012).

In children, hypophosphatemia is revealed by vitamin D-resistant rickets that results in phosphaturia, inappropriately low levels of $1,25(OH)_2D_3$, spontaneous dental abscesses, bone pain, variable degrees of delayed walking, waddling gait, bowing of lower extremities, enlarged cartilages and growth failure (short stature) (Figure 5). The mineralisation defect endures in adulthood with continuing osteomalacia, which leads to long-term complications including bone pain, fractures, severe dental anomalies, hearing loss and fatigue (Linglart et al., 2014). Both rickets and osteomalacia are considered to be conditions of metabolic bone disease (Horvai and Boyce, 2011; Jakob, 2007).

Figure 5: Radiography from a 2.5-year-old boy with XLH. Leg bowing with cupping of the metaphyseal ends of the bone are typical radiographic findings of XLH (from Dr. K. L. Mohnike, Magdeburg, Germany).

Contrary to disorders of renal phosphate wasting, there are also hyperphosphatemic disorders defined by inappropriately low serum levels of FGF23 and abnormally high serum levels of phosphate (Table 1; marked in green). Familial tumoural calcinosis (FTC), an autosomal recessive condition causing FGF23 deficiency, is characterised by hyperphosphatemia, hypercalcemia and increased serum levels of active vitamin D. In addition, pathological deposits of phosphate and calcium give rise to ectopic calcifications (calcinosis) as shown in Figure 6.

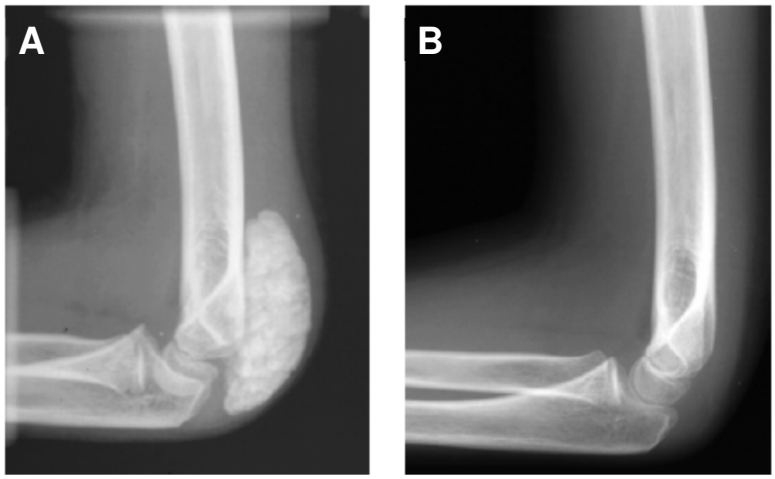

Figure 6: Characteristic findings of FTC in a 12-year-old boy. Calcinosis usually occurs in and just under skin tissue around the joints, most often the hips, shoulders and elbows. Radiographs show the left elbow (A) before and (B) after resection of a discoid lobulated calcified tumour-like (tumoural) mass in the soft tissue of the extensior site of the left distal humerus (Benet-Pages et al., 2005).

In FTC, inactivating mutations in *FGF23* or *GALNT3* result in defects of FGF23 O-glycosylation, which usually stabilises the protein (Benet-Pages et al., 2005; Topaz et al., 2004). Without posttranslational processing, FGF23 is rapidly degraded by proteases. Hence, patients have low levels of intact FGF23 but elevated levels of FGF23 fragments (Ichikawa et al., 2007). Homozygous missense mutations in the human *KLOTHO* gene have also been identified as a cause of tumoural calcinosis (Ichikawa et al., 2007).

1.3.2. Acquired Disorders

Besides inherited forms of altered renal phosphate handling, disorders can arise spontaneously (Table 2). Tumour-induced osteomalacia (TIO), also known as oncogenic osteomalacia, is a rare paraneoplastic syndrome, in which patients present with bone pain, fractures and muscle weakness. In TIO, high levels of FGF23 are secreted by mesenchymal, usually benign tumours that are typically very small and difficult to locate (Shimada et al., 2001). In addition, it was reported that elevated serum levels of FGF23 are found in association with mosaic cutaneous disorders that affect large proportions of the skin and appear in patterns corresponding to the migration of ectodermal progenitors. Activating somatic mutations in *HRAS* and *NRAS* were identified to be causal for this hypophosphatemic disorder (Lim et al., 2014).

Table 2: Acquired disorders of renal phosphate wasting.

Disease	Gene	Occurrence	Mutation	FGF23 levels	Pi levels
TIO	*MEPE*	spontaneous?	overexpression	normal	low
TIO	*sFRP4*	spontaneous?	overexpression	normal	low
TIO	*FGF7*	spontaneous?	overexpression	normal	low
TIO	*FGF23*	spontaneous?	overexpression	high	low
Mosaic cutaneous and skeletal lesions	*HRAS, NRAS*	spontaneous?	gain of function	high	low

Red colour indicates increased serum levels of FGF23. Pi = inorganic phosphate; TIO = tumour-induced osteomalacia; MEPE = matrix extracellular phosphoglycoprotein; sFRP4 = secreted frizzled-related protein 4; FGF7, 23 = fibroblast growth factor 7, 23; HRAS = Harvey rat sarcoma viral oncogene homologue; NRAS = neuroblastoma RAS viral (v-ras) oncogene homologue

In addition to FGF23, other factors like MEPE, sFRP4 and FGF7 were demonstrated to have phosphaturic properties and to be overexpressed by tumours that cause TIO (Table 2) (Carpenter et al., 2005; De Beur et al., 2002; Rowe et al., 2000).

1.3.3. Treatment Strategies in Hypo- and Hyperphosphatemic Disorders

The current strategy for the treatment of hereditary hyperphosphatemic disorders like FTC caused by low serum levels of FGF23 is surgery to remove tumoural masses. Surgery is combined with lowering intestinal absorption of phosphate using both dietary phosphate restriction and oral phosphate-binding agents such as aluminium hydroxide and sevelamer (Farrow et al., 2011a). However, the success is only nominal, proposing that neither surgical nor present medical treatment is effective in controlling ectopic and vascular calcifications (Alkhatib et al., 2014; Carmichael et al., 2009).

On the other hand, conventional medical therapy of FGF23-related hypophosphatemic disorders in children is aimed at counteracting the consequences of FGF23 excess, i.e. oral phosphate supplementation with multiple daily intakes to compensate for renal phosphate wasting and active vitamin D analogues to counter the $1,25(OH)_2D_3$ deficiency. In adulthood, therapy is usually continued in symptomatic patients and generally intends to reduce osteomalacia and bone pain (Linglart et al., 2014; Verge et al., 1991). In some cases, corrective surgery may also help to overcome major bone deformities like leg bowing. Nevertheless, conventional treatment strategies are not causative. They improve clinical symptoms, but renal phosphate wasting persists due to the inappropriately high levels of circulating FGF23. Furthermore, parameters like height, serum calcium, alkaline phosphatase, PTH, phosphate serum levels and urinary calcium/creatinine ratio should be determined in a frequent follow-up. This close monitoring of patients is necessary, since the treatment with oral phosphate and active vitamin D preparations can be associated with complications including nephrocalcinosis (Verge et al., 1991), hyperparathyroidism (Schmitt and Mehls, 2004), hypertension (Alon et al., 2003) and cardiovascular abnormalities (Nehgme et al., 1997).

In the recent years, novel treatment strategies for hypophosphatemic conditions that target FGF23 as a key effector of phosphate wasting have been described. Several of them aim at inhibiting downstream FGF23 signalling. Monoclonal anti-FGF23 antibodies to neutralise endogenous FGF23 action have been generated by Yamazaki and co-workers in 2008

(Yamazaki et al., 2008). The humanised anti-FGF23 antibody, KRN23, ameliorated hypophosphatemia in patients with XLH after a single-dose treatment. Within the test phase, patients did not exhibit side effects like nephrocalcinosis (Carpenter et al., 2014). A phase I/II clinical trial has been successfully completed in the USA and Canada in 2013 (ClinicalTrials.gov identifiers NCT00830674, NCT01340482 and NCT01571596). Another approach was taken by Goetz et al. (Goetz et al., 2010). They demonstrated that the C-terminal fragment of FGF23 competes with the intact protein for receptor binding, yet without activating downstream signalling. There is no information indicating a possible clinical transition for this elegant approach as of today. The pharmacological inhibition of downstream FGF23 signalling was also probed as a potential novel treatment strategy in animal models. By means of the selective pan-specific FGFR antagonist NVP-BGJ398, tyrosine kinase activity of FGFR was inhibited (Wohrle et al., 2013). In addition, an inhibition of downstream FGF23 signalling within the MAPK signalling cascade by the small-molecule MEK inhibitor PD0325901 led to comparable results (Zhang et al., 2012). Although both small-molecule inhibitors have already been tested in clinical trials for cancer therapy in humans (Haura et al., 2010; Wolf et al., 2012), the application to hypophosphatemic rickets will warrant further investigation concerning the selectivity, notably towards other FGFR-mediated physiological processes beyond phosphate metabolism.

1.4. GAINING NEW INSIGHTS INTO MOLECULAR GENETICS OF PHOSPHATE HOMEOSTASIS

Despite significant advances in the mineral metabolism field, many open questions regarding principal molecular mechanisms regulating phosphate homeostasis, links between the known key regulators as well as the existence and contribution of additional members in the bone-kidney axis have to be addressed. In this work, three different approaches are proposed to improve the understanding of the molecular genetics of phosphate homeostasis.

1.4.1. Novel Candidate Disease Genes in Human Hypo- and Hyperphosphatemic Disorders

Next-generation sequencing (NGS) is becoming the primary discovery tool in human genetics. It is based on highly parallel DNA sequencing, which produces many hundreds of thousands or millions of short reads for low cost and in a short time (Metzker, 2010; Shendure

and Ji, 2008). Initially, the term arose to describe the first sequencing technologies that took alternative approaches to Sanger sequencing to determine the DNA nucleotide order (Sanger et al., 1977).

NGS is a successful strategy for mutation detection in rare monogenic diseases, often referred to as orphan diseases (Boycott et al., 2013). Although the individual diseases are rare (defined as affecting less than 200,000 people in the USA or fewer than 1 in 2,000 people in Europe), they are collectively common, affecting millions of individuals worldwide (Carter, 1977). It is estimated that as many as 5,000 to 7,000 distinct diseases exist and as much as 6% to 8% of the population of the European Union is affected by one (European Organisation for Rare Diseases, 2005). NGS overcomes problems of traditional gene discovery approaches in rare diseases like locus heterogeneity and the availability of only a small number of patients or families to study. Both genome and exome sequencing are powerful approaches for identifying genetic variation within an individual. However, as a consequence of the breadth and complexity of genome sequencing, exome sequencing is currently the more prevalent platform for the discovery of genes associated with rare diseases (Boycott et al., 2013). Exome sequencing is the term used to describe the targeted enrichment and sequencing of the approximately 1% protein-coding portion of the human genome (the "exome"). The technique was widely adopted and used to detect new disease genes in recessive (Ng et al., 2010) and dominant disorders (Ng et al., 2009). Over the last years, the number of identified rare-disease-causing variants by means of exome sequencing has increased rapidly (Boycott et al., 2013).

Hereditary phosphate balance disorders also belong to the group of rare diseases. There is convincing evidence that part of the hypo- and hyperphosphatemic disorders cannot be explained by mutations in the known genes associated with the regulation of phosphate homeostasis. In the "Institute of Human Genetics (IHG), Helmholtz Zentrum München" (Munich, Germany), a patient population of approximately 260 families with phosphate balance disorders is available. Thereof, no causative mutation has been identified in about 50 index cases up to now. Here, exome sequencing may be a helpful strategy in the gene discovery process.

1.4.2. Mouse Models for Metabolic Bone Disease and Abnormalities in Skeletal Development

In addition to the identification of novel candidate genes associated with human hereditary phosphate balance disorders, animal models may help to understand the molecular mechanisms responsible for imbalances in phosphate regulation in disturbed bone development, mineralisation and turnover. Metabolic bone disease is a collective term referring to bone disorders caused by a broad spectrum of abnormalities of minerals (such as phosphate and calcium), endocrine functions, bone mass or bone structure (Horvai and Boyce, 2011; Reuss-Borst, 2014). Serum inorganic phosphate (Pi) is routinely used combined with total calcium (Ca) and alkaline phosphatase (ALP) activity as a marker to identify early stages in metabolic bone disease (Backstrom et al., 2000; Duursma et al., 1974; Sabrautzki et al., 2012).

Mice have already been shown to successfully serve as model organism to study defects of bone mineralisation (Eicher et al., 1976; Farrow et al., 2011b; Feng et al., 2008; Sabrautzki et al., 2012). Random N-ethyl-N-nitrosourea (ENU) mutagenesis is a promising approach to obtain mouse models for hereditary human diseases (Hrabe de Angelis and Balling, 1998). Within the Munich ENU Mutagenesis Project, a genome-wide large-scale screen of mutant mice was performed at the "Institute of Experimental Genetics (IEG), Helmholtz Zentrum München" (Munich, Germany) (Hrabe de Angelis et al., 2000). 190 phenodeviants of 9,540 first generation (G1) animals showed alterations in at least one of the three parameters of interest (Pi, Ca and ALP) in two repeated blood measurements and were mated to wild-type C3HeB/FeJ mice in test breeding (Fuchs et al., 2012; Sabrautzki et al., 2012). On the basis of published mutation rates for ENU mutagenesis (Takahasi et al., 2007), it was estimated that each of the G1 animals would carry approximately one *de novo* single nucleotide variant (SNV) per Mb (Andrews et al., 2012; Bull et al., 2013). Considering classical formal genetics, in each generation 50% of the SNVs are lost and only the mutation for which the specific phenotype continues to be selected is maintained in the cohort (Balling, 2001). Based on the backcrossing strategy with consecutive mating of mutant with wild-type mice, it may be calculated that mice born after five generations should carry approximately 97% of the recipient genome and only the mutation of interest (Keays et al., 2006).

However, these mouse mutants with alterations in bone metabolism and skeletal development are not maximally useful to study the regulation of phosphate homeostasis until the

underlying mutation of interest is identified. Until recently, the bottleneck of the ENU approach has been in identifying a single disease-causing mutation in an entire genome (Fairfield et al., 2011). The gene discovery process in mice has been greatly hindered by the time and expense incurred by phenotype-based candidate gene approaches including high-resolution genetic mapping (Sabrautzki et al., 2012). Now, the widespread availability of massively parallel DNA sequencing strategies has brought about a paradigm shift in forward genetics by closing the gap between genotype and phenotype (Bamshad et al., 2011; Shendure and Ji, 2008). In initial mouse studies, we and other groups started to use NGS data to identify ENU-induced mutations by sequencing whole chromosomes (Sabrautzki et al., 2013) or BAC libraries (Boles et al., 2009; Zhang et al., 2009). Arnold et al. applied genome sequencing to detect putative mutations and, following this, they performed extensive validation by Sanger sequencing and genetic mapping (Arnold et al., 2011). Yabas et al. mapped a novel ENU mutation to a region of the X-chromosome and identified the mutation by oligonucleotide bait-mediated capture and deep sequencing of exonic DNA fragments within this region (Yabas et al., 2011). Most of the approaches turned out to be time-consuming and material-intensive. Finally, Fairfield et al. demonstrated that exome sequencing is a novel robust approach for discovery of both homozygous and heterozygous ENU-induced mutations (Fairfield et al., 2011).

1.4.3. Small-Molecule Regulators of FGF23 Signalling

Furthermore, it might be useful to investigate FGF23 as the major regulator of systemic phosphate turnover in a functional approach to unravel its molecular mode of action. Most notably, within the last decade, high-throughput screening (HTS) of small-molecule compounds (typically organic compounds with a molecular weight under ~ 900 Da) has been evaluated as a suitable experimental tool to define complex cellular processes and to identify new biological targets (Eggert, 2013; Hughes et al., 2011). In pharmaceutical research and development, this approach has revolutionised the identification of first-in-class molecules in the drug discovery process (Bickle, 2010; Macarron et al., 2011; Swinney and Anthony, 2011). Examples of approved drugs with origins in HTS hits are Gefitinib, Erlotinib and Lepatinib, which were identified as tyrosine kinase inhibitors with indication for patients suffering from cancer (Wunder et al., 2008).

The “Assay Development and Screening Platform (ADSP), Helmholtz Zentrum München” (Munich, Germany), which was established in 2010, is a central unit to move projects from

basic research to lead molecules. With searching for small molecules, it is finally intended to detect novel methodologies for the treatment of diseases and to identify novel tool compounds for understanding biological questions. The so-called "Helmholtz Zentrum München Library" contains 30,000 diverse small-molecule compounds from different providers. The aim is to rather use this smaller set of compounds to investigate complex biological processes than to compete with pharmaceutical companies by performing classical target assays and analysing enormous numbers of small-molecule compounds (Schorpp and Hadian, 2014).

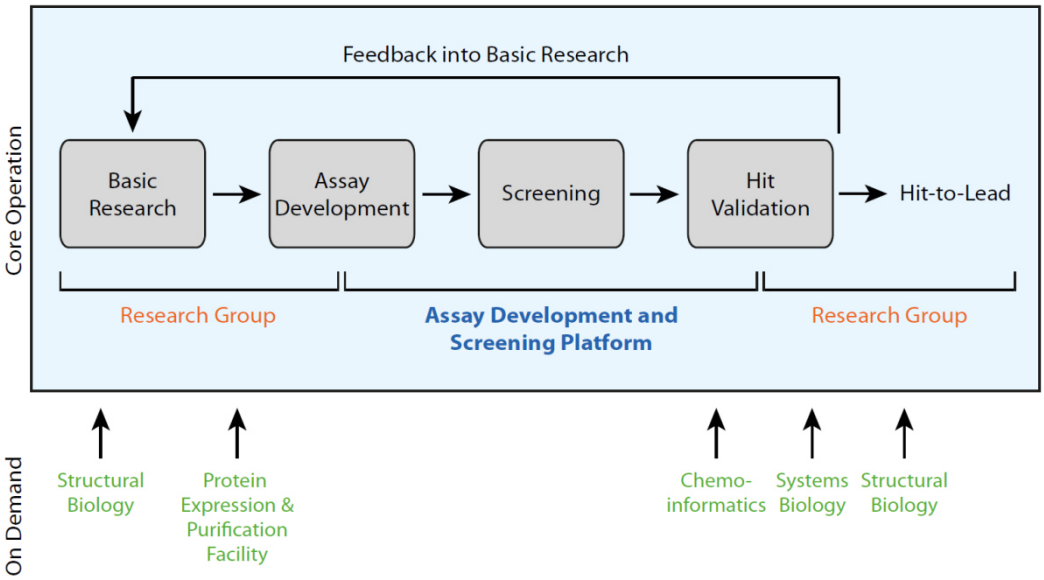

Figure 7: From basic research to hit validation using small-molecule compound screens. Basic research and assay development is conducted at the research group in close cooperation with ADSP. Once the assay is established, the small-molecule compound screening is performed at ADSP. Thereafter, the project goes back to the research group for further investigation (Schorpp and Hadian, 2014).

As explicated in Figure 7, project ideas originate from basic research groups. After assay development in close cooperation with ADSP, the small-molecule compound screening is performed at ADSP using the different liquid handling working stations and instrumentations. The project returns to the research group after the hit validation phase. Further investigation for hit-to-lead transition is done by selecting promising hits with the help of chemoinformatics, system biology and structural biology groups at the research centre. Validated hits will then be further used to verify project hypotheses of basic research, to analyse specific research questions and to develop hit compounds into lead molecules (Schorpp and Hadian, 2014).

In the context of phosphate homeostasis, the identification of small-molecule compounds that modulate FGF23 signalling could help to improve the understanding of principal molecular mechanisms of phosphate balance in the body by using them as tools to study the second messenger pathway after binding of FGF23 to FGFR1c/Klotho and to detect possible novel target genes of FGF23 signalling. Moreover, nominated candidate hits interacting with FGF23 signalling would provide the basis to manipulate this pathway and would potentially validate this pathway as druggable.

1.5. AIM OF THE STUDY

Phosphate homeostasis is controlled by a complex system mainly based on an endocrine cross-organ communication between bone and kidney with FGF23 as a primary regulator of extracellular phosphate concentration. To close gaps in understanding molecular regulatory mechanisms, the three abovementioned approaches should be used in this thesis as follows:

- Human phosphate balance disorders: Given the finding that in approximately 50 index cases of the DNA collection of patients with hypo- and hyperphosphatemic disorders available at IHG no causative mutations could be identified in the coding regions of the known disease genes, it is tempting to speculate that additional genes contribute to the regulatory events of phosphate homeostasis. Novel genes should be identified by exome sequencing.
- Mouse models: Exome sequencing should be applied as a novel approach for mutation discovery in 18 ENU-derived mouse models with changes in metabolism and development of bone showing alterations in serum levels of Pi, Ca and/or ALP activity.
- Small-molecule compound screening: Small-molecule compounds which affect FGF23/FGFR1c/Klotho signalling should be identified. For this, an FGF23-inducible cell model will be developed. On the basis of this cell model, reporter assays suited for HTS will be established. In a pilot screen, robustness of the screening strategy should be verified and first candidate hits should be nominated.

2. MATERIAL AND METHODS

2.1.MATERIAL

2.1.1. Nucleic Acids

2.1.1.1. DNA

DNA samples of patients with hypo- and hyperphosphatemic disorders belong to the DNA collection of IHG (Helmholtz Zentrum München, Munich, Germany). For all samples, informed consent was obtained. DNA samples of ENU-derived mutant mice as well as wild-type mice of different inbred strains were provided by IEG (Helmholtz Zentrum München, Munich, Germany).

2.1.1.2. RNA

For semiquantitative multiplex RT-PCR (section 2.2.1.2), total RNA was extracted from murine calvaria and femur using Trizol reagent (Life Technologies, Carlsbad, CA, USA) following the manufacturer's instructions. For RNA-Seq (section 2.2.2.3), total RNA was extracted from eukaryotic cells with the RNeasy Plus Mini kit from Qiagen (Hilden, Germany) as recommended by the manufacturer.

2.1.1.3. cDNA

Mouse Marathon-Ready cDNAs from different tissues (mouse embryo 17 d, liver, kidney and heart) were purchased from Clontech Laboratories (Mountain View, CA, USA).

2.1.2. Oligonucleotides

Primer sequences were determined with the ExonPrimer software (http://ihg.helmholtz-muenchen.de/ihg/ExonPrimer.html). All oligonucleotides used in the PCR reactions were synthesised by the manufacturer Metabion (Martinsried, Germany).

Standard PCR and Sanger sequencing

Alb_ex6_F	5'-AAACTTTGGGAGGTGTGTGTG-3'

Alb_ex6_R	5'-TCAACAGAAAGATGCGAACTG-3'
Alb_ex7_F	5'-AATTGGCAACAGACCTGACC-3'
Alb_ex7_R	5'-AAACACAGGCGCTCAACTG-3'
Ednra_ex2_F	5'-CACATCAGAGCAAGCGTCAG-3'
Ednra_ex2_R	5'-AGTGTATGAGGAACGGCCC-3'
Ero1l_ex6_F	5'-TGCACACTTTCACAAACGTC-3'
Ero1l_ex6_R	5'-AACTGGGAAAGAGAATAATGCAG-3'
Fam46a_ex2_F	5'-CGGGCAAGAAGTCTAACAGG-3'
Fam46a_ex2_R	5'-TGGCCTAGGCTACAAGGACC-3'
Ftl1_ex2_F	5'-ACATGCTCGGTAGTGCCC-3'
Ftl1_ex2_R	5'-TGTCTGACTGGAACTCGCTG-3'
Mmp20_ex8_F	5'-GCAACGAATAGATGCTGCTG-3'
Mmp20_ex8_R	5'-GCAGGCTTATTGTTAAGTAGCTTGTC-3'
Myst4_ex5_F	5'-TCTGTTGTATTACAGGATAACATGC-3'
Myst4_ex5_R	5'-CACCTGCACTCCCAGCTC-3'
Satb2_ex6_F	5'-TCCTAATACTTATTTACAACCCTTCC-3'
Satb2_ex6_R	5'-GCAACCAAGTGCCAGGAG-3'
Scube3_ex8_F	5'-CAGATATAGACGAGTGCCGC-3'
Scube3_ex8_R	5'-CAGCTCCTTTCGTTGATGAG-3'
Sik3_ex6_F	5'-GGGAGCACACTGCAGAATC-3'
Sik3_ex6_R	5'-TACTCCACATGCCTGCCTC-3'
Sipa1_ex17_F	5'-GTCAGGCTCTCTCCTCACCC-3'
Sipa1_ex17_R	5'-CACTGCTTCCGCTGAGTTC-3'
Sulf1_ex22_F	5'-GGATGGGAAGGTTAGTCAGTCC-3'
Sulf1_ex22_R	5'-GCCCTCAGGTAGTTAGTCCAG-3'
Trp63_ex6_F	5'-AGACAGCTTCTTAGGCCACC-3'
Trp63_ex6_R	5'-CGGTGATAAATGCTAGATCCC-3'
Ryr1_ex91_F	5'-GTCCTCGTCCTCCTCCG-3'
Ryr1_ex91_R	5'-TCATCTTCGACGTGGTGAAC-3'

RT-PCR

Fam46a_Cex2_F1	5'-CTACAAGGACCTGGACCTCATC-3'
Fam46a_Cex3_R1	5'-TCTACACTGAATTCAAACTGCCTC-3'

2.1.3. FGFs

Recombinant human basic FGF (AA 1 - 157; hereafter named "bFGF") was purchased from R&D Systems (Minneapolis, MN, USA). It was *E. coli*-derived with a predicted molecular mass of 17 kDa and a purity of > 97%. Recombinant human FGF23 (R179Q mutant; in the following named "FGF23R179Q") was purchased from Adipogen (Liestal, Switzerland). It was expressed in genetically modified human embryonic kidney cells (HEK293). FGF23 (AA 1 - 251) was fused at the C-terminus to a His-tag. It showed a purity of > 90% with a predicted molecular mass of 32 kDa. Moreover, we decided to produce the same recombinant human FGF23R179Q protein together with Proteros (Martinsried, Germany) by means of an in-house generated HEK293 cell line stably expressing FGF23R179Q. The purity was again > 90%.

2.1.4. Antibodies

anti-Klotho polyclonal goat Ab	Santa Cruz Biotechnology, Dallas, TX, USA
anti-EGR1 monoclonal mouse Ab	Santa Cruz Biotechnology, Dallas, TX, USA
anti-ERK1/2 monoclonal rabbit Ab	Cell Signaling Technology, Danvers, MA, USA
anti-p-ERK1/2 monoclonal rabbit Ab	Cell Signaling Technology, Danvers, MA, USA
anti-His(C-term) HRP-linked Ab	Life Technologies, Carlsbad, CA, USA
anti-goat HRP-linked Ab	Cell Signaling Technology, Danvers, MA, USA
anti-mouse HRP-linked Ab	Cell Signaling Technology, Danvers, MA, USA
anti-rabbit HRP-linked Ab	Cell Signaling Technology, Danvers, MA, USA

2.1.5. Cell Lines

Human embryonic kidney cells (HEK293) were provided by "Deutsches Krebsforschungszentrum (DKFZ)" (Heidelberg, Germany).

2.1.6. Chemicals and Solutions

Unless otherwise stated, chemicals and solutions were purchased from Merck (Darmstadt, Germany) or Sigma-Aldrich (St. Louis, MO, USA).

2.2.METHODS

2.2.1. PCR

2.2.1.1. Standard PCR

Polymerase chain reaction (PCR) was used to amplify DNA sequences. Negative controls were always used and positive controls if required. For 30 - 50 ng genomic DNA template, the reaction mixture (25 µl) consisted of premixed, ready-to-use Promega PCR Master Mix solution containing *Taq* DNA polymerase, dNTPs, $MgCl_2$ and reaction buffers (Promega, Madison, WI, USA) as well as 10 pmol of both forward and reverse primer (listed in section 2.1.2). PCR was performed in a thermal cycler (PeqStar; PeqLab Biotechnology, Erlangen, Germany) with the following conditions (touchdown PCR): 95 °C for 5 min; 95 °C for 30 s, 65 °C for 30 s, 72 °C for 30 s, -1 °C for each of the next 7 cycles; 95 °C for 30 s, 58 °C for 30 s, 72 °C for 30 s during 25 cycles and a final extension of 72 °C for 3 min. The size of the obtained PCR products was determined by agarose gel electrophoresis (section 2.2.1.3).

2.2.1.2. Semiquantitative Multiplex RT-PCR

In gene expression analysis, semiquantitative multiplex reverse transcription (RT)-PCR can be utilised not only to detect specific mRNAs but also to evaluate their expression levels by comparing the expression levels of a housekeeping gene with a specific gene in the same PCR reaction (multiplex). First-strand cDNA was synthesised from total RNA (500 ng) using the SuperScript III First-strand Synthesis SuperMix (Life Technologies, Carlsbad, CA, USA) according to the manufacturer's protocols. First-strand cDNA (1 µl) was used as template to perform a multiplex PCR (25 µl) with the Advantage cDNA PCR kit (Clontech Laboratories, Mountain View, CA, USA) by use of the following touchdown PCR conditions: 94 °C for 1 min; 94 °C for 30 s, 65 °C for 30 s, 68 °C for 1 min, -1 °C for each of the next 7 cycles; 94 °C for 30 s, 58 °C for 30 s, 68 °C for 1 min during 25 cycles and a final extension of 68 °C for 5 min. Primers used are listed in section 2.1.2.

2.2.1.3. Agarose Gel Electrophoresis

Electrophoresis through 0.7 - 1.5% horizontal agarose gels (depending on the size of the expected DNA fragment) was used to separate and identify DNA fragments. Gels were prepared by dissolving agarose (Biozym DNA Agarose; Biozym Scientific, Oldendorf, Germany) in 1x TBE buffer (840 mM Tris, 900 mM boric acid, 20 mM EDTA, dH_2O up to

1 l, pH 8). The fluorescent dye Serva DNA Stain Clear G (Serva Electrophoresis, Heidelberg, Germany), which binds to DNA, was added to the solution. It can be visualised, when excited by UV light under a 300 nm UV light transilluminator (UVT-40M; Herolab, Wiesloch, Germany). PCR products were mixed with gel loading buffer (0.05% (w/v) Orange G in 25% (w/v) Ficoll) and loaded onto the gel. 1x TBE was used as the running buffer. The electrophoresis was carried out at a voltage of 120 V for about 30 min. To interpret the results, a DNA 1 kb DNA ladder (Life Technologies, Carlsbad, CA, USA) was utilised.

2.2.2. Sequencing

2.2.2.1. Sanger Sequencing

PCR products were cleaned through Millipore PCR Cleanup filter plates (Merck, Darmstadt, Germany). Bidirectional Sanger sequencing was performed in a capillary-based automated sequencer (ABI 3730 Genetic Analyzer; Life Technologies, Carlsbad, CA, USA) subsequent to a cycle sequencing reaction using the ABI BigDye Terminator v.3.1 Cycle Sequencing kit (Life Technologies, Carlsbad, CA, USA). 1 µl of the purified PCR product was mixed with 0.5 µl BigDye Terminator v.3.1 Ready Reaction mix, 1 µl sequencing buffer (5x), 1 µl primer (10 pmol/µl; forward or reverse) and dH_20 up to a final volume of 5 µl. The protocol included following conditions: 96 °C for 1 min; 96 °C for 10 s, 50 °C for 5 s, 60 °C for 1 min 30 s during 25 cycles. Primer sequences are listed in section 2.1.2. After cycle sequencing reaction, the DNA was precipitated in 100% ethanol, incubated for 10 min and centrifuged (3,000 x g, 30 min, RT). The pellet was washed in 70% ethanol and centrifuged (2,000 x g, 15 min, RT). Afterwards, the DNA pellet was dried at RT in the dark and dissolved in DHPLC-H_2O (LiChrosolv; Merck, Darmstadt, Germany). Dissolved DNA was transferred onto a microtiter plate, which was placed into the automated ABI 3730 sequencer. The resulting data were collected and analysed using Staden Package (http://staden.sourceforge.net).

2.2.2.2. Exome Sequencing

In-solution targeted enrichment of exonic sequences from human DNA samples was performed using the Agilent SureSelect XT Human All Exon 50 Mb kit. For mouse DNA samples, the Agilent SureSelect XT Mouse All Exon kit was applied. Both kits were purchased from Agilent Technologies (Santa Clara, CA, USA) and utilised as recommended by the manufacturer.

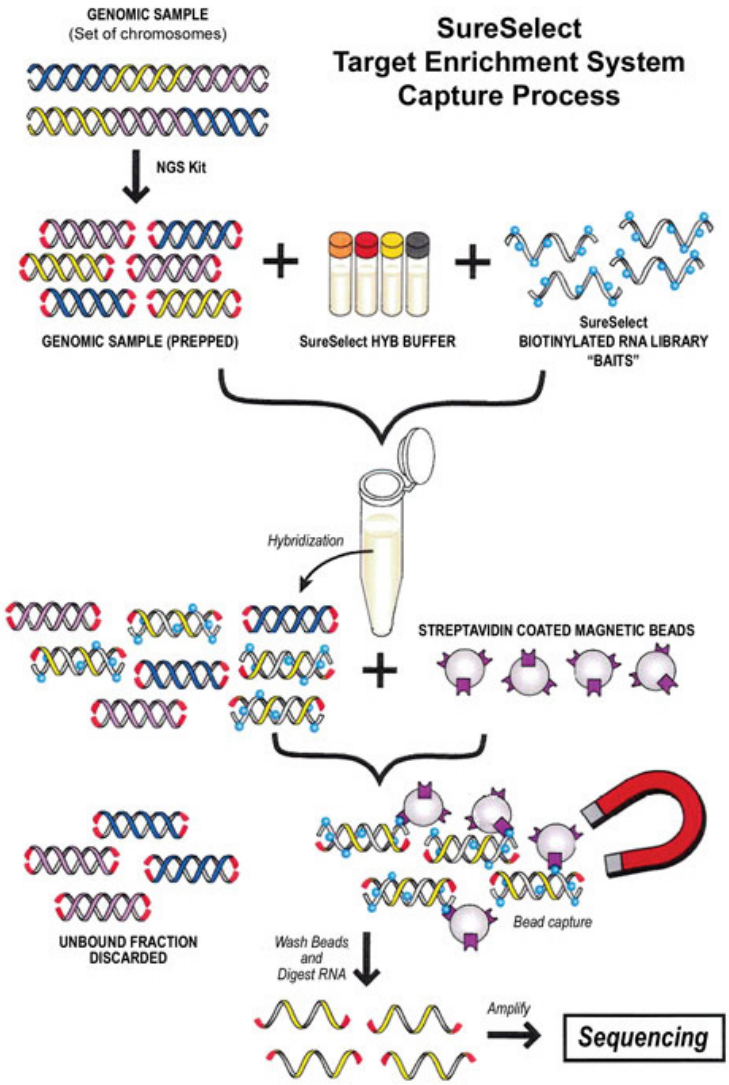

Figure 8: SureSelect target enrichment system capture process. Genomic library is mixed in solution with capture probes. Specific probes bind complementary exomic sequences and are captured via magnetic beads. Available at: www.agilent.com.

Starting with 3 µg of high quality genomic DNA, samples were sheared to generate small DNA fragments with a base pair peak of 150 to 200 bp. Shearing was achieved with the Covaris E220 focused-ultrasonicator (Covaris, Woburn, MA, USA). This system works by sending acoustic energy wave packets to shear DNA in a highly controlled manner. After DNA shearing, libraries were prepared following the Illumina Paired-End Sequencing Library protocol based on the addition of Illumina compatible adapters and indices. Processes were automated by use of the Bravo and Bravo BenchCel 4 R liquid handling platform of Agilent Technologies (Santa Clara, CA, USA). Genomic libraries were mixed in solution with an excess of 120 bp long, biotinylated RNA oligonucleotides, termed probes or baits, which are complementary in sequence to the targeted exons. These RNA baits annealed to their targets

and were pulled down with streptavidin-coated magnetic beads. The caught sequences were then PCR-amplified with universal primers. At the end, quality and quantity was assessed on an Agilent 2100 Bioanalyzer with the Agilent DNA 1000 kit (Agilent Technologies, Santa Clara, CA, USA), and the samples were subjugated to clustering and sequencing as 100 bp paired-end runs on a HiSeq2000 system (Illumina, San Diego, CA, USA). The workflow is visualised by Figure 8.

2.2.2.3. RNA-Seq

Indexed paired-end libraries of mRNA from cells were prepared with the Illumina TruSeq RNA Sample Preparation kit according to manufacturer's instructions. Initially, total RNA was quantified on an Agilent 2100 Bioanalyzer with the Agilent 6000 Nano kit (Agilent Technologies, Santa Clara, CA, USA), and RNA integrity was confirmed as all samples had an RNA integrity number (RIN) of 10.

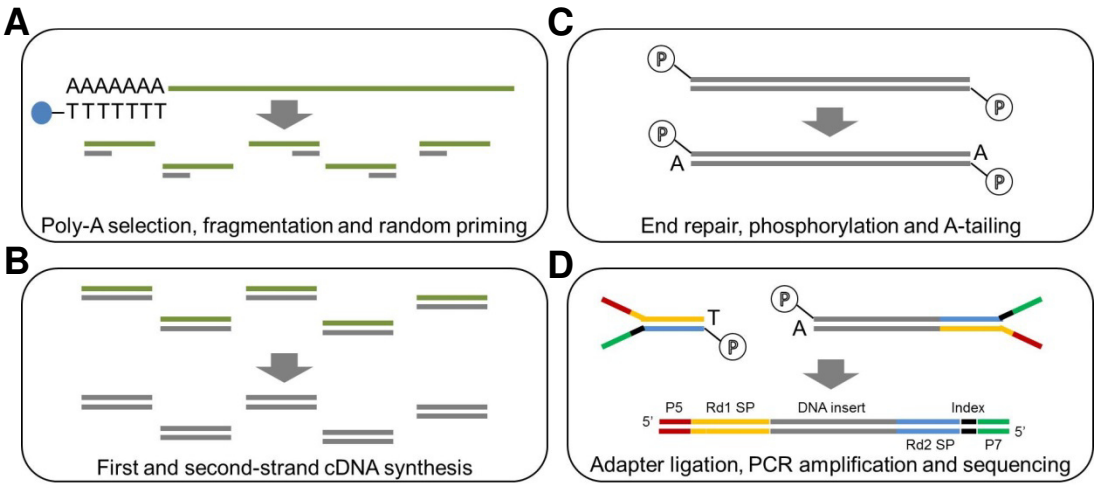

Figure 9: Illumina TruSeq RNA sample preparation. (A) Library preparation begins with 1 µg of high quality total RNA, which is poly-A selected with magnetic beads. Double-stranded cDNA (B) is phosphorylated and A-tailed (C) ready for adapter ligation. The library is PCR-amplified (D) and ready for clustering and sequencing. P5 and P7 are primers used for PCR amplification. Rd1 SP and Rd2 SP are sequencing primers. Figure modified from: bitesizebio.com/13542/what-everyone-should-know-about-rna-seq.

Starting with 1 µg of high quality RNA, the first step in the workflow involved isolation of the poly-A containing mRNA molecules with poly-T oligo-attached magnetic beads. Following purification, the mRNA was fragmented into small pieces using divalent cations under elevated temperature (Figure 9 A). The cleaved RNA fragments were copied into first-strand cDNA by the use of reverse transcriptase and random primers. Strand specificity was achieved by replacing TTP with UTP in the Second Strand Marking Mix (SMM), followed by

second-strand cDNA synthesis using DNA Polymerase I and RNase H. The incorporation of dUTP in second-strand synthesis efficiently quenches the second strand during amplification, because the polymerase used in the assay will not incorporate past this nucleotide (Figure 9 B). Afterwards, overhangs of the double-stranded (ds) cDNA fragments resulting from fragmentation were converted into 5'-phosphorylated blunt ends by end repair and single "A" nucleotides were added to the 3' ends (Figure 9 C). Subsequently, indexing-specific paired-end adapters were ligated to the ends of the ds cDNA fragments. The products were then purified and enriched with PCR to create the final cDNA libraries (Figure 9 D). Another time, quality and quantity were assessed on an Agilent 2100 Bioanalyzer with the Agilent DNA 1000 kit (Agilent Technologies, Santa Clara, CA, USA). Libraries were clustered and sequenced on a HiSeq2000 system (Illumina, San Diego, CA, USA).

2.2.3. Molecular Cloning

2.2.3.1. DNA Cloning and Transformation

Full-length human *KLOTHO* cDNA (3,056 bp) was previously cloned into a pcDNA3.1/*myc*-His(-) B vector in frame with a *myc* and 6x His tag (5,520 bp; Life Technologies, Carlsbad, CA, USA) by GenScript (Piscataway, NJ, USA). A scheme of the vector is shown in the figure below:

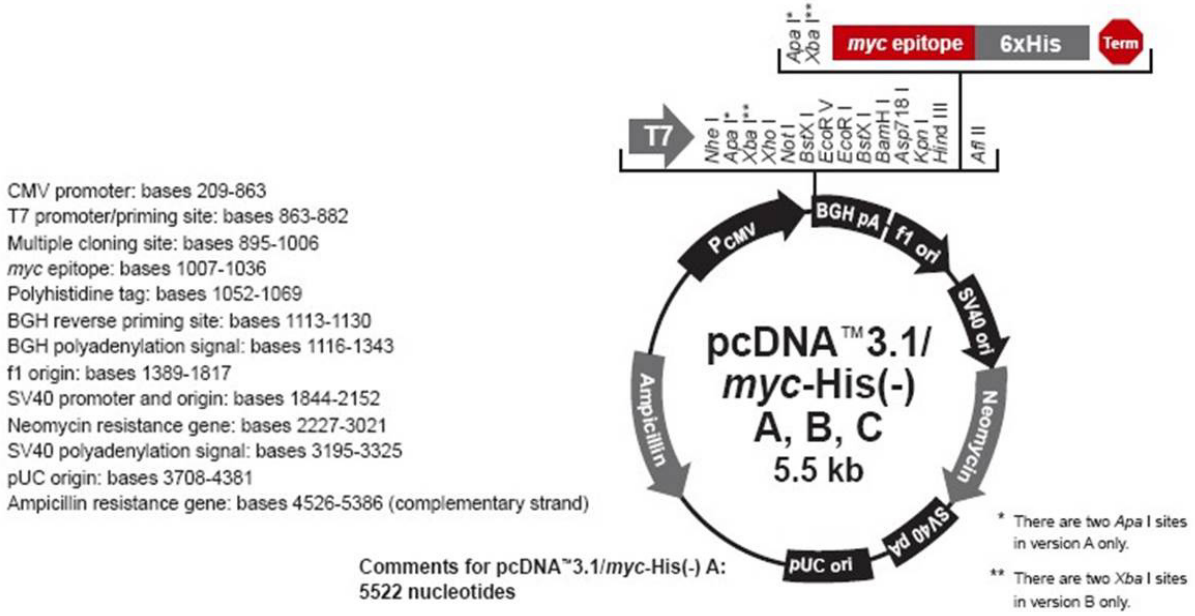

Figure 10: Features of the pcDNA3.1/*myc*-His(-) vector. Figure available at: http://www.lifetechnologies.com.

Plasmid DNA was transformed into XL10-Gold ultracompetent cells (Stratagene, La Jolla, CA, USA) according to manufacturer's instructions.

2.2.3.2. Plasmid DNA Preparation

For transfection, preparations of plasmid DNA were performed using the EndoFree Plasmid Purification kit (Qiagen, Hilden, Germany) as recommended by the manufacturer. Plasmid DNA concentration and purity were determined using the Nano Drop 2000 spectrophotometer (PeqLab Biotechnology, Erlangen, Germany).

2.2.3.3. Restriction Digest

In order to check plasmid DNA, 0.5 µl of plasmid DNA were incubated at 37 °C for 1 h using 1 µl of both XbaI and BamHI restriction enzymes and 2.5 µl of the recommended Tango restriction buffer (Thermo Fisher Scientific, Waltham, MA, USA). The final volume was 25 µl. Restriction digests were incubated using a thermomixer (Eppendorf, Hamburg, Germany). Product sizes were determined via agarose gel electrophoresis (see section 2.2.1.3).

2.2.4. Cell Culture

2.2.4.1. Cell Culture of Adherent Cells

Adherent HEK293 cells were maintained in DMEM growth medium containing 4.5 g/l D-glucose, L-glutamine and pyruvate. 10% foetal bovine serum (FBS) and PenStrep (5,000 U/ml penicillin and 5,000 µg/ml streptomycin) were added. All reagents were purchased from Life Technologies (Carlsbad, CA, USA). The cells were kept in 75 cm^2 (15 ml) or 175 cm^2 (25 ml) cell culture flasks (Greiner bio-one, Frickenhausen, Germany) suitable for adherent cell culture and incubated at 37 °C, 90% humidity and 5% CO_2 in a cell culture incubator (Sanyo, Watford, UK). According to cellular growth and use of the cells, they were passaged once or twice a week. HEK293 cells were detached from the culture vessel at 80 - 90% confluency using 0.05% Trypsin/EDTA (GE Healthcare, Chalfont St. Giles, UK). After detachment, cells were resuspended in the respective culture medium and passaged 1:5 or 1:10.

2.2.4.2. Stable Transfection of Adherent Cells

HEK293 cells were stably transfected with the expression plasmid pcDNA3.1/*KLOTHO*/*myc*-His (see section 2.2.3.1) using the PolyFect transfection reagent

from Qiagen (Hilden, Germany), which is a solution of specifically designed activated-dendrimers. PolyFect reagent assembles DNA into compact structures that bind to the cell surface and are taken into the cell by non-specific endocytosis. The reagent buffers the pH of the endosome leading to pH inhibition of endosomal nucleases, which ensures stability of PolyFect-DNA complexes. Transfection was conducted according to the manufacturer's instructions. After transfection, cells were incubated for 48 h to allow for gene expression. Selection of successfully transfected cells was started by the use of Geneticin (G418 sulphate) solution (Carl Roth, Karlsruhe, Germany). Resistance to Geneticin is conferred by the Neomycin resistance gene of the pcDNA3.1/*myc*-His(-) B vector (Figure 10).

Figure 11: Stable transfection of HEK293 cells. 48 h after transfection, selection of successfully transfected cells was started by the use of 1,000 µg/ml of Geneticin (G418 sulphate). Medium was changed every two to three days. Non-transfected cells died. After four weeks, cell colonies were picked and cell clones were expanded. The concentration of Geneticin was reduced to 100 µg/ml.

Stable transfectants were selected over a time period of four weeks for the resistance to Geneticin. Cell clones were picked and expanded. Within the next four weeks, the starting concentration of Geneticin (1,000 µg/ml) was slowly reduced to 100 µg/ml. HEK293 cells that stably expressed Klotho were named "HEK293-KL" cells.

2.2.4.3. Induction Experiments

For protein analysis, non-transfected and transfected HEK293 cells were plated at 1.2 x 10^6 cells per 6-well plate (BD, Franklin Lakes, NJ, USA) and treated when ~ 70% confluent with bFGF (10 ng/ml) and FGF23R179Q (0 - 100 ng/ml) (section 2.1.3), respectively, for 20 min or overnight in a cell culture incubator. Then, cell lysates were prepared (section 2.2.4.5). For RNA-Seq, cells were plated at 3.5 x 10^6 cells per 100 mm dish (Thermo Fisher Scientific, Waltham, MA, USA) and induced when ~ 70% confluent with FGF23R179Q (100 ng/ml) in a cell culture incubator for 1 h. RNA was isolated as described in section 2.1.1.2.

2.2.4.4. Treatment with Inhibitors

The inhibitors SU5402 (3-[3-(2-carboxyethyl)-4-methylpyrrol-2-methylidenyl]-2-indolinone) and U0126 (1,4-diamino-2,3-dicyano-1,4-bis(2-aminophenylthio)butadiene) were purchased from Merck (Darmstadt, Germany). HEK293-KL cells were plated at 1.2 x 10^6 cells per 6-well plate and treated when ~ 70% confluent. Cells were incubated with SU5402 (65 nM and 40 µM) or U0126 (100 nM and 10 µM) in serum-free medium in a cell culture incubator for 1 h and were then stimulated with bFGF (10 ng/ml) or FGF23R179Q (100 ng/ml) for 20 min.

2.2.4.5. Preparation of Cell Lysates

Adherent cells were lysed using lysis buffer (30 mM Tris, pH 7.4, 150 mM NaCl), which contained protease (Complete, Roche, Mannheim, Germany) and phosphatase inhibitor cocktails (PhosStop, Roche, Mannheim, Germany). All steps were performed on ice. Medium was removed from the cells, 100 µl of lysis buffer per well of a 6-well plate was added and incubated with gentle agitation for 5 min. Using a cell scraper (Sarstedt, Nümbrecht, Germany), cell suspension was transferred into 1.5 ml microcentrifuge tubes (Eppendorf, Hamburg, Germany) and homogenised by thorough mixing with a vortexer (Scientific Industries, New York City, NY, USA) every 10 min for three times. The resulting homogenate was centrifuged (10,000 x g, 10 min, 4 °C). This separated the total protein (supernatant) from cellular debris (pellet). The supernatant was transferred into new tubes and processed for further analysis or stored at -80 °C for long-term storage.

2.2.5. Western Blot

Western blot is a widely used analytical technique to detect specific proteins in cell lysates.

2.2.5.1. Measuring Protein Concentrations after Bradford

The concentration of proteins in cell lysates can be quantified by the Bradford method (Bradford, 1976). It is a dye-binding assay based on the differential colour change of the dye Coomassie Brilliant Blue G-250 in response to various concentrations of protein. When binding to protein occurs, the dye stabilises from a doubly-protonated red form to an unprotonated blue form. The maximum absorbance of the acidic solution of Coomassie Brilliant Blue G-250 shifts from 465 nm to 595 nm. Quick Start Bradford protein assay kit (Bio-Rad Laboratories, Hercules, CA, USA) was used following the manufacturer's

instructions. Absorbance was measured at 595 nm. A regression curve with a protein standard (BSA, 0.125 - 2 mg/ml) was set up to help the quantification of the results.

2.2.5.2. SDS-PAGE

Sodium dodecyl sulphate polyacrylamide gel electrophoresis (SDS-PAGE) was performed as a vertical flat-bed electrophoresis in a discontinuous buffer system. Proteins were separated dependent on their size through presence of SDS forming SDS-protein-micelles with constant negative charge per mass unit (1.4 g SDS per 1 g protein). Precast gels (with gradient (4 - 20%) or without gradient (10%)) were used in the Mini-PROTEAN Tetra Cell system (Bio-Rad Laboratories, Hercules, CA, USA). Samples were diluted in 2x Laemmli sample buffer (Bio-Rad Laboratories, Hercules, CA, USA) and heated at 95 °C for 3 min. Gels were run in SDS-running buffer (25 mM Tris, pH 8.3, 192 mM glycine, 0.1% (w/v) SDS) with constant current of 120 mA for approximately 2 h. As a standard, a ready-to-use protein molecular weight marker (Precision Plus Protein Dual Color standard, Bio-Rad Laboratories, Hercules, CA, USA) was applied.

2.2.5.3. Protein Blotting

Proteins were eluted through the electrical field perpendicular to the gel and immobilised on a polyvinylidene difluoride (PVDF) membrane (0.45 µm pore size, Immobilon-P; Millipore, Billerica, MA, USA). First of all, the PVDF membrane was rinsed in methanol, equilibrated in ice-cold transfer buffer (20% (v/v) methanol, 20 mM Tris, pH 8.3, 150 mM glycine) and set on the protein gel in between two 3MM Whatman paper (GE Healthcare, Chalfont St. Giles, UK). Proteins were blotted in the cooled Mini Trans-Blot cell system (Bio-Rad Laboratories, Hercules, CA, USA) with ice-cold transfer buffer at a constant voltage of 80 V for 2 h.

2.2.5.4. Ponceau S Staining

To confirm the uniformity and overall effectiveness of the transfer of proteins from the gel to the membrane, the entire area of the PVDF membranes were stained with the removable dye Ponceau S. Membranes were incubated in a Ponceau S staining solution (0.5 g Ponceau S, 1% (v/v) acetic acid in dH_2O) for 3 min followed by 5 min fading in fading solution (10% (v/v) acetic acid, 50% (v/v) methanol in dH_2O).

2.2.5.5. Immunodetection

Proteins covalently bonded to PVDF membranes can be detected with the help of antibodies. Membranes were pre-wetted in methanol and equilibrated in Tris-buffered saline and Tween 20 (TBST; 10 mM Tris, 150 mM sodium chloride, 0.05% (v/v) Tween 20) for 5 min. Unreacted binding sites of the membranes were blocked in 1x Roti-Block reagent (Carl Roth, Karlsruhe, Germany) at RT for 1 h with agitation to suppress non-specific adsorption of antibodies. After washing with TBST (1 x 15 min and 2 x 5 min), membranes were incubated with specific primary antibodies under different conditions:

anti-Klotho polyclonal goat Ab	working dilution 1:200; RT, 1 h
anti-EGR1 monoclonal mouse Ab	working dilution 1:400; RT; 1 h
anti-ERK1/2 monoclonal rabbit Ab	working dilution 1:1,000; 4 °C; overnight
anti-p-ERK1/2 monoclonal rabbit Ab	working dilution 1:1,500; 4 °C; overnight
anti-His(C-term) HRP-linked Ab	working dilution 1:5,000; RT; 2 h

All antibodies were diluted in 1x Roti-Block reagent and membranes were incubated with gentle shaking. Membranes were again washed and incubated with appropriate horseradish peroxidase (HRP)-coupled secondary antibodies (working dilution 1:5,000 in 1x Roti-Block reagent) for 1 h. All antibodies are detailed in section 2.1.4. Thorough washing with TBST for six times was followed by enzyme-substrate (Amersham ECL Plus Western blotting detection system; GE Healthcare, Chalfont St. Giles, UK) incubation for 5 min. Detection of chemiluminescence was accomplished using X-ray films (Amersham Hyperfilm ECL; GE Healthcare, Chalfont St. Giles, UK) with antibody-dependent exposition times between 10 s and 15 min. For repeated immunodetection, membranes were stripped at 50 °C for 30 min under agitation in stripping buffer (62.5 mM Tris hydrochloride, pH 6.7, 2% (w/v) SDS, 100 mM β-mercaptoethanol) to remove bound antibodies. Membranes were washed three times for 10 min with TBST and were ready for a new immunodetection.

2.2.6. ELISA

Levels of intact FGF23 in serum of humans and mice were measured by means of a two-site enzyme-linked immunosorbent assay (ELISA) from Kainos Laboratories (Tokyo, Japan). Two specific murine monoclonal antibodies bind to intact FGF23 forming a sandwich complex. One antibody is immobilised onto the well of a microtiter plate for capture. The

second antibody is conjugated to HRP for detection. The enzymatic activity of the complex bound to the well is directly proportional to the amount of intact FGF23 in the sample. Serum samples were isolated immediately after blood withdrawal by centrifugation (2,000 x g, RT, 10 min) and were stored at -80 °C before biochemical analysis. Assay procedure was performed following the manufacturer's instructions. Absorbance was measured in a Synergy HT Multi Detection Microplate Reader (BioTek, Winooski, VT, USA).

2.2.7. Small-Molecule Compound Screening

2.2.7.1. AlphaScreen SureFire Assay

The AlphaScreen SureFire p-ERK1/2 assay from PerkinElmer (Waltham, MA, USA) was used to measure the phosphorylation of ERK1/2 in cellular lysates (Figure 12).

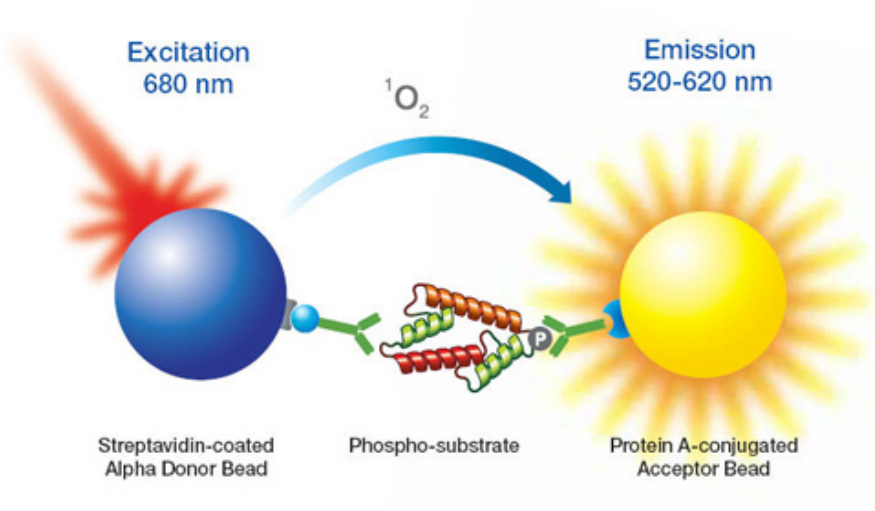

Figure 12: AlphaScreen SureFire assay principle. The technology allows the detection of phosphorylated ERK1/2 in cellular lysates in a highly sensitive and quantitative manner. Sandwich antibody complexes, which are only formed in the presence of the analyte, are captured by AlphaScreen donor and acceptor beads, bringing them into close proximity. The excitation of the donor beads provokes the release of singlet oxygen molecules that triggers a cascade of energy transfer in the acceptor beads resulting in the emission of light at 520 - 620 nm. Figure available at: www.perkinelmer.com.

Alpha (amplified luminescent proximity homogenous assay) technology requires two bead types: donor beads and acceptor beads. Donor beads contain a photosensitizer, phthalocyanine, which converts ambient oxygen to an excited and reactive form of O_2, singlet oxygen, upon illumination at 680 nm. Within its half-life, singlet oxygen can diffuse approximately 200 nm in solution. If an acceptor bead is within this distance, energy is transferred from the singlet oxygen to thioxene derivates within the acceptor bead resulting in

light production at 520 - 620 nm. To bring the beads in close proximity in the presence of p-ERK1/2 in cellular lysates, the assay uses the formation of sandwich antibody complexes. Biotinylated antibodies, which recognise a distal epitope on ERK1/2, are bound to the streptavidin-coated donor beads. Non-biotinylated antibodies, which recognise the p-Thr^{202}/Tyr^{204}-epitope, are bound to the Protein A-conjugated acceptor beads. The intensity of light emission, hereinafter called "Alpha signal (counts)", is proportional to ERK1/2 phosphorylation in cellular lysates. The assay was performed according to manufacturer's instructions.

2.2.7.2. HTRF Cellul'erk Assay

The HTRF Cellul'erk p-ERK1/2 assay from Cisbio (Codolet, France) makes also use of the formation of sandwich antibody complexes to detect endogenous ERK1/2, when it is phosphorylated (Figure 13).

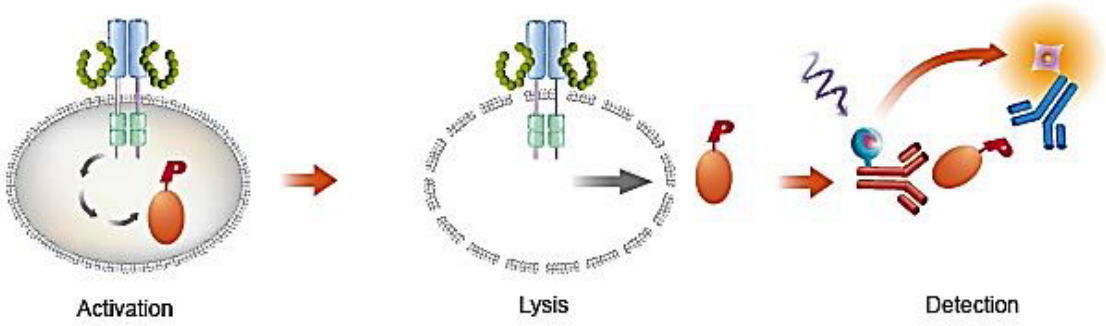

Figure 13: HTRF Cellul'erk assay principle. ERK1/2 is activated leading to phosphorylation. After cell lysis of the cell membrane, the phosphorylated ERK1/2 can be detected via a sandwich assay format using two different specific monoclonal antibodies: the anti-ERK1/2 antibody labelled with Eu^{3+}-cryptate and the anti-p-ERK1/2 antibody labelled with d2. Figure available at: www.htrf.com.

This assay format is based on the homogenous time-resolved fluorescence (HTRF) technology, which utilises two different specific antibodies, one labelled with Eu^{3+}-cryptate (donor) and the second with d2 (acceptor). When the dyes are in close proximity, the excitation of the donor with a light source (laser) triggers a time-resolved fluorescence resonance energy transfer (TR-FRET) towards the acceptor.

HTRF emissions were measured at 620 nm (donor) and at 665 nm (acceptor). Emissions at 620 nm were used as an internal reference, while emissions at 665 nm were used as an indicator of the biological reaction being assessed. Within ratiometric reduction of data, the so-called "HTRF Ratio" (HTRF emission $_{665\ nm}$/HTRF emission $_{620\ nm}$ x 10^4) was calculated.

This ratio should reduce well-to-well variations and signal quenching from assay components and media. The specific ratio modulates positively in proportion to p-ERK1/2. Assay procedure was performed following the manufacturer's instructions.

2.2.7.3. HTS of a Diverse Small-Molecule Library

For the high-throughput screening (HTS) of small-molecule compounds, plate and liquid handling was performed using a Cell::Explorer HTS platform sytem, a Sciclone G3 Liquid Handler with a Twister II Robotic Arm and Flexdrop Dispenser from PerkinElmer (Waltham, MA, USA) as well as an ELx405 Plate Washer and a MultiFlo Dispenser (Biotek Instruments, Bad Friedrichshall, Germany). Cells were incubated in a Cytomat Incubator (Thermo Fisher Scientific, Waltham, MA, USA). AlphaScreen SureFire and HTRF Cellul'erk measurements were performed using an EnVision Multilabel Reader (PerkinElmer, Waltham, MA, USA). Assays were carried out in white 384-well ProxiPlates or OptiPlates (PerkinElmer, Waltham, MA, USA). The plates were coated with poly-D-lysine (Sigma-Aldrich, St. Louis, MO, USA) to facilitate a better cell adherence. For the pilot HTS, a diverse small-molecule library was acquired from Prestwick Chemical (Illkirch, France). The Prestwick Chemical Library contains 1,280 small-molecule compounds, which are 100% approved drugs (Food and Drug Administration (FDA), European Medicines Agency (EMA) and other agencies). The purity of the compounds was > 90% as reported by the provider of the compounds. Comparable to section 2.2.4.4, nominated hit compounds were finally tested with different concentrations (0 - 30 µM) in the HEK293-KL cell model followed by Western blotting.

2.2.7.4. Cell Viability Test

To investigate the toxicity of small-molecule compounds on HEK293-KL cells, the CellTiter-Blue cell viability assay (Promega, Madison, WI, USA) was utilised. This assay enables the estimation of viable cells present in multiwell plates. Viable cells maintain the ability to reduce resazurin into resorufin, which is highly fluorescent. Nonviable cells rapidly lose metabolic capacity, do not reduce the indicator dye, and thus do not generate a fluorescent signal. Usually, the fluorescent signal from the CellTiter-Blue reagent is proportional to the number of viable cells. HEK293-KL cells were cultured in 384-well plates (13,000 cells/well) for 24 h and incubated with small-molecule compounds for 1 h. Subsequently, the CellTiter-Blue cell viability assay was conducted following the manufacturer's instructions.

2.2.8. Statistical Analysis

Statistical difference (*p*-value) between different conditions in either ELISA, AlphaScreen SureFire or HTRF Cellul'erk measurements was assessed by unpaired Student's *t*-test (giving mean ± standard deviation (SD) values) using GraphPad Prism version 6 (GraphPad Software, San Diego, CA, USA).

Statistical difference (*p*-value) in expression of transcripts was determined with the R package DESeq (Anders and Huber, 2010).

2.2.9. Computer Programs and Databases

2.2.9.1. Computer Programs

BWA	http://bio-bwa.sourceforge.net
CLUSTAL O	http://www.clustal.org/omega
DESeq	http://bioconductor.org/packages/release/bioc/html/DESeq.html
ExonPrimer	http://ihg.helmholtz-muenchen.de/ihg/ExonPrimer.html
GePS	http://www.genomatix.de
GraphPad Prism	http://www.graphpad.com/scientific-software/prism
Human Splicing Finder	http://www.umd.be/HSF
NetPhos	http://www.cbs.dtu.dk/services/NetPhos
NNSPLICE	http://www.fruitfly.org/seq_tools/splice.html
SAMtools	http://samtools.sourceforge.net
Staden Package	http://staden.sourceforge.net

2.2.9.2. Databases

dbSNP	http://www.ncbi.nlm.nih.gov/SNP
Ensembl	http://www.ensembl.org
ExAc Browser (Beta)	http://exac.broadinstitute.org

GeneCards	http://www.genecards.org
HGMD	http://www.hgmd.cf.ac.uk/ac/index.php
MGI	http://www.informatics.jax.org
NCBI	http://www.ncbi.nlm.nih.gov
OMIM	http://www.omim.org
PubChem	https://pubchem.ncbi.nlm.nih.gov
PubMed	http://www.ncbi.nlm.nih.gov/pubmed
RefSeq	http://www.ncbi.nlm.nih.gov/refseq
UCSC Genome Browser	http://genome.ucsc.edu
UniProt	http://www.uniprot.org

3. RESULTS

3.1. DETECTION OF NOVEL CANDIDATE DISEASE GENES ASSOCIATED WITH HUMAN PHOSPHATE BALANCE DISORDERS

For the detection of novel candidate disease genes associated with altered phosphate homeostasis, a patient population of 260 families with hypo- and hyperphosphatemic disorders is available at IHG (Helmholtz Zentrum München). In about 50 index cases, no mutation in one of the known genes involved in monogenic phosphate balance disorders has yet been detected.

Exome sequencing was performed for six unrelated single cases, for one patient and her affected mother, for three patients and their parents (trios) and for one family with several affected members suffering from hypophosphatemia. In total, 22 exomes were enriched in solution and indexed with SureSelect XT Human All Exon 50 Mb kit from Agilent Technologies. Sequencing was performed as pooled 100-bp paired-end runs on a HiSeq2000 system from Illumina. Within bioinformatic data analysis, Burrows-Wheeler Aligner (BWA, version 0.5.9) (Li and Durbin, 2009, 2010) was used for read alignment against the human genome assembly hg19 (GRCh37, UCSC). Single nucleotide variant (SNV) and small insertion and deletion (indel) calling specifically for the regions targeted by the exome enrichment kit was done using SAMtools (version 0.1.7) (Li et al., 2009). Annotation and filtering of the variants included information about known transcripts (UCSC Known Genes and RefSeq genes), known variants (dbSNP 135 and in-house database of approximately 5,200 exomes), variant quality (Mapping quality score > 50, SNV quality score > 40), type of mutation and, if applicable, amino acid change in the corresponding protein. Analysis of exome sequencing data is described in more detail for mouse samples in section 3.2.2.

In eight patients from our cohort analysed by exome sequencing, no novel variants which seem to be of pathogenic relevance for the diagnosed hypophosphatemia in at least two unrelated index cases could be detected. In one trio with healthy parents and one affected daughter showing hypophosphatemic rickets, markedly elevated bone mineral density and chronic unexplained renal disease in the absence of any nephrocalcinosis, a heterozygous *de*

novo 4-bp deletion within exon 5 of the *PHEX* gene (NM_000444.4:c.545_548delAGAG, NP_000435.3:p.Arg183Serfs37*) was identified by exome sequencing in the DNA of the affected daughter. The 4-bp deletion was confirmed with Sanger sequencing. The deletion was not found in the DNA of the unaffected parents. In another family with affected mother and daughter, a heterozygous stop mutation in exon 9 of the *PHEX* gene (NM_000444.5:c.1038C>G, NP_000435.3:p.Tyr346*) was detected by exome sequencing in both patients and was confirmed by Sanger sequencing. This stop mutation can also be found in the Human Gene Mutation Database (HGMD; CM113238). Subsequently, serum levels of intact FGF23 were assessed using a commercially available intact FGF23 ELISA. FGF23 levels were slightly elevated in the serum of the mother, whereas FGF23 levels in the serum of the daughter were within the normal range. The identified variants in the *PHEX* gene are also present in other families of our patient cohort and can be considered as causal mutations. In a German multiplex-family (Figure 14) with X-linked dominant or autosomal dominant inheritance, hypophosphatemia with inadequate phosphate balance and morphological changes of the skeleton was diagnosed in at least six family members within three generations (#3, #4, #6, #7, #10 and #11).

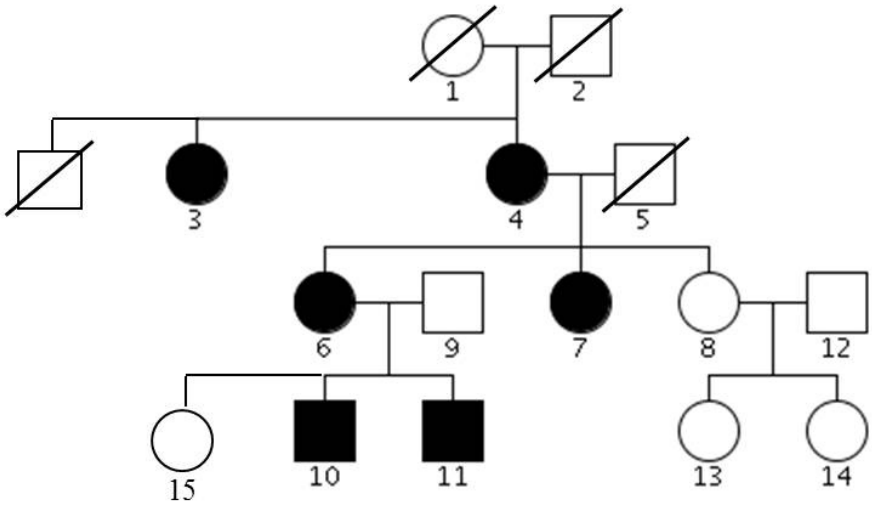

Figure 14: Pedigree of a German multiplex-family comprising at least six affected members with hypophosphatemia. Exome sequencing was performed for family members with the identification number #4, #6, #7, #10 and #11.

For DNA sample #10, Sanger sequencing was conducted for all 22 exons of the *PHEX* gene without any indication for mutations in the coding regions and the splice sites. It is worth mentioning that the mutation discovery rate in the *PHEX* gene is more than 90% in male patients, making the presence of XLH, the most common form of hereditary

hypophosphatemia, unlikely in this patient. Exome sequencing of five affected family members (#4, #6, #7, #10 and #11) resulted in one possible private loss-of-function SNV in the *COL24A1* (collagen XXIV, α1) gene. This variant (NM_152890.5:c.3558+1G>T) affects a nucleotide 1 bp upstream of exon 40 at the canonical donor splice site. In all investigated family members with hypophosphatemia, a heterozygous genotype was detected. Interestingly, family member #15, who has no symptoms of hypophosphatemia so far, also showed a heterozygous genotype. This could be due to incomplete penetrance of the phenotype. The detected variant is predicted to change the splice site, and hence affect protein features (Human Splicing Finder, version 2.4.1; NNSPLICE, version 0.9). An alternate splice product could result in an aberrant protein. However, the variant was not detected in any other investigated unrelated hypophosphatemic patient of our cohort. Due to the missing "second case", it remains unclear whether this SNV is of pathogenic relevance.

3.2. IDENTIFICATION OF ENU-DERIVED MOUSE MODELS FOR ABNORMALITIES IN BONE METABOLISM AND SKELETAL DEVELOPMENT

3.2.1. Mutation Discovery Using Exome Sequencing

In cooperation with IEG (Helmholtz Zentrum München), we focused on the identification of novel genes involved in bone metabolism and skeletal development by selecting mutant mouse lines from the Munich ENU Mutagenesis Project with at least one altered serum parameter for metabolic bone disease (Pi, Ca and ALP). In total, 18 mutant mouse lines and one wild-type C3HeB/FeJ mouse were subjected to exome analysis using massively parallel sequencing strategies (Figure 15). In this cohort, 15 mouse lines showed a dominant and three mouse lines a recessive mode of inheritance.

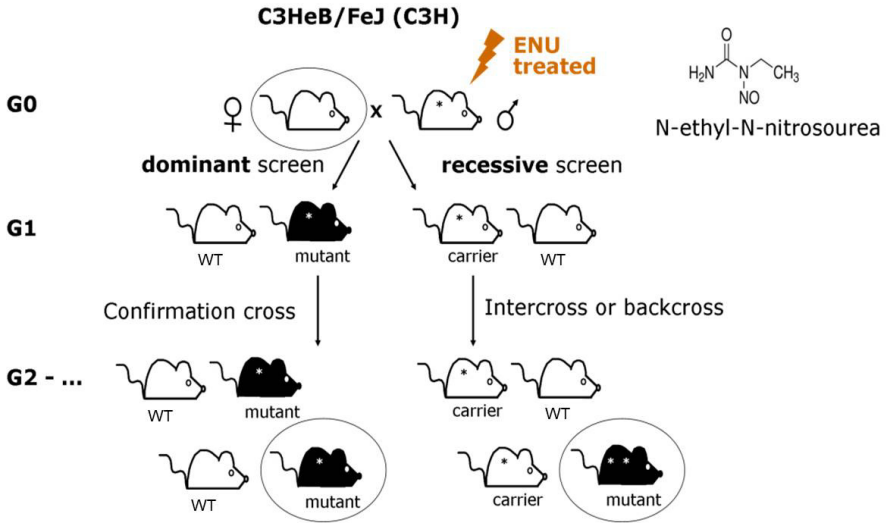

Figure 15: Scheme of the large-scale genome-wide Munich N-ethyl-N-nitrosourea (ENU) Mutagenesis Project. Mice in circles were used for exome sequencing.

As mutant mice were generated on a well-known inbred strain (C3HeB/FeJ) with a homogeneous genetic configuration, only one mutant mouse (generations G5 - G10) per mouse line was analysed, and the results were compared with the data of the untreated wild-type (WT) background mouse as a control in the first setup (mouse lines 1 - 12).

Additionally, after these first experiences of exome sequencing of mouse samples, the procedure for the analysis of another six mutant mouse lines was optimised and accelerated in the second setup (mouse lines 13 - 18). Here, two affected littermates (generations G5 - G10) per mouse line and one wild-type C3HeB/FeJ mouse were sequenced. By this second strategy, we aimed to avoid analysis problems caused by technical artefacts like amplification, sequencing and/or computational analysis errors found in the first setup.

3.2.2. Capture of Exonic Sequences and Data Analysis

For enrichment of exonic sequences and search for the causative mutations, the Agilent SureSelect XT Mouse All Exon kit for in-solution sequence capture was used followed by Illumina HiSeq2000 NGS. Paired-end reads were mapped to the mouse genome assembly mm9 (NCBI37, UCSC) using Burrows-Wheeler Aligner (BWA, version 0.5.9). SAMtools (version 0.1.7) was used for SNV and indel calling. Between 5.45 Gb and 11.68 Gb of raw sequence data corresponding to read counts between 53,925,582 and 115,676,475 were generated, and between 96.83% and 98.60% of reads were mapped leading to an average coverage between 63x and 138x, respectively (Table 3).

Table 3: Next-generation sequencing technical data.

Mouse line	Mutant number	Seq (Gb)	Total number of reads	Reads mapped (%)	Reads on target (%)	Coverage 1x (%)	Coverage 20x (%)	Average coverage	Ts/Tv
1	60339	10.02	99,225,831	97.66	77.83	99.81	95.40	119.93	2.64
2	60342	9.71	96,124,207	97.71	76.54	99.79	95.21	113.77	2.64
3	60343	9.18	90,869,007	95.79	78.09	99.79	93.18	108.65	2.65
4	60344	9.78	96,859,843	97.91	78.23	99.79	93.82	118.54	2.66
5	60345	11.61	114,921,675	97.01	78.75	99.82	94.89	138.44	2.66
6	60346	8.72	86,299,515	97.63	77.45	99.78	93.95	103.09	2.64
7	60347	9.78	96,808,078	97.31	78.62	99.86	94.73	117.35	2.66
8	60348	9.45	93,565,698	97.41	77.96	99.81	95.57	112.37	2.64
9	60350	8.59	85,038,099	97.54	78.11	99.75	89.15	102.99	2.65
10	60352	10.00	99,043,969	97.59	77.08	99.82	96.04	117.04	2.66
11	60355	8.03	79,457,229	96.83	77.49	99.79	92.79	95.56	2.64
12	60358	9.03	89,452,869	97.92	76.39	99.77	94.19	107.06	2.64
13	65610	10.43	103,282,928	98.27	75.18	99.80	95.53	121.87	2.65
	66533	8.30	82,161,746	98.43	73.48	99.77	93.63	93.97	2.65
14	65611	10.52	104,203,635	98.29	74.23	99.79	95.57	121.05	2.64
	66525	10.35	102,433,897	98.39	72.51	99.79	95.42	115.64	2.63
15	65612	11.68	115,676,475	98.34	72.99	99.80	96.03	132.28	2.64
	66531	7.67	75,906,966	97.39	74.42	99.79	92.27	86.86	2.65
16	65620	11.60	114,853,903	98.28	72.53	99.81	96.35	129.45	2.65
	66537	9.35	92,579,856	98.60	73.32	99.78	94.69	106.00	2.64
17	65622	8.39	83,033,828	97.72	73.77	99.80	93.59	95.41	2.64
	66532	5.45	53,925,582	97.87	75.07	99.71	84.54	62.65	2.66
18	65623	10.33	102,240,037	98.16	74.73	99.80	95.52	119.32	2.65
	66527	10.80	106,939,546	98.14	70.04	99.80	95.42	115.56	2.65
	60360 (C3HeB/FeJ, WT)	9.20	91,056,920	97.73	78.84	99.78	92.93	112.19	2.65

Seq = raw sequencing data generated in Gb; Ts/Tv = transition versus transversion rate

By comparing the sequencing data with the mouse reference sequence mm9 (NCBI37, UCSC), in total approximately 126,000 variants were called including on average 38,000 high-quality coding variants (Mapping quality score > 50, SNV quality score > 40). Coding variants could be divided into 24,000 synonymous and 14,000 non-synonymous variants. Non-synonymous variants were further filtered to remove variants found in both mutant and wild-type (C3HeB/FeJ) sequences as well as variants known to be present in the database of single nucleotide polymorphisms (dbSNP 128) and within 142 in-house generated mouse exomes. Finally, the variants were catalogued on the basis of mutation type and consequence. The undermentioned variants were chosen for further analysis: (1) SNVs which resulted in an amino acid substitution, (2) SNVs which were predicted to cause either the gain or loss of a stop codon, (3) SNVs which changed a nucleotide at the canonical 5' donor or 3' acceptor splice site and (4) indels which caused a frameshift. Altogether, around 12 variants per mutant mouse line were identified (Figure 16).

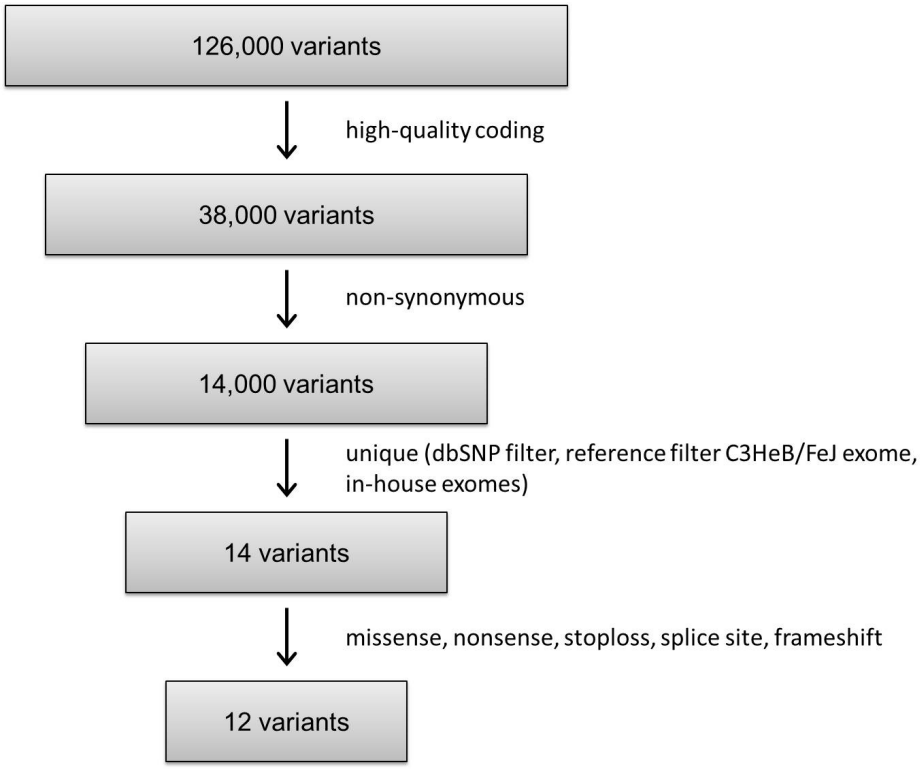

Figure 16: Filter criteria of exome sequencing data to identify putative causative coding mutations. Average numbers of variants detected in the mouse lines are depicted.

Detailed filtering of exome sequencing data for each mutant mouse line and the wild-type mouse is shown in Table 4.

Table 4: Filtering of exome sequencing data for each mouse line.

Mouse line (inheritance)	**Mutant number**	**Variants different from mm9**	**Synonymous variants**	**Non-synonymous variants**	**Not in dbSNP 128 and 142 in-house exomes**	**Nonsense missense splice site stoploss frameshift**
1 (ad)	60339	126,068	23,571	14,070	13	11
2 (ad)	60342	125,349	23,532	14,027	12	9
3 (ar)	60343	125,923	23,590	14,128	4	3
4 (ad)	60344	125,186	23,531	14,065	14	12
5 (ad)	60345	126,112	23,559	14,119	39	33
6 (ad)	60346	124,904	23,525	14,054	16	11
7 (ad)	60347	125,390	23,523	14,067	11	11
8 (ad)	60348	126,109	23,552	14,112	14	12
9 (ad)	60350	125,031	23,538	14,118	28	27
10 (ad)	60352	126,654	23,601	14,181	31	28
11 (ad)	60355	125,090	23,586	14,085	15	12
12 (ar)	60358	124,530	23,488	13,985	7	3
13 (ad)	65610 66533	125,960 125,501	23,557 23,558	14,137 14,126	1	1
14 (ar)	65611 66525	125,960 126,145	23,580 23,538	14,136 14,121	12	11
15 (ad)	65612 66531	126,099 125,603	23,579 23,570	14,126 14,176	1	1
16 (ad)	65620 66537	126,663 125,665	23,562 23,568	14,174 14,113	18	17
17 (ad)	65622 66532	125,758 123,339	23,599 23,592	14,185 14,182	5	4
18 (ad)	65623 66527	126,097 125,881	23,571 23,571	14,143 14,110	8	7
	60360 (C3HeB/FeJ, WT)	124,877	23,540	14,045	-	-

Quality criteria: Mapping quality score > 50; SNV quality score > 40; mm9 = mouse genome assembly NCBI37, UCSC; ad = autosomal dominant; ar = autosomal recessive

3.2.3. Validation of Putative Causative Candidate Mutations

All variants of interest were further analysed by capillary sequencing using the original DNA sample from exome sequencing to confirm NGS data. In addition, DNA samples from more mutant mice from the maintenance breeding with generations even higher than the exome mouse (> G10) and from control littermates were screened for the putative candidate variant to confirm co-segregation of the genotype and the phenotype (Table 5). Variants not present in phenotypically mutant mice were excluded as candidates, while variants present in phenotypically wild-type mice were still included in the analysis because of the possibility of incomplete penetrance of the phenotype.

In 13 of the 18 mutant mouse lines, one unique variant has been found by capillary sequencing to be a correct call and to segregate in a corresponding mouse cohort of affected and unaffected littermates (Table 5). More than one potentially causal variant was identified to correlate with the phenotype in one mutant mouse line (mutant 60347) (Table 5). For the remaining four mutant mouse lines, no possible candidate variant in protein coding sequences and splice sites at all could be detected. We expanded our search to untranslated regions (5'and 3' UTRs) but with no appreciable success.

Altogether, two nonsense, one splice site and 12 missense candidate mutations (including two different variants in one mutant mouse) were determined within the 18 mutant mouse lines analysed by exome sequencing. Sequencing of two mutant littermates with generations G5 - G10 per mutant mouse line and comparison with one wild-type C3HeB/FeJ mouse sequence turned out to be the more efficient strategy in mutation discovery at first glance. Within this second setup, we identified the causative mutation in all six mutant mouse lines analysed (mutation detection rate 100%). In the first setup with sequencing of only one mutant mouse with generations G5 - G10 and comparison with one wild-type C3HeB/FeJ mouse sequence, the causative mutation was detected in eight of the 12 mutant mouse lines analysed (mutation detection rate 67%).

The results collectively indicate that exome sequencing is a straightforward and robust approach for mutation discovery in ENU-derived mouse models not only for metabolic bone disease. The strategy for the second setup analysing two mutants per mouse line reduced the number of remaining candidate variants during the validation process and expressively increased the success rate for detection of the causative mutation.

Table 5: Variants identified using exome sequencing data.

Mouse line	Mutant number	Screening parameters	Observed phenotype	Variants	Candidate gene	Location (mm9)	Ref allele	Var allele	AA change	Detected alleles	Function	Segregation observed genotype-phenotype correlation
1	60339	high ALP	craniofacial	11	*Ednra*	chr8:80,243,961	A	T	p.Tyr129Phe	het./hom.	missense	8/8 hom. affected, 16/16 het. intermediate, 10/10 WT unaffected
2	60342	high ALP, low Ca, low albumin	metabolic	9	*Alb*	chr5:90,896,485	T	C	p.Cys277Arg	het.	missense	61/65 het. affected, 54/59 WT unaffected
3	60343	high ALP, high Ca	metabolic	3	NA	-	-	-	-	-	-	-
4	60344	high ALP	skeletal	12	*Satb2*	chr1:56,948,007	G	T	p.Val234Leu	het.	missense	11/11 het. affected, 11/11 WT unaffected
5	60345	high ALP, high Ca	skeletal	33	NA	-	-	-	-	-	-	-
6	60346	high ALP	skeletal	11	*Fam46a*	chr9:85,219,964	G	T	p.Glu157*	het./hom.	nonsense	7/7 hom. affected, 47/52 het. intermediate, 49/54 WT unaffected

7	60347	high ALP	small	11	*Myst4*	chr14:22,438,503	C	T	p.Leu305Phe	het.	missense	10/12 het. affected, 15/20 WT unaffected,
					Ero1l	chr14:45,921,413	T	C	p.Trp154Arg	het.	missense	10/12 het. affected, 19/20 WT unaffected
8	60348	high ALP, low Ca, low albumin	metabolic	12	*Alb*	chr5:90,894,954	T	C	p.Cys224Arg	het.	missense	9/9 het. affected, 19/19 WT unaffected
9	60350	low Pi	metabolic	27	NA	-	-	-	-	-	-	-
10	60352	low Pi	metabolic	28	NA	-	-	-	-	-	-	-
11	60355	low Pi	metabolic	12	*Trp63*	chr16:25,863,819	T	A	p.Tyr450*	het.	nonsense	6/15 het. affected, 39/77 WT unaffected
12	60358	high Ca, low Pi	skeletal	3	*Scube3*	chr17:28,299,313	C	A	p.Asn294Lys	hom.	missense	15/15 hom. affected, 10/10 WT unaffected
13	65610 66533	NA	teeth	1	*Sipa1*	chr19:5,651,695	T	G	p.Ser971Ala	het.	missense	2/2 het. affected, 6/6 WT unaffected
14	65611 66525	NA	teeth	11	*Mmp20*	chr9:7,655,132	T	A	p.Tyr414Asn	hom.	missense	14/14 hom. affected, 10/10 WT unaffected
15	65612 66531	NA	teeth	1	*Ftl1*	chr7:52,714,602	A	G	3' acceptor splice site	het.	splice	10/10 het. affected, 11/11 WT unaffected
16	65620 66537	NA	small	17	*Sik3*	chr9:45,986,624	T	C	p.Phe284Ser	het.	missense	3/3 het. affected, 5/5 WT unaffected
17	65622 66532	NA	small	4	*Sulf1*	chr1:12,848,991	G	A	p.Asp82Asn	het.	missense	7/7 het. affected, 20/20 WT unaffected
18	65623 66527	NA	small	7	*Ryr1*	chr7:29,805,182	A	G	p.Glu4247Gly	het.	missense	13/16 het. affected, 23/23 WT unaffected

NA = not available; mm9 = mouse genome assembly NCBI37, UCSC; Ednra = endothelin receptor type A; Alb = albumin; Satb2 = special AT-rich sequence binding; Fam46a = family with sequence similarity 46, member A; Myst4 = histone acetyltransferase monocytic leukaemia 4; Ero1l = ERO1-like; Trp63 = transformation-related protein 63; Scube3 = signal peptide CUB EGF domain-containing protein 3; Sipa1 = signal-induced proliferation associated gene 1; Mmp20 = matrix metallopeptidase 20; Ftl1 = ferritin light chain 1; Sik3 = SIK family kinase 3; Sulf1 = sulfatase 1; Ryr1 = ryanodine receptor 1, skeletal muscle

3.2.4. Exome Sequencing Identifies a Novel Nonsense Mutation in the *Fam46a* Gene Associated with Skeletal Abnormalities in BAP014 Mice

In cooperation with IEG, we intended to further investigate one mouse line of our cohort of ENU-derived mice, named BAP014 (Bone screen alkaline phosphatase #14; mutant 60346 (Table 5)), which was initially defined by changes in the bone turnover parameter ALP and by abnormalities in bone content and structure.

3.2.4.1. Phenotypic Biochemical Identification of the New ENU-Derived Mouse Model BAP014

BAP014 mice of a confirmation cross appeared morphologically normal with no noticeable phenotype at first glance. When analysed at 12, 24 and 36 weeks of age, mutants had significantly higher ALP activity values compared to wild-type mice. Conversely, total Ca and Pi serum values of BAP014 mice remained in the physiological range (data not shown; measurements performed at IEG). FGF23 serum levels were also not significantly different between BAP014 and wild-type mice (Figure 17).

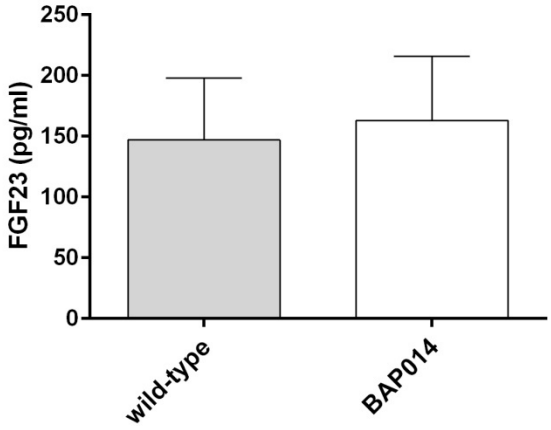

Figure 17: Measurement of serum levels of intact FGF23 in wild-type (grey bar) and BAP014 (white bar) mice by ELISA. The data are expressed as the mean ± SD (n = 20). Significance was determined with the unpaired Student's *t*-test. There was no significant difference of FGF23 serum levels between wild-type and BAP014 mice.

Since increased ALP activities suggested a deregulation of bone content and structure, peripheral quantitative computed tomography (pQCT) measurements of the femur of 9- and 12-month-old female and male BAP014 mice were taken at IEG. Compared to wild-type mice, total bone mineral density was significantly elevated in the metaphysis of 9- and 12-

month-old female BAP014 mice and in the diaphysis of 12-month-old female BAP014 mice as well as slightly increased in the diaphysis of 9- and 12-month-old male BAP014 mice (data not shown). Despite the apparently normal bone morphology of BAP014 mice at first sight, this indicated possible abnormalities in long bone formation of mutants.

3.2.4.2. Exome Sequencing Identifies a *Fam46a* Nonsense Mutation

As described above, exome sequencing was used to identify causative mutations in ENU-derived mice. For BAP014 mice, 11 candidate variants (ten SNVs and one indel) were obtained. We analysed all variants of interest within a cohort of eight phenotypically wild-type and eight phenotypically mutant mice by capillary sequencing. Only one SNV on mouse chromosome 9 segregated in all mutant mice with the phenotype. This perfectly matched the linkage data available for BAP014 mice with a candidate linkage interval on mouse chromosome 9 (mm9_chr9:37,503,221 - 110,962,308; size 73.5 Mb). The detected private SNV was a heterozygous nonsense mutation within the *Fam46a* (family with sequence similarity 46, member A) gene leading to a premature stop codon after 156 amino acids (NM_001160378.1:c.469G>T, NP_001153850.1:p.Glu157*) (Figure 18). Therefore, the BAP014 mouse line was renamed to *Fam46a*^{E157*Mhda}. Comparison of this position (mm9_chr9:85,219,964) with published resequencing data of 18 different mouse strains (Ensembl Genome Browser 72: *Mus musculus*) revealed that all mouse strains were homozygous for the G allele (G/G) as the reference. In addition, we investigated four further inbred strains (BALB/c, DBA/2, FVB, SJL) by capillary sequencing and got the same result.

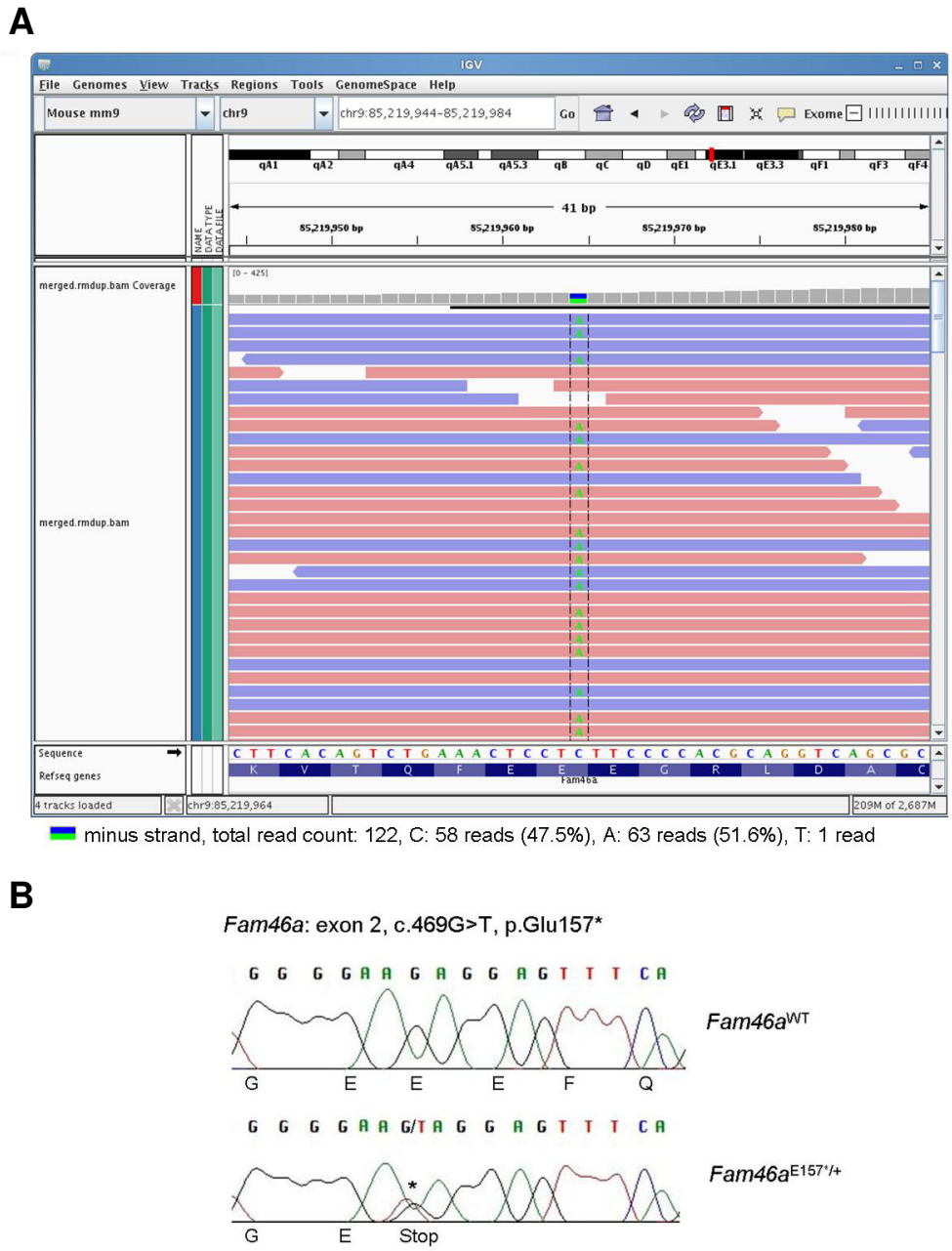

Figure 18: Identification of a nonsense mutation in the *Fam46a* gene by exome sequencing. Exome sequencing revealed a heterozygous nonsense mutation (NM_001160378.1:c.469G>T, NP_001153850.1:p.Glu157*) within the *Fam46a* (family with sequence similarity 46, member A) gene leading to a premature termination of translation. (A) Exome sequencing data are visualised with IGV (Integrative Genomics Viewer, (Robinson et al., 2011)). In total, 122 reads were mapped successfully to *Fam46a* by the use of BWA. They covered the nonsense mutation at genomic position mm9_chr9:85,219,964. *Fam46a* is located on the minus strand. 58 reads (47.5%) covered the complementary C reference allele, while 63 reads (51.6%) covered the complementary mutant A allele. (B) The nonsense mutation (marked by an asterisk) was confirmed by capillary sequencing of *Fam46a*$^{E157*/+}$ and *Fam46a*^{WT} mouse DNA samples.

3.2.4.3. Generation of Homozygous *Fam46a*^{E157*} Mice and Phenotypic Abnormalities

To examine the functional consequence of the putative loss-of-function mutation in more detail, heterozygote intercross mating was done at IEG to generate homozygous *Fam46a*^{E157*} mice resulting in a cohort of 49 phenotypically wild-type, 47 heterozygous and seven homozygous *Fam46a*^{E157*} mice. The observed low number of homozygous mice representing an atypical Mendelian ratio may reflect a decreased viability of *Fam46a*$^{E157*/-}$ mice in the perinatal period. Surviving *Fam46a*$^{E157*/-}$ mice had phenotypic abnormalities with variable expression.

ALP activity was also assessed for *Fam46a*$^{E157*/-}$ mice at the age of 12 weeks. Compared to wild-type and heterozygous mice, ALP activity was significantly increased in homozygous mutant mice. It was even twice as high as in heterozygous mice (data not shown; measurements taken at IEG). Homozygous *Fam46a*^{E157*} mice showed morphologically distinct skeletal and growth phenotypes. Compared to *Fam46a*^{WT} and heterozygous littermates, a significantly reduced body size (short stature) was apparent in all seven *Fam46a*$^{E157*/-}$ mice (Figure 19 A, Figure 20 A). Furthermore, *Fam46a*$^{E157*/-}$ mice displayed an abnormal gait due to shortened and twisted hind and/or front limbs. In one severely affected 22-week-old male *Fam46a*$^{E157*/-}$ mouse, the talocalcaneal joint of the left hind limb appeared thickened and reddened (Figure 19 B). At the right hind limb, the femur was shortened and the talocalcaneal joint seemed twisted (Figure 19 C). X-ray analysis revealed that the right femur was shortened and thickened and also showed an anomalous morphology (Figure 19 D). Both humeral bones had similar malformations and the thoracic vertebral column presented distorted (Figure 19 D). To analyse these abnormal skeletal changes in more detail, micro computed tomography (µCT, SkyScan) analysis of the whole skeleton was performed (Figure 19 E - J). The SkyScan analysis manifested profound abnormalities of long bones, joints, ribs and vertebrae. The thickening of the left talocalcaneal joint became more distinct as an obvious malformation of the distal tibia (Figure 19 E). The right femur was shortened and highly malformed possibly due to a fracture. Additionally, in the right talocalcaneal joint, the calcaneus was shortened, malformed and embedded in a hypertrophic mass of unknown tissue (Figure 19 F and G). Malformation of the left humerus appeared at the region of the deltoid tuberosity (Figure 19 H). Comparison of whole skeleton preparations of a *Fam46a*^{WT} and another *Fam46a*$^{E157*/-}$ mouse displayed shortened and severely malformed ribs with calluses, compression of the rib cage, atypical scapulae and a left shortened and thickened

humerus (Figure 19 J). In contrast, no obvious skeletal abnormalities were seen in the *Fam46a*^{WT} mouse (Figure 19 I).

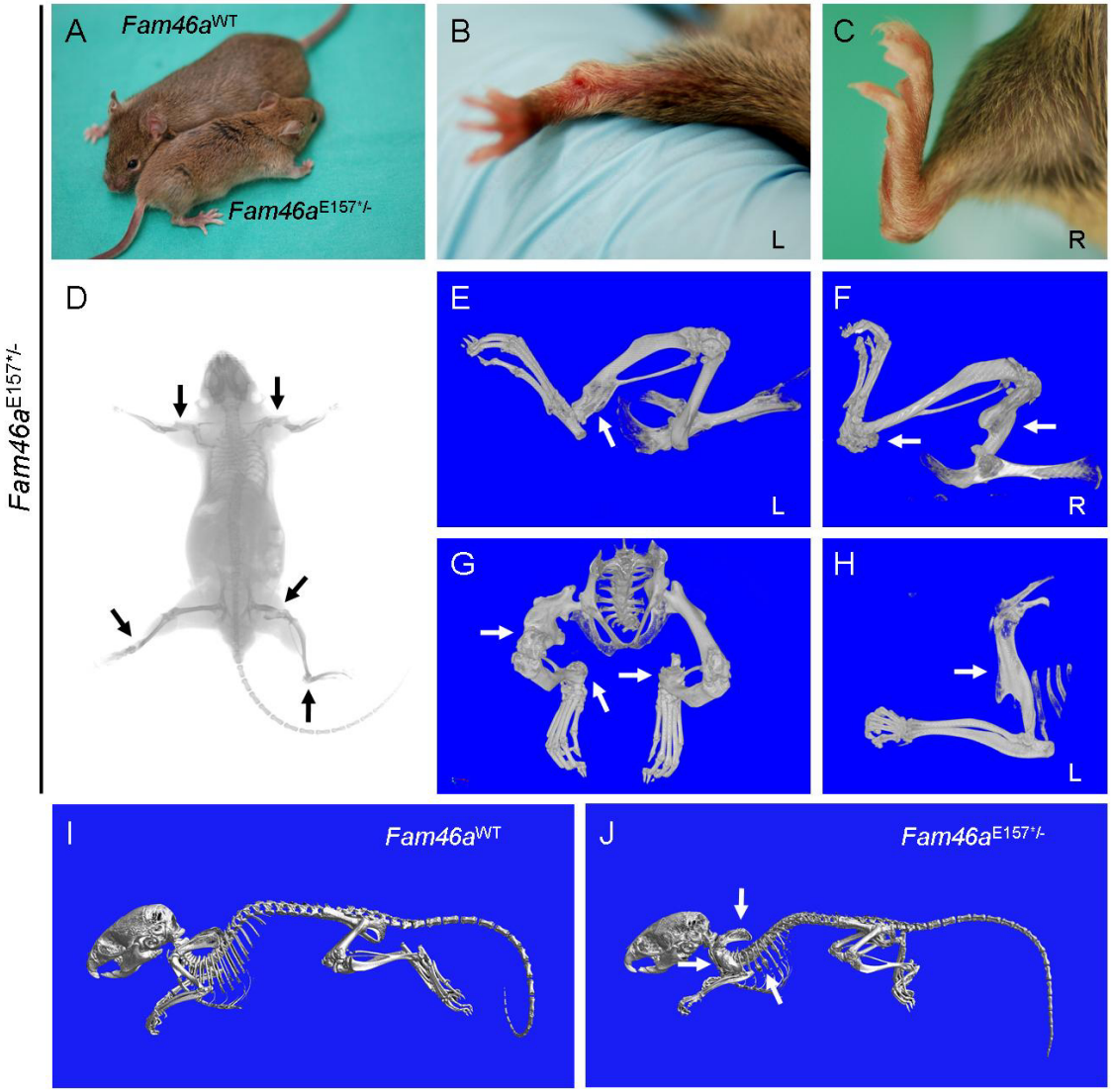

Figure 19: Phenotypic appearance of *Fam46a*$^{E157*/-}$ mice. (A) When compared to a *Fam46a*^{WT} littermate, the homozygous mutant showed a distinct phenotype with significantly reduced body size (short stature) and abnormal limbs. (B) The talocalcaneal joint of the left hind limb appeared thickened and reddened. (C) Shortening of the femur was present with an abnormally twisted talocalcaneal joint at the right hind limb. (D) X-ray analysis confirmed the hind limb abnormalities. In addition, thickened humoral bones and a distorted thoracic vertebral column were found (black arrows). (E - H) SkyScan analysis of this *Fam46a*$^{E157*/-}$ mouse was conducted. (E) In the *Fam46a*$^{E157*/-}$ mouse, thickening of the left talocalcaneal was identified to be more likely a malformation of the distal tibia. (F) The right femur was shortened and seemed to be twisted possibly due to a fracture. The calcaneus in the right talocalcaneal joint was shortened, malformed and appeared to be embedded in a hypertrophic mass of unknown tissue. (G) These findings were also observed in the craniodorsal scan view. (H) Thickening of the left humerus of the *Fam46a*$^{E157*/-}$ mouse was detected at the region of the deltoid tuberosity. (I and J) Images of whole mouse skeletons revealed shortened and severely malformed ribs with calluses, compression of the rib cage, atypical scapulae and a left shortened and thickened humerus in another *Fam46a*$^{E157*/-}$ mouse (white arrows) not to be seen in the wild-type.

In addition to the identified morphological abnormalities, we aimed to check for ossification defects. For this, whole skeletons of 25-week-old *Fam46a*$^{E157*/-}$ and *Fam46a*^{WT} mice were stained with Alizarin Red (mineralised bone) and Alcian Blue (cartilaginous matrix) at IEG.

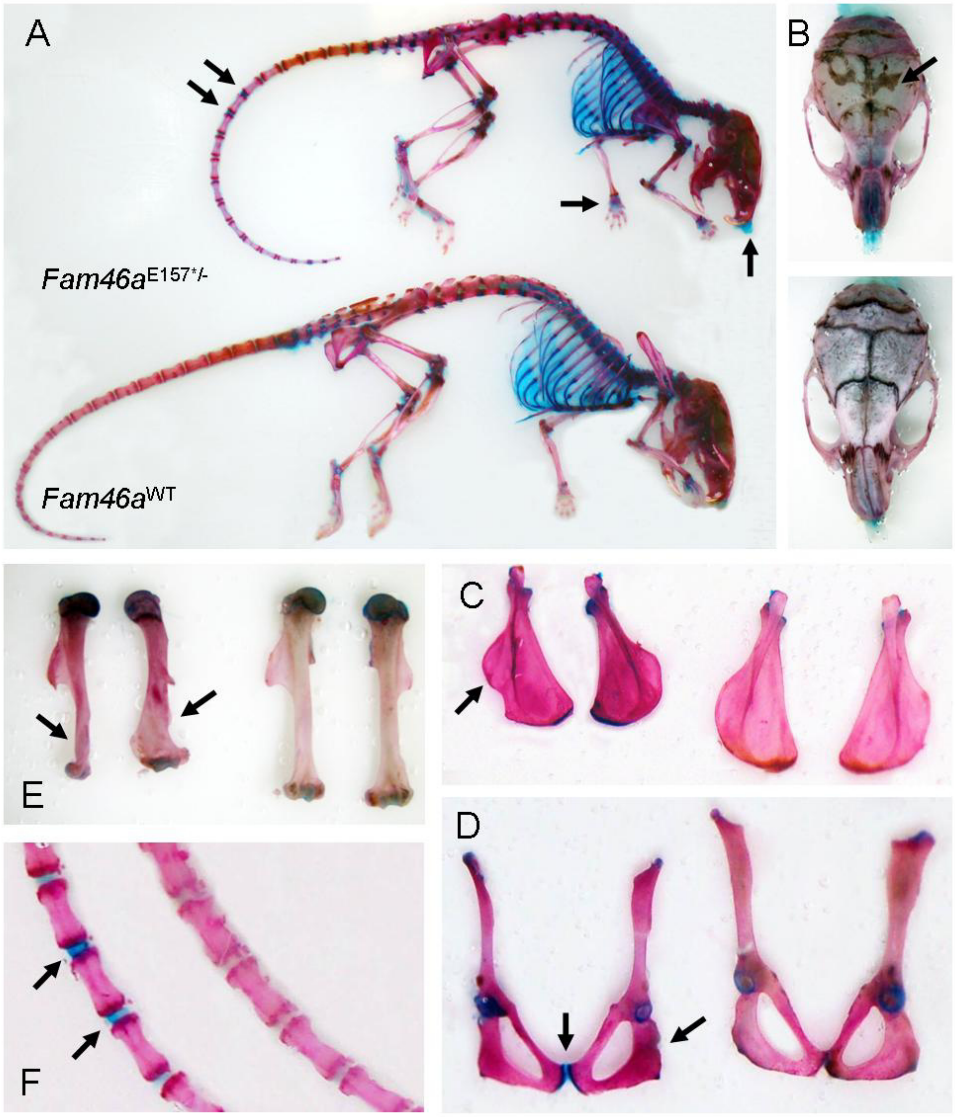

Figure 20: Alizarin Red/Alcian Blue staining of the skeleton of a 25-week-old *Fam46a*$^{E157*/-}$ mouse. (A) Extensive blue staining of cartilaginous matrix (black arrows) revealed a possible delayed ossification within the mouse tail, pelvis, paws and snout of the *Fam46a*$^{E157*/-}$ mouse in comparison to the wild-type. (B) The *Fam46a*$^{E157*/-}$ mouse had a smaller skull with very thin parchment-like calvaria (upper picture). (C and D) Scapulae and ischium bones appeared smaller and abnormally shaped in the *Fam46a*$^{E157*/-}$ mouse (left *Fam46a*$^{E157*/-}$, right *Fam46a*^{WT}; black arrows). (E) Humeri also showed malformations like thickening and twisting in this homozygous mutant (left *Fam46a*$^{E157*/-}$, right *Fam46a*^{WT}; black arrows). (F) Magnification of a possible delayed ossification within the mouse tail (left *Fam46a*$^{E157*/-}$, right *Fam46a*^{WT}; black arrows).

A possible delayed ossification within the mouse tail, pelvis, paws and snout could be revealed by extensive blue staining of cartilaginous matrix in the *Fam46a*$^{E157*/-}$ mouse

(Figure 20 A and F). The mutant had smaller skulls with very thin, probably hypomineralised calvaria suggesting severe defects in intramembranous ossification (Figure 20 B). Scapulae and ischium bones showed smaller size and atypical shapes in the *Fam46a*$^{E157*/-}$ mouse (Figure 20 C and D). In addition, humeri displayed malformations like thickening and twisting, which could possibly result from defects in endochondral ossification (Figure 20 A and E).

Homozygous animals that survived to adulthood were classified as moderately-to-severely affected and displayed reduced body size, severe brittleness and atypical shapes of long bones, pelvis, scapulae and calvaria as well as a possible delay in ossification.

3.2.4.4. Expression of *Fam46a* in Bone Tissue

To investigate a potential role of Fam46a in bone formation and turnover in postnatal development, *Fam46a* expression was analysed in adult mouse bone tissue. We isolated total RNA from whole femur and from calvaria of adult wild-type C3HeB/FeJ mice and performed semi-quantitative multiplex RT-PCR experiments.

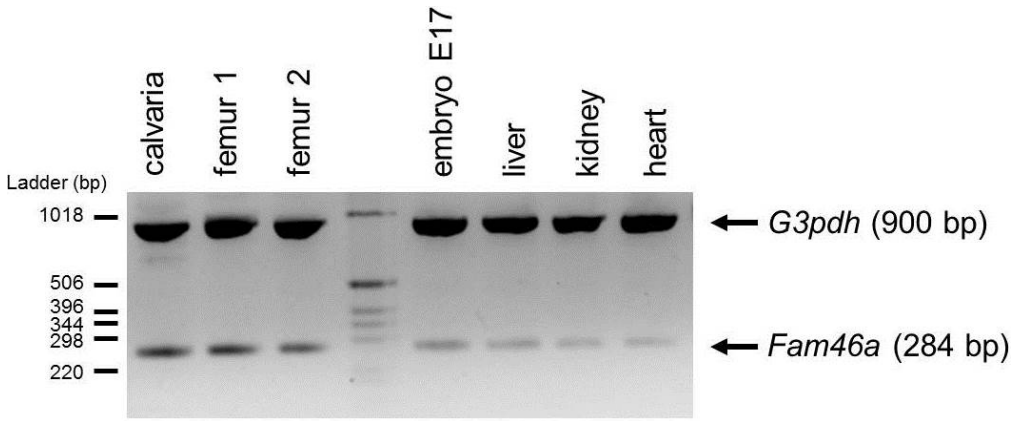

Figure 21: Expression analysis of *Fam46a* in different mouse tissues. Expression analysis of *Fam46a* was performed using semiquantitative multiplex RT-PCR using *Fam46a* and *G3pdh* (glyceraldehyde 3-phosphate dehydrogenase) primers within the same reaction. Expression of *Fam46a* in bone tissue was analysed in comparison to the expression in other embryonic and adult mouse tissues.

Specific RT-PCR products were generated from adult mouse control tissues (liver, kidney and heart), mouse embryo E17 as well as from calcified tissues. Compared with the expression level of the housekeeping gene *G3pdh* (glyceraldehyde 3-phosphate dehydrogenase), *Fam46a* exhibited a strong expression in calvaria and femur (Figure 21) suggesting also a possible role in postnatal bone homeostasis.

3.2.4.5. FAM46 Protein Family

FAM46A is a highly conserved protein in vertebrates (Lagali et al., 2002). It is present in eutherians, marsupials, amphibians and fish. The identity between the human (Uniprot ID: Q96IP4-2) and mouse (Uniprot ID: D3Z5S8) amino acid sequences is 94% and differs mainly within the variable number of tandem repeats (VNTRs)-encoded PS50315 domain (Figure 22).

The human *FAM46A* gene, originally named *C6orf37*, is located on chromosome 6q14.1. For the human and the mouse gene, a few alternative splice variants have been reported (Etokebe et al., 2014). The human gene product contains 523, 461 or 442 amino acids depending on the transcribed isoform. The consensus mouse Fam46a protein contains 447 amino acids. Any known intracellular organelle targeting signals and putative hydrophobic transmembrane domains are missing within the FAM46A amino acid sequence, which indicates a soluble, globular structure with a possible localisation in the cytoplasm (Lagali et al., 2002).

Sequence assembly of the four known FAM46 family members (FAM46A, FAM46B, FAM46C and FAM46D) and *in silico* domain homology search revealed similarity of the core region of the FAM46 protein family to a protein family that contains a domain of unknown function (DUF1693) (Figure 22). This family comprises many hypothetical proteins including four nematode prion-like proteins.

The nonsense mutation identified in *Fam46a*^{E157*} mice is located near the start of the DUF1693 domain. It may cause, if transcribed and translated, a truncated and presumably functionless protein.

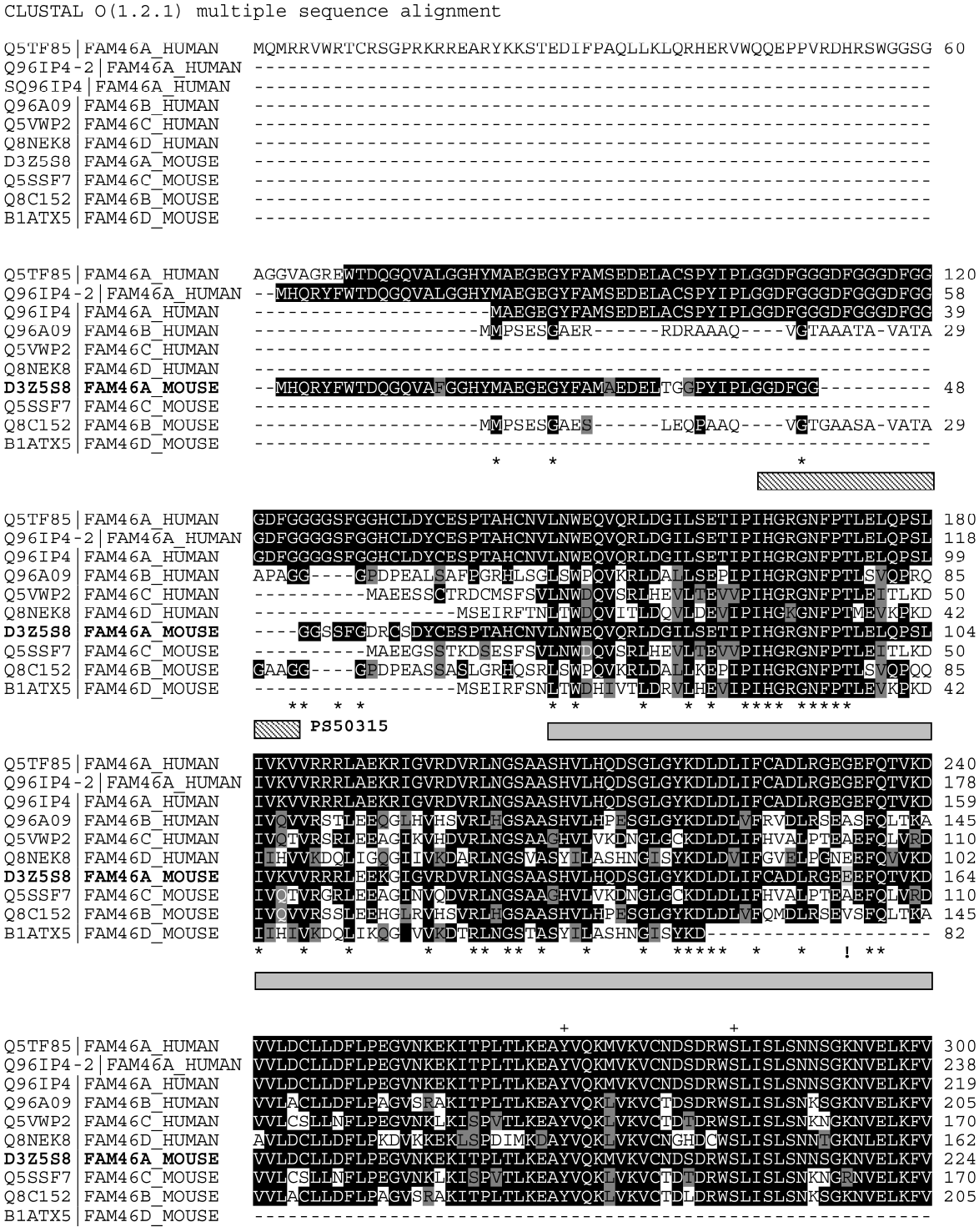
CLUSTAL O(1.2.1) multiple sequence alignment
Q5TF85|FAM46A_HUMAN MQMRRVWRTCRSGPRKRREARYKKSTEDIFPAQLLKLQRHERVWQQEPPVRDHRSWGGSG 60
Q96IP4-2|FAM46A_HUMAN
SQ96IP4|FAM46A_HUMAN
Q96A09|FAM46B_HUMAN
Q5VWP2|FAM46C_HUMAN
Q8NEK8|FAM46D_HUMAN
D3Z5S8|FAM46A_MOUSE
Q5SSF7|FAM46C_MOUSE
Q8C152|FAM46B_MOUSE
B1ATX5|FAM46D_MOUSE
Q5TF85|FAM46A_HUMAN AGGVAGREWTDQGQVALGGHYMAEGEGYFAMSEDELACSPYIPLGGDFGGGDFGGGDFGG 120
Q96IP4-2|FAM46A_HUMAN --MHQRYFWTDQGQVALGGHYMAEGEGYFAMSEDELACSPYIPLGGDFGGGDFGGGDFGG 58
Q96IP4|FAM46A_HUMAN MAEGEGYFAMSEDELACSPYIPLGGDFGGGDFGGGDFGG 39
Q96A09|FAM46B_HUMAN MMPSESGAER-----RDRAAAQ----VGTAAATA-VATA 29
Q5VWP2|FAM46C_HUMAN
Q8NEK8|FAM46D_HUMAN
D3Z5S8|FAM46A_MOUSE --MHQRYFWTDQGQVAFGGHYMAEGEGYFAMAEDELTGCPYIPLGGDFGG---------- 48
Q5SSF7|FAM46C_MOUSE
Q8C152|FAM46B_MOUSE MMPSESGAES-----LEQPAAQ----VGTGAASA-VATA 29
B1ATX5|FAM46D_MOUSE
Q5TF85|FAM46A_HUMAN GDFGGGGSFGGHCLDYCESPTAHCNVLNWEQVQRLDGILSETIPIHGRGNFPTLELQPSL 180
Q96IP4-2|FAM46A_HUMAN GDFGGGGSFGGHCLDYCESPTAHCNVLNWEQVQRLDGILSETIPIHGRGNFPTLELQPSL 118
Q96IP4|FAM46A_HUMAN GDFGGGGSFGGHCLDYCESPTAHCNVLNWEQVQRLDGILSETIPIHGRGNFPTLELQPSL 99
Q96A09|FAM46B_HUMAN APAGG----GPDPEALSAFPGRHLSGLSWPQVKRLDALLSEPIPIHGRGNFPTLSVQPRQ 85
Q5VWP2|FAM46C_HUMAN ----------MAEESSCTRDCMSFSVLNWDQVSRLHEVLTEVVPIHGRGNFPTLEITLKD 50
Q8NEK8|FAM46D_HUMAN ----------MSEIRFTNLTWDQVITLDQVLDEVIPIHGKGNFPTMEVKPKD 42
D3Z5S8|FAM46A_MOUSE ----GGSSFGDRCSDYCESPTAHCNVLNWEQVQRLDGILSETIPIHGRGNFPTLELQPSL 104
Q5SSF7|FAM46C_MOUSE ----------MAEEGSSTKDSESFSVLNWDQVSRLHEVLTEVVPIHGRGNFPTLEITLKD 50
Q8C152|FAM46B_MOUSE GAAGG----GPDPEASSASLGRHQSRLSWPQVKRLDALLKEPIPIHGRGNFPTLSVQPQQ 85
B1ATX5|FAM46D_MOUSE ----------MSEIRFSNLTWDHIVTLDRVLHEVIPIHGRGNFPTLEVKPKD 42
PS50315
Q5TF85|FAM46A_HUMAN IVKVVRRRLAEKRIGVRDVRLNGSAASHVLHQDSGLGYKDLDLIFCADLRGEGEFQTVKD 240
Q96IP4-2|FAM46A_HUMAN IVKVVRRRLAEKRIGVRDVRLNGSAASHVLHQDSGLGYKDLDLIFCADLRGEGEFQTVKD 178
Q96IP4|FAM46A_HUMAN IVKVVRRRLAEKRIGVRDVRLNGSAASHVLHQDSGLGYKDLDLIFCADLRGEGEFQTVKD 159
Q96A09|FAM46B_HUMAN IVQVVRSTLEEQGLHVHSVRLHGSAASHVLHPESGLGYKDLDLVFRVDLRSEASFQLTKA 145
Q5VWP2|FAM46C_HUMAN IVQTVRSRLEEAGIKVHDVRLNGSAACHVLVKDNGLGCKDLDLIFHVALPTEAEFQLVRD 110
Q8NEK8|FAM46D_HUMAN IIHVVKDQLIGQGIIVKDARLNGSVASYILASHNGISYKDLDVIFGVELPGNEEFQVVKD 102
D3Z5S8|FAM46A_MOUSE IVKVVRRRLEEKGIGVRDVRLNGSAASHVLHQDSGLGYKDLDLIFCADLRGEEEFQTVKD 164
Q5SSF7|FAM46C_MOUSE IVQTVRGRLEEAGINVQDVRLNGSAACHVLVKDNGLGCKDLDLIFHVALPTEAEFQLVRD 110
Q8C152|FAM46B_MOUSE IVQVVRSSLEEHGLRVHSVRLHGSAASHVLHPESGLGYKDLDLVFQMDLRSEVSFQLTKA 145
B1ATX5|FAM46D_MOUSE IIHIVKDQLIKQGVVVKDTRLNGSTASYILASHNGISYKD---------- 82
Q5TF85|FAM46A_HUMAN VVLDCLLDFLPEGVNKEKITPLTLKEAYVQKMVKVCNDSDRWSLISLSNNSGKNVELKFV 300
Q96IP4-2|FAM46A_HUMAN VVLDCLLDFLPEGVNKEKITPLTLKEAYVQKMVKVCNDSDRWSLISLSNNSGKNVELKFV 238
Q96IP4|FAM46A_HUMAN VVLDCLLDFLPEGVNKEKITPLTLKEAYVQKMVKVCNDSDRWSLISLSNNSGKNVELKFV 219
Q96A09|FAM46B_HUMAN VVLACLLDFLPAGVSRAKITPLTLKEAYVQKLVKVCTDSDRWSLISLSNKSGKNVELKFV 205
Q5VWP2|FAM46C_HUMAN VVLCSLLNFLPEGVNKLKISPVTLKEAYVQKLVKVCTDTDRWSLISLSNKNGKNVELKFV 170
Q8NEK8|FAM46D_HUMAN AVLDCLLDFLPKDVKKEKLSPDIMKDAYVQKLVKVCNGHDCWSLISLSNNTGKNLELKFV 162
D3Z5S8|FAM46A_MOUSE VVLDCLLDFLPEGVNKEKITPLTLKEAYVQKMVKVCNDSDRWSLISLSNNSGKNVELKFV 224
Q5SSF7|FAM46C_MOUSE VVLCSLLNFLPEGVNKLKISPVTLKEAYVQKLVKVCTDTDRWSLISLSNKNGRNVELKFV 170
Q8C152|FAM46B_MOUSE VVLACLLDFLPAGVSRAKITPLTLKEAYVQKLVKVCTDLDRWSLISLSNKSGKNVELKFV 205
B1ATX5|FAM46D_MOUSE

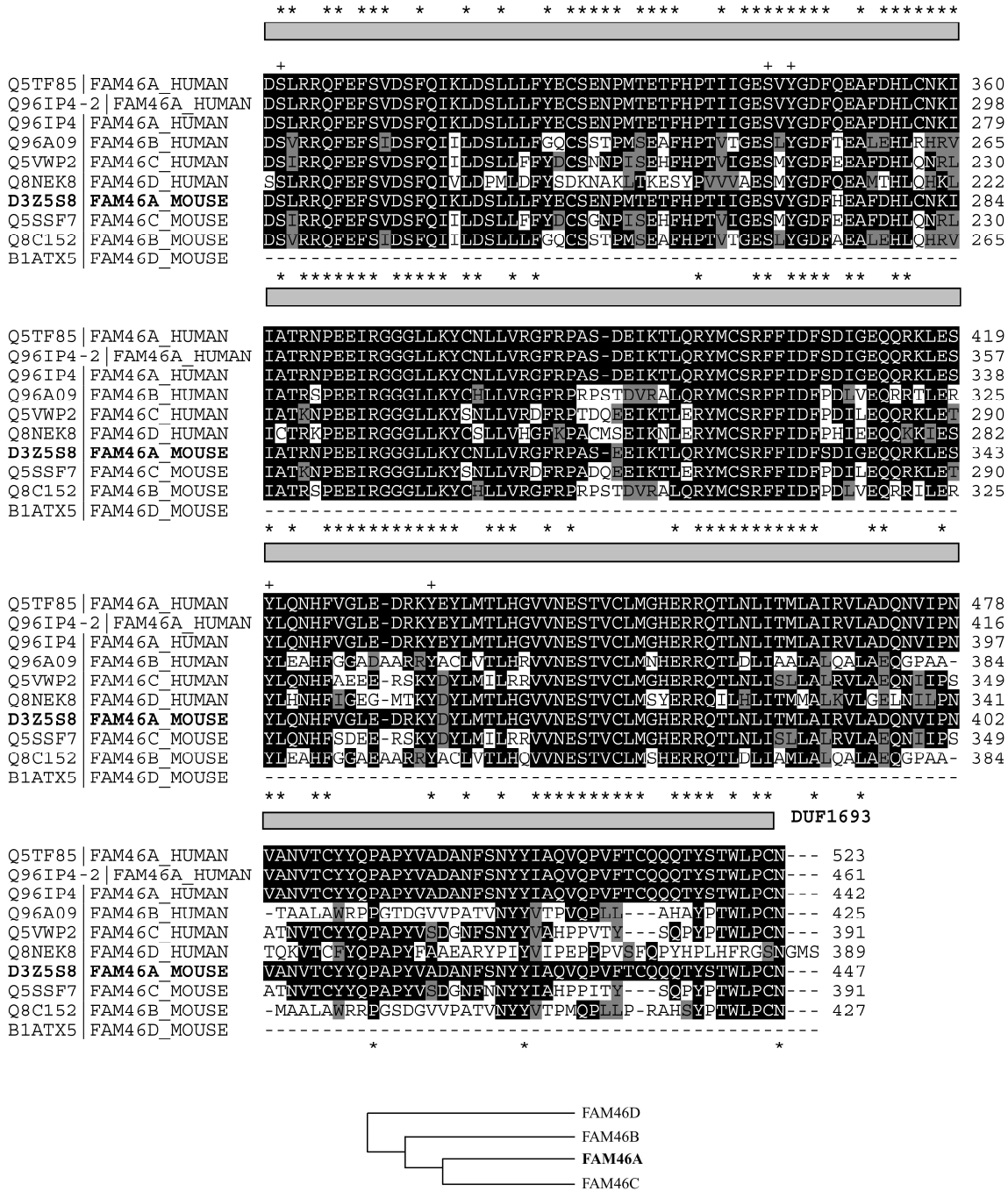

Figure 22: Sequence alignment of the FAM46 family of human and mouse protein members. The amino acid sequences of the human and mouse FAM46 family members were aligned using CLUSTAL O program (version 1.2.1). Three different isoforms of the human FAM46A protein are shown (Uniprot ID: Q5TF85 length 523 AA, Q96IP4-2 length 461 AA and Q96IP4 length 442 AA). Hyphens represent gaps within the alignment. Identical amino acid residues are represented on a black background and conservative amino acid substitutions are grey-shaded. Amino acid residues identical in all four FAM46 family members in humans and mice are marked with asterisks ("*"). The identified nonsense mutation (p.Glu157*) is designated with an exclamation mark ("!"). Predicted phosphorylation sites (NetPhos 2.0) identified in all four FAM46 family members are labelled with crosses ("+") at the top of the alignment. The PS50315 domain encoded by VNTRs is marked with a stripped bar under the alignment. The light grey bar under the alignment represents the dimension of the predicted domain of unknown function 1693 (DUF1693). A guide tree of the four FAM46 family members is depicted on the bottom of the alignment.

3.3. SMALL-MOLECULE COMPOUND SCREENING TO DISCOVER REGULATORS OF FGF23 SIGNALLING

HTS is a popular method for discovering small molecules as starting points for drug discovery purposes (Macarron et al., 2011). In cooperation with ADSP (Helmholtz Zentrum München), a method has been developed to identify novel small-molecule compounds that regulate FGF23/FGFR1c/Klotho signalling by monitoring the phosphorylation status of ERK1/2 in a HTS approach.

3.3.1. Development of a Cell Model: FGF23-Inducible HEK293-KL Cells

3.3.1.1. Stable Expression of Klotho in HEK293 Cells

First of all, a cell system of FGF23-inducible HEK293 cells that stably express Klotho was established (Figure 23).

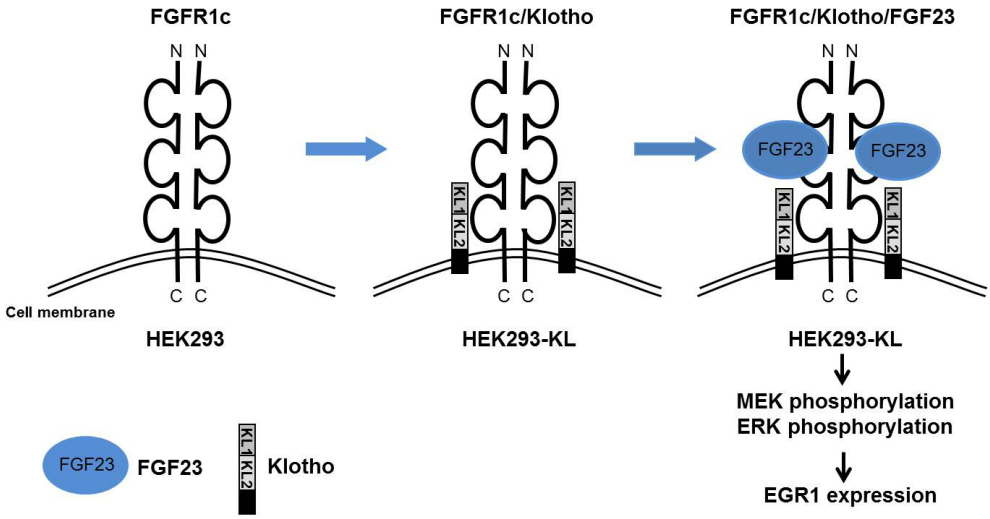

Figure 23: Schematic model of FGF23-inducible HEK293 cells stably expressing Klotho (HEK293-KL cells).

For this, HEK293 human embryonic kidney cells, which endogenously express detectable levels of FGFR1c (data not shown) but no detectable levels of Klotho (Figure 24), were stably transfected with an expression plasmid encoding the full length human *KLOTHO* cDNA (pcDNA3.1/*KLOTHO*/*myc*-His). Stable transfectants were selected over a time period of four weeks for the resistance to Geneticin (1,000 µg/ml). Cell clones were picked, expanded and expression of Klotho was confirmed by Western blot analysis using antibodies against human Klotho and the C-terminal His-tag of the fusion protein Klotho/myc-His (Figure 24).

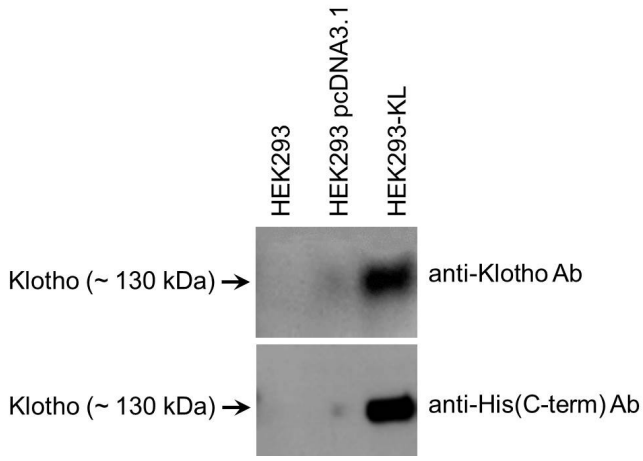

Figure 24: Stable expression of human Klotho in HEK293 cells (HEK293-KL cells). 10 µg of whole cell lysate of non-transfected HEK293 cells, of cells transfected with the pcDNA3.1/*myc*-His(-) B vector control and of cells transfected with pcDNA3.1/*KLOTHO*/*myc*-His was loaded on 4 - 20% SDS PAGE and subjected to immunoblotting using antibodies against human Klotho and the C-terminal His-tag.

HEK293 cells that stably expressed Klotho were designated "HEK293-KL" cells, and two different HEK293-KL cell clones (clone D1 and D4) with adequate levels of Klotho expression were utilised for further experiments.

3.3.1.2. Induction of HEK293-KL Cells with FGF23

Upon binding of FGF23 to the receptor complex FGFR1c/Klotho, MAPK signalling cascade is activated resulting in the phosphorylation of MEK1/2 and ERK1/2 and an increased expression of downstream targets, e.g. EGR1 (Figure 23). To test whether our obtained HEK293-KL cell clones are FGF23-inducible, induction experiments were performed using a mutant form of recombinant human FGF23 (FGF23R179Q), which is known to be resistant to proteolytic cleavage and is broadly used as a tool to study FGF23 signalling (Saito et al., 2003). As a positive control, recombinant human basic FGF (bFGF) was utilised, which binds with high affinity to all four FGFRs without the need of the co-receptor Klotho (Ornitz and Itoh, 2001; Ornitz et al., 1996). Non-transfected HEK293 cells, HEK293 cells transfected with the vector control and HEK293-KL cells (clone D1 and D4) were treated with bFGF (10 ng/ml) or FGF23R179Q (0 - 100 ng/ml) for 20 min. Afterwards, whole cell lysates were loaded on 10% SDS-PAGE and Western blotting was performed with antibodies against total ERK1/2 (used as loading control) and against the phosphorylated form of ERK1/2 (p-ERK1/2) to demonstrate the early activation of MAPK signalling pathway (Figure 25).

HEK293-KL cells were FGF23-inducible, in contrast to non-transfected parental HEK293 cells and HEK293 cells only transfected with the vector control, which showed no signal for p-ERK1/2. The induction of HEK293-KL cell clones with FGF23 was concentration-dependent and displayed slight differences between the investigated cell clones. For all following induction experiments, we decided to use a final FGF23R179Q concentration of 100 ng/ml.

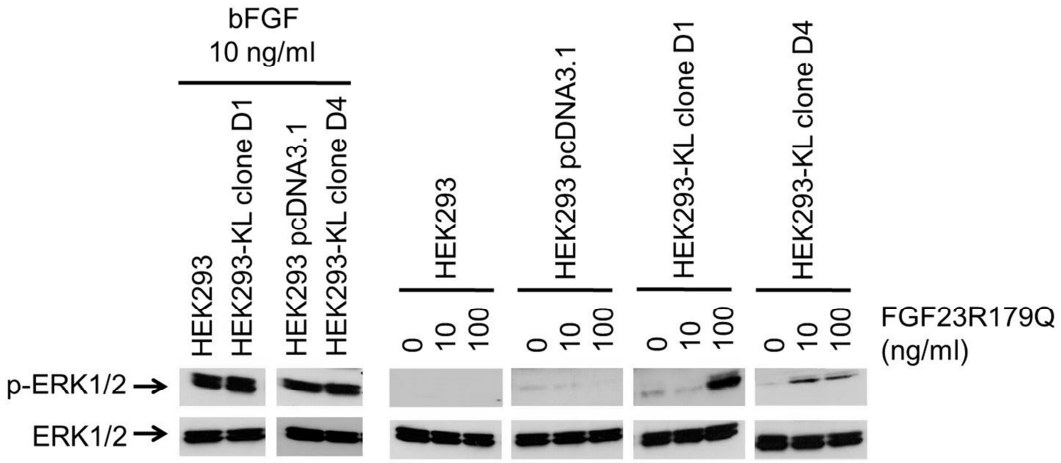

Figure 25: HEK293-KL cells are FGF23-inducible. Increasing levels of the mutant form of human FGF23 (FGF23R179Q) enhance p-ERK1/2 in HEK293-KL cells (clone D1 and D4) but not in non-transfected cells or cells transfected with the pcDNA3.1/*myc*-His(-) B vector control. FGF basic (bFGF), which binds with high affinity to FGF receptors, was utilised as a positive control. Cells were stimulated for 20 min. Western blot was performed with antibodies against p-ERK1/2 and total ERK1/2 (44/42 kDa).

Additionally, the differential expression of the transcription factor EGR1 was analysed. HEK293-KL cells (clone D1 and D4) were treated with FGF23R179Q overnight. An antibody against EGR1 was used to demonstrate its expression by Western blot analysis (Figure 26).

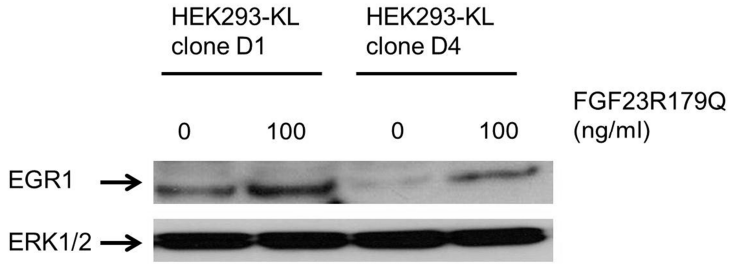

Figure 26: FGF23R179Q enhances the expression of EGR1 in HEK293-KL cells. Total ERK1/2 was used as loading control.

Similar to the results for p-ERK1/2, an increase in the signal for EGR1 was detectable after the induction with FGF23R179Q. This indicated that the induction not only activated early stages in FGF23/FGFR1c/Klotho signalling (phosphorylation of ERK1/2) but also later ones (increased expression of EGR1).

3.3.1.3. Effect of Small-Molecule Compounds on the Cell Model

In order to study whether the induction of HEK293-KL cells with FGF23R179Q can be reduced by small-molecule compounds, the effect of two known inhibitors of MAPK signalling pathway was investigated: SU5402 and U0126 (Shalhoub et al., 2011) (Figure 27).

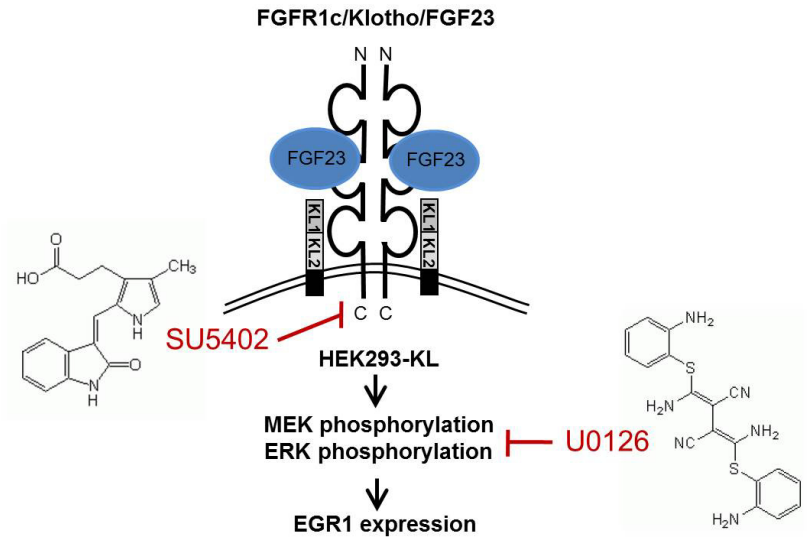

Figure 27: Inhibitors affecting the induction of FGFR1c/Klotho signalling pathway in HEK293-KL cells. SU5402 interacts with FGFR1. U0126 is a specific inhibitor of MEK1/2 in MAPK signalling pathway.

SU5402 is a cell-permeable, reversible and ATP-competitive inhibitor of the tyrosine kinase activity of FGFR1 by interacting with its catalytic domain (Mohammadi et al., 1997). U0126 is a potent and specific inhibitor of MEK1/2. The inhibition is non-competitive with respect to MEK substrates (Favata et al., 1998).

HEK293-KL cells (clone D1 and D4) were incubated with SU5402 or U0126 in serum-free medium for 1 h and were then stimulated with bFGF (10 ng/ml) or FGF23R179Q (100 ng/ml) for 20 min. Two different concentrations were used for each small-molecule inhibitor. Immunoblotting was conducted with antibodies against p-ERK1/2 and total ERK1/2 (Figure 28).

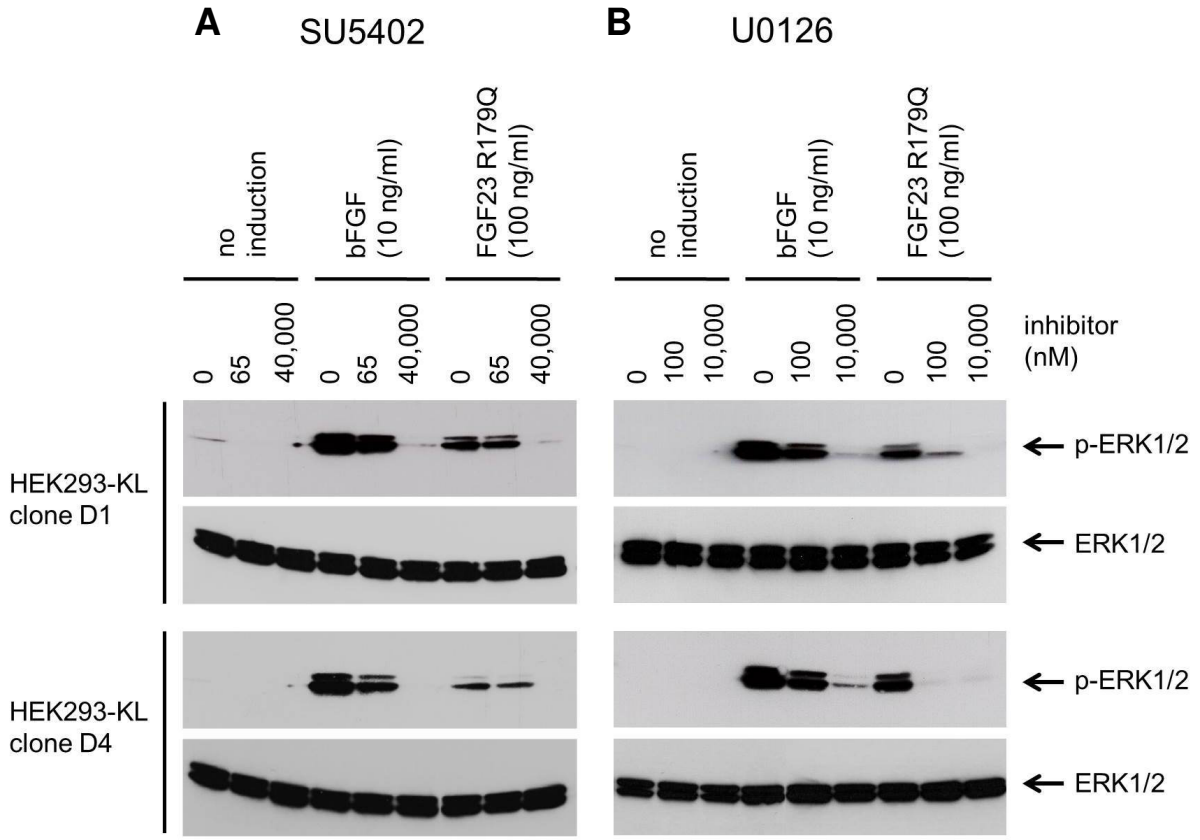

Figure 28: FGFR1 inhibitor SU5402 (A) and MEK1/2 inhibitor U0126 (B) reduce activation of MAPK signalling pathway in FGF23-induced HEK293-KL cells. Inhibitor alone and bFGF served as controls. Cell lysates were analysed by Western blot using antibodies against p-ERK1/2 and total ERK1/2.

Both inhibitors reduced the activation of MAPK signalling after the induction with bFGF or FGF23R179Q in a concentration-dependent manner.

Taken together, an *in vitro* model of FGF23-inducible HEK293-KL cells has been successfully established. This cell model is suited to investigate the effect of small-molecule compounds on FGF23 signalling.

3.3.1.4. A Comprehensive Transcriptome Analysis of HEK293-KL Cells after the Induction with FGF23

To further define and validate our established cell model on a gene expression level, we performed transcriptome analysis. The "transcriptome" encompasses the complete set and quantity of transcripts in a cell for a specific developmental stage or physiological condition (Wang et al., 2009). Genome-wide transcriptional changes in HEK293-KL cells (clone D1) specifically caused by FGF23 were defined by comparing the transcriptome of FGF23-induced HEK293-KL cells with the transcriptome of uninduced HEK293-KL cells. Before

total RNA was isolated, HEK293-KL cells were stimulated with FGF23R179Q for 1 h. Untreated HEK293-KL cells served as a control. We made use of the technology of RNA-Seq, which is a massively parallel sequencing approach to allow genome-wide analysis of gene expression profiles at a far higher resolution than is available with microarray-based methods (Sultan et al., 2008; Wang et al., 2009). Pooled indexed paired-end libraries were prepared with the Illumina TruSeq RNA Sample Preparation kit according to the manufacturer's protocol. RNA-Seq was performed on a HiSeq2000 system (Illumina).

In this study, the R package DESeq (Anders and Huber, 2010) was utilised for variance estimation, normalisation and finding differentially expressed transcripts. The results are depicted in the scatter plot below (Figure 29).

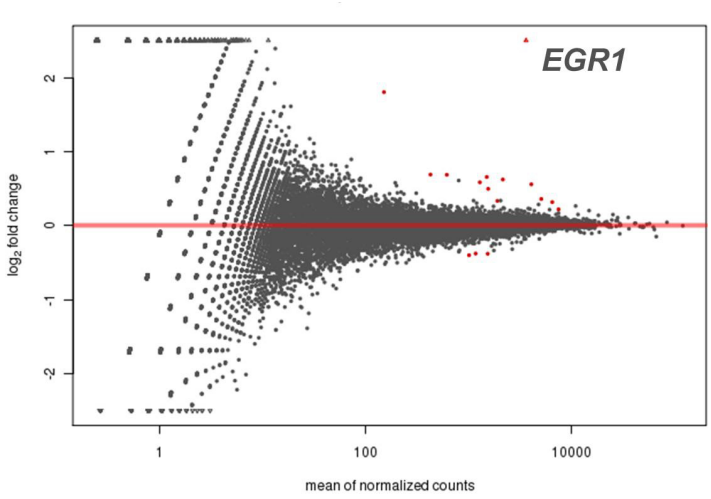

Figure 29: Scatter plot of differentially expressed transcripts. Each data point stands for a single transcript. The y-axis typifies the $\log_2$ fold change of transcript expression between the two conditions, FGF23-induced HEK293-KL cells and untreated HEK293-KL cells. The x-axis represents the mean of the normalised read counts. Red coloured markers indicate differentially expressed transcripts that are significant at 10% false discovery rate (FDR).

We identified 20 transcripts showing significant difference in expression between the two conditions (treated and untreated HEK293-KL cells, n = 3): 17 were significantly up- and three significantly downregulated (Table 6).

Table 6: Significant transcriptome-wide changes in HEK293-KL cells after the induction with FGF23.

Gene symbol	Location (hg19)	log_2 fold change	*p*-value	Regulation
EGR1	chr5:137,801,180-137,805,004	4.52	5.9637E-33	up
GPR3	chr1:27,719,147-27,722,317	2.13	8.8190E-06	up
c-FOS	chr14:75,745,480-75,748,937	1.81	8.2044E-12	up
DUSP5	chr10:112,257,624-112,271,302	1.12	5.3766E-08	up
OLIG2	chr21:34,398,215-34,401,503	1.02	1.1584E-06	up
SPRY2	chr13:80,910,111-80,915,086	0.69	1.2557E-06	up
CTGF	chr6:132,269,316-132,272,518	0.69	5.8682E-05	up
DUSP1	chr5:172,195,092-172,198,203	0.66	1.9855E-05	up
BHLHE40	chr3:5,021,096-5,026,865	0.62	7.0138E-14	up
IER2	chr19:13,261,281-13,265,718	0.59	2.3731E-08	up
TRIB1	chr8:126,442,562-126,450,644	0.56	5.3624E-07	up
OTUD1	chr10:23,728,197-23,731,310	0.50	1.4676E-09	up
PMAIP1	chr18:57,567,191-57,571,538	0.36	6.0596E-10	up
HES1	chr3:193,853,930-193,856,401	0.34	2.4050E-04	up
RGS16	chr1:182,567,757-182,573,548	0.33	1.0072E-05	up
ADAMTS1	chr21:28,208,605-28,217,728	0.32	3.9228E-08	up
SOX4	chr6:21,593,971-21,598,849	0.22	3.7938E-05	up
GOLGA8A	chr15:34,671,269-34,729,667	-0.38	8.8712E-06	down
HERC2P2	chr15:23,282,264-23,378,259	-0.38	7.7438E-07	down
GOLGA8B	chr15:34,817,483-34,875,771	-0.40	8.5163E-06	down

Data are presented based on the ranking of log_2 fold change. hg19 = human genome assembly GRCh37, UCSC; EGR1 = early growth response 1; GPR3 = G protein-coupled receptor 3; c-FOS = FBJ murine osteosarcoma viral oncogene homologue; DUSP5 = dual specificity phosphatase 5; OLIG2 = oligodendrocyte lineage transcription factor 2; SPRY2 = sprouty homologue 2; CTGF = connective tissue growth factor; DUSP1 = dual specificity phosphatase 1; BHLHE40 = basic helix-loop-helix family, member e40; IER2 = immediate early response 2; TRIB1 = tribbles pseudokinase 1; OTUD1 = OTU deubiquitinase 1; PMAIP1 = phorbol-12-myristate-13-acetate-induced protein 1; HES1 = hes family bHLH transcription factor 1; RGS16 = regulator of G protein signalling 16; ADAMTS1 = ADAM metallopeptidase with thrombospondin type 1 motif, 1; SOX4 = SRY (sex determining region Y)-box 4; GOLGA8A = golgin A8 family, member A; HERC2P2 = hect domain and RLD 2 pseudogene 2; GOLGA8B = golgin A8 family, member B

Among the identified transcripts, the expression of a group of transcription factors and immediate early response genes was elevated in HEK293-KL cells after the induction with FGF23 (*EGR1*, *c-FOS*, *DUSP5*, *OLIG2*, *CTGF, DUSP1*, *BHLHE40, IER2*, *PMAIP1, HES1*, *ADAMTS1*, *SOX4*). Moreover, FGF23 increased the expression of genes involved in MAPK signalling and its regulation (*EGR1*, *c-FOS*, *DUSP5*, *SPRY2*, *DUSP1*, *TRIB1*, *PMAIP1*). For three transcripts, a direct link to FGF23 has already been described in animal models: *Egr1* (Farrow et al., 2010), *Adamts1* (Hu et al., 2013a) and *Dusp5* (Roman-Garcia et al., 2012).

To determine interactions between the identified transcripts, we used Genomatix Pathway System (GePS). Connections are demonstrated in a "Simple Network" on a "Function Word Level" (Figure 30).

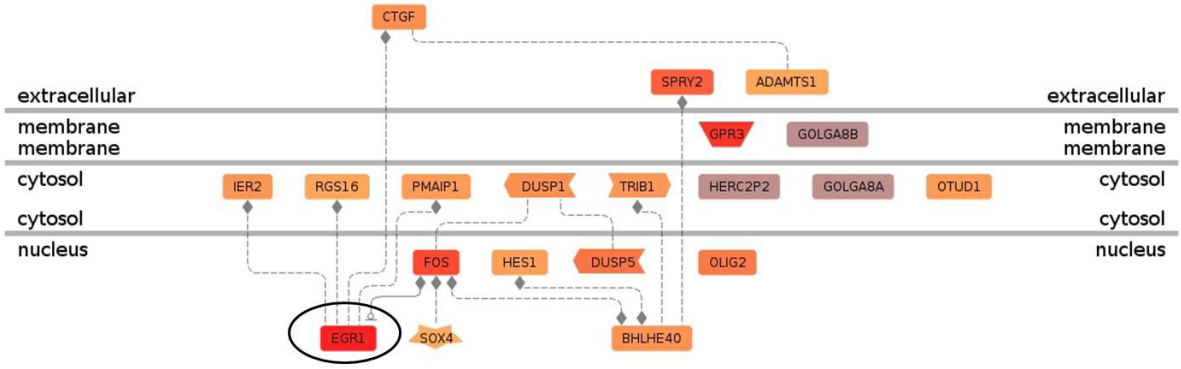

Figure 30: Prediction of interactions between the identified transcripts by Genomatix Pathway System (GePS). Connections are demonstrated in a "Simple Network" on a "Function Word Level". Upregulated transcripts are orange/red (darker colour indicates higher expression), downregulated ones are purple. *EGR1* is marked with a black circle.

Among the 17 significantly upregulated transcripts, *EGR1* was the most upregulated one (Figure 29) confirming our results from Western blot analysis (Figure 26). Pathway analysis highlighted *EGR1* to be of central importance as an FGF23-responsive target gene. It is predicted to have a binding site in the promoter region of four other genes (*IER2*, *RGS16*, *CTGF* and *PMAIP1*) that showed a significantly enhanced expression in HEK293-KL cells after the induction with FGF23 (Figure 30; modulation of gene expression is indicated as hash key).

In conclusion, we could confirm our results from Western blot analysis, proposing that MAPK signalling pathway is mainly activated in HEK293-KL cells after the induction with FGF23. This leads to an increased expression of several FGF23-responsive target genes, among which *EGR1* seems to have an enormous significance.

Hence, our well-defined cell model of FGF23-inducible HEK293-KL cells was ready for the establishment of reporter assays applicable for HTS to identify small-molecule compounds with an influence on FGF23 signalling.

3.3.2. Establishment of Cell-Based Reporter Assays

The following steps were conducted in cooperation with ADSP.

3.3.2.1. Establishment of the Primary Screening Assay

The primary cell-based reporter assay was adapted from the AlphaScreen SureFire p-ERK1/2 technology from PerkinElmer. It allows the detection of p-ERK1/2 in cellular lysates by the formation of sandwich antibody complexes, which are captured by AlphaScreen donor and acceptor beads. This triggers a cascade of energy transfer resulting in light emission. The intensity of light emission, referred to as "Alpha signal (counts)", is proportional to ERK1/2 phosphorylation. We applied this assay format to monitor the activation of MAPK pathway in HEK293-KL cells (clone D1) after the induction with FGF23.

To make the primary assay suitable for HTS approaches, a number of different configurations had to be optimised:

(1) 384-well plates: We aimed to perform our screening in a miniaturised format in 384-well plates. As best suited plates for the automated screening process, OptiPlates from PerkinElmer were determined.
(2) Coating of plates: Coating of plates with poly-D-lysine increased cell adherence and simplified assay performance before cell lysis.
(3) Cell density: Adherent HEK293-KL cells were seeded at cell densities between 5,000 cells/well and 20,000 cells/well and were cultivated at 37 °C in a cell culture incubator for 24 h. At a cell density of 13,000 cells/well, cells grew in a confluent monolayer, which was optimal for the assay. When confluent, many signalling pathways like MAPK signalling pathway can become quiescent and synchronised (Vinals and Pouyssegur, 1999). After stimulation with FGF23, the cells can respond uniformly.
(4) Concentration of FGF23: The best concentration of FGF23 to induce HEK293-KL cells in the AlphaScreen SureFire p-ERK1/2 assay was examined by stimulating cells with increasing concentrations of FGF23R179Q for 20 min (Figure 31). We obtained

an EC_{50} value of ~ 110 ng/ml. According to our previous results from induction experiments (see section 3.3.1.2), a concentration of 100 ng/ml seemed to be appropriate, since it allowed to detect modulations of the Alpha signal in both directions (big signal window).

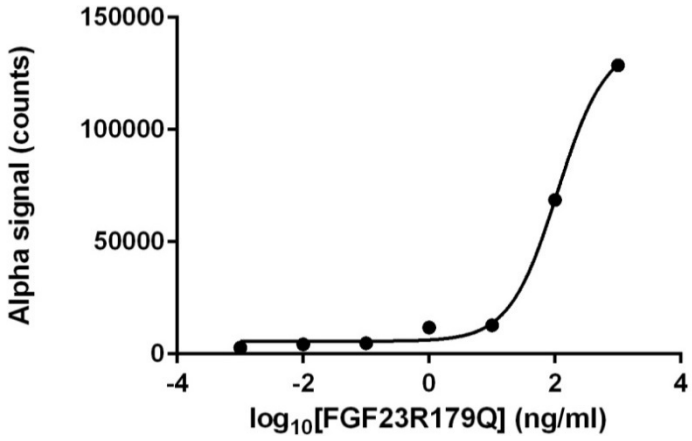

Figure 31: Concentration profile of FGF23. HEK293-KL cells were stimulated with different concentrations of FGF23R179Q (0.001 - 1,000 ng/ml) for 20 min. Induction was measured with the AlphaScreen SureFire p-ERK1/2 technology from PerkinElmer by monitoring the phosphorylation of ERK1/2 in cellular lysates, which is depicted as Alpha signal (counts). Data are expressed as the mean ± SD (n = 3). The activation curve is drawn up by plotting the Alpha signal (counts) versus the decadic logarithm of the concentration of FGF23R179Q. We obtained an EC_{50} value of 109.6 ng/ml.

(5) Stimulation time with FGF23: Significant changes in the phosphorylation status of ERK1/2 were detectable in HEK293-KL cell lysates after stimulation with FGF23R179Q for 20 min, 40 min and 60 min (Figure 32). Already after 20 min, the cells were strongly stimulated and the signal remained stable over time.

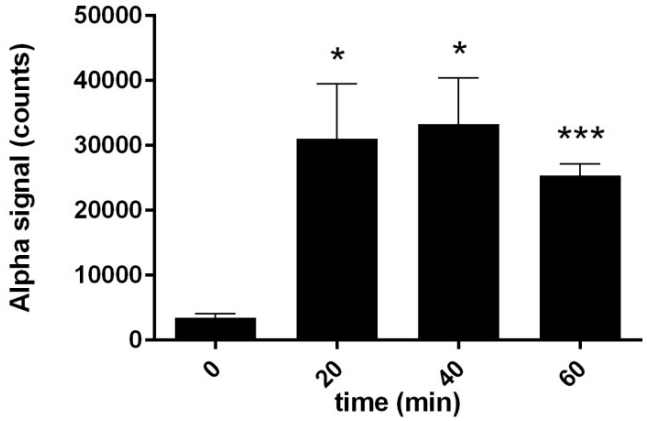

Figure 32: Time course study of the effects of inducing HEK293-KL cells with FGF23R179Q (100 ng/ml) for 0 min, 20 min, 40 min and 60 min. Bars represent the mean ± SD (n = 3). Significance was determined with the unpaired Student's *t*-test (* $p < 0.05$, *** $p < 0.001$; compared to 0 min stimulation with FGF23R179Q).

To identify small molecules, which act in the very early phase of the FGF23-dependent MAPK signalling, and to avoid effects that were produced due to feedback loops in the signalling cascade, we chose a stimulation time of 20 min for further experiments.

(6) Specificity of the assay: In addition, we could confirm that our assay detected an increase of the Alpha signal only in HEK293-KL cells and not in the parental HEK293 cell line after the induction with FGF23. Without FGF23, just a cellular background (basal activation of MAPK pathway) was detectable in HEK293 and HEK293-KL cells (Figure 33).

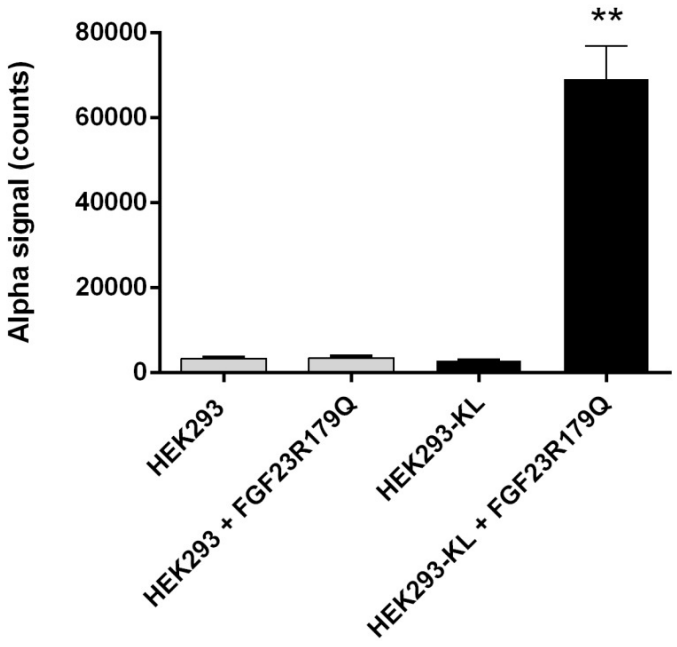

Figure 33: Specificity of the developed primary screening assay. HEK293 cells (grey bars) and HEK293-KL cells (black bars) were either not treated or treated with FGF23R179Q (100 ng/ml) for 20 min. AlphaScreen SureFire assay was performed for all samples (n = 3). Shown are the mean ± SD values. Significance was determined with the unpaired Student's *t*-test (** $p < 0.01$).

(7) DMSO compatibility: Dimethyl sulfoxide (DMSO) is routinely used as solvent for compound libraries. To check whether DMSO reduced the sensitivity of our assay by decreasing the signal maximum, HEK293-KL cells were incubated with a final volume concentration of 0%, 1%, 2% and 5% DMSO for 1 h and were then induced by FGF23R179Q (100 ng/ml) for 20 min. In comparison to 0% DMSO, the Alpha signal was significantly reduced for a volume concentration of 2% or higher (Figure 34). In our case, small-molecule compounds screens were carried out with a final

volume concentration of 0.8% DMSO, assuming that it caused no significant reduction of the assay performance.

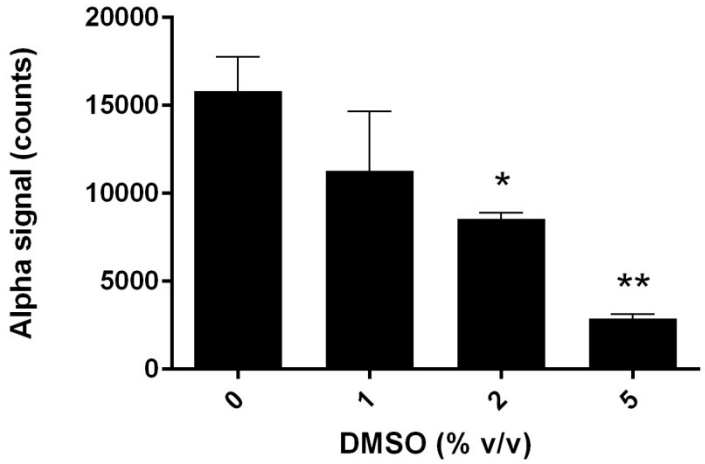

Figure 34: Tolerance to DMSO. Increasing volume concentrations (% v/v) of DMSO were added to the cells 1 h before induction with FGF23R179Q (100 ng/ml) for 20 min and assay performance. The mean ± SD (n = 3) of the data is displayed. Significance was determined with the unpaired Student's *t*-test (* $p < 0.05$, ** $p < 0.01$; versus volume concentration of 0% DMSO).

(8) Small-molecule compounds: We investigated the applicability of the developed assay for identifying small-molecule compounds that modulate the effect of FGF23 signalling. For this, we utilised the known small-molecule inhibitors SU5402 and U0126 (Figure 27, Figure 28). HEK293-KL cells were incubated with increasing inhibitor concentrations (0.1 - 100 µM) for 1 h and were then stimulated with FGF23R179Q (100 ng/ml) for 20 min (Figure 35).

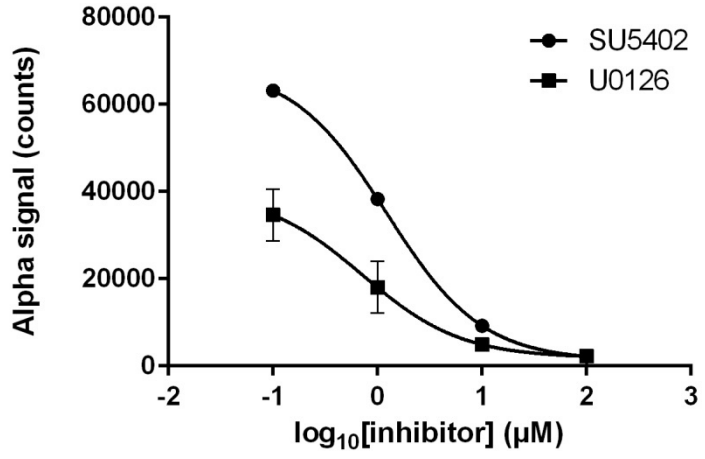

Figure 35: Concentration profile of the inhibitors SU5402 (●) and U0126 (■). After an incubation with increasing inhibitor concentrations (0.1 - 100 µM) for 1 h, HEK293-KL cells were stimulated with FGF23R179Q (100 ng/ml) for 20 min. The data are expressed as the mean ± SD (n = 3). Inhibition curves are drawn up by plotting the Alpha signal (counts) versus the decadic logarithm of the inhibitor concentrations. IC_{50} values were 1.23 µM for SU5402 and 0.72 µM for U0126.

We obtained a concentration-dependent reduction of the Alpha signal with IC_{50} values of 1.23 µM (SU5402) and 0.72 µM (U0126), suggesting that our assay is adequate for compound screens.

(9) Automation of the screening process: Finally, the assay procedure was automatised using the liquid handling workstation and robotics at ADSP. Inter-plate and inter-day tests in automation mode were conducted to minimise variation. We assessed the suitability of our assay for HTS by calculating performance measures: Z' factor, signal window (SW) and coefficient of variation (CV). All criteria exceeded the minimum pass criteria for HTS: Z' > 0.5, SW > 2 and CV < 20% (Iversen et al., 2004; Schorpp et al., 2013; Zhang et al., 1999) indicating an excellent assay performance and robustness (Figure 36).

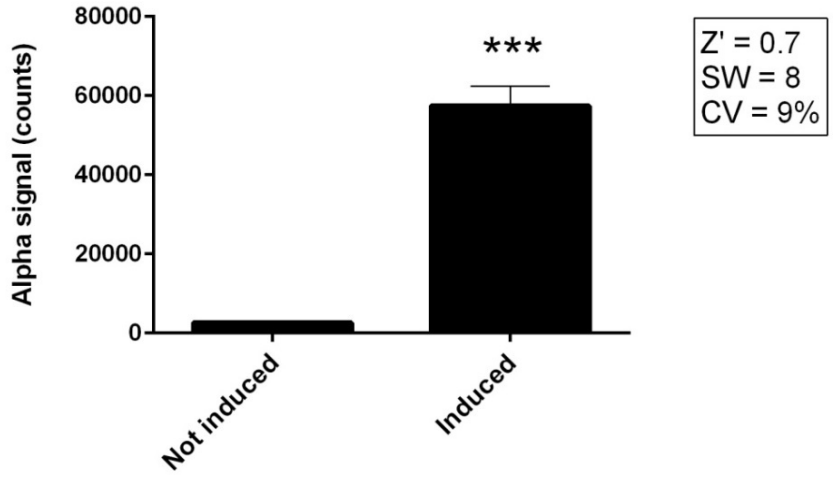

Figure 36: Automation of the screening process. HEK293-KL cells were either not treated or induced with FGF23R179Q (100 ng/ml) for 20 min. Data are shown as the mean ± SD (n = 288). Significance was determined with the unpaired Student's *t*-test (*** $p < 0.001$).

3.3.2.2. Establishment of the Secondary Screening Assay

In parallel, a secondary assay for the validation phase was generated using the Cisbio HTRF Cellul'erk p-ERK1/2 platform. It similarly measures p-ERK1/2 in lysates of HEK293-KL cells, but makes use of another technology for detection. It uses a TR-FRET sandwich immunoassay format containing two specific monoclonal anti-ERK1/2 antibodies, one labelled with Eu^{3+}-cryptate (donor; 620 nm) and the other labelled with d2 (acceptor; 665 nm). The "HTRF Ratio" (HTRF emission $_{665\ nm}$/HTRF emission $_{620\ nm}$ x 10^4) is proportional to substrate phosphorylation.

The assay was set up in a comparable manner as the primary assay. We maintained most of the established configurations: Before assay performance, HEK293-KL cells were seeded in coated OptiPlates (13,000 cells/well), cultivated for 24 h and then stimulated with FGF23R179Q (100 ng/ml) for 20 min. The assay was highly specific, as it detected a significant increase of p-ERK1/2 levels only in lysates of HEK293-KL cells after an induction with FGF23R179Q (Figure 37).

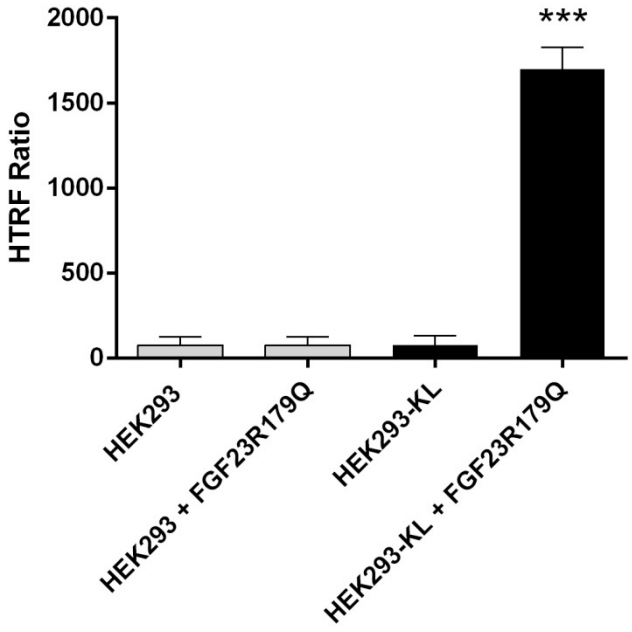

Figure 37: Establishment of a secondary cell-reporter assay based on the HTRF Cellul'erk technology from Cisbio. HEK293 cells (grey bars) or HEK293-KL cells (black bars) were either uninduced or induced with FGF23R179Q (100 ng/ml) for 20 min. Data are expressed as the mean of the HTRF Ratio ± SD (n = 3). Significance was calculated with the unpaired Student's *t*-test (*** $p < 0.001$).

Moreover, we investigated the DMSO tolerance of the secondary assay and obtained similar results as in the primary assay: There was no significant reduction of the HTRF Ratio measurable for a final DMSO volume concentration smaller than 2% (Figure 38). Consequently, the secondary assay was also applicable to screen small molecules with a final DMSO volume concentration of 0.8%.

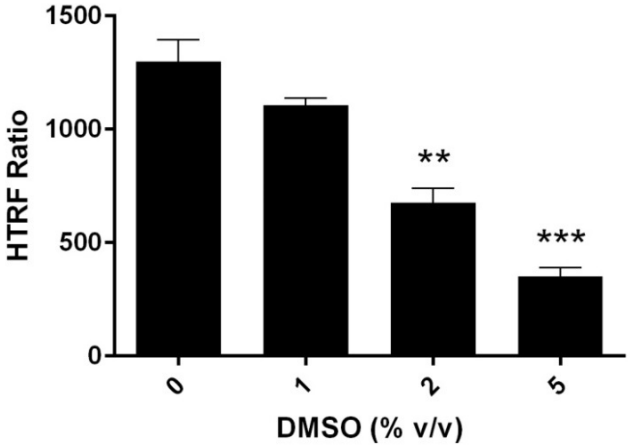

Figure 38: DMSO tolerance of the secondary assay. Tolerance was investigated by increasing final volume concentrations (% v/v) of DMSO. HEK293-KL cells were incubated for 1 h with DMSO and were then induced by FGF23R179Q (100 ng/ml) for 20 min followed by assay performance. The mean ± SD (n = 3) of the data is displayed. Significance was determined with the unpaired Student's *t*-test (** $p < 0.01$; versus volume concentration of 0 % DMSO).

As we aimed to screen small-molecule compounds at a final concentration of 8 µM, we analysed the effect of the known FGFR1 inhibitor SU5402 on our second cell-reporter assay and could detect a significant reduction of the HTRF Ratio in presence of the inhibitor (Figure 39).

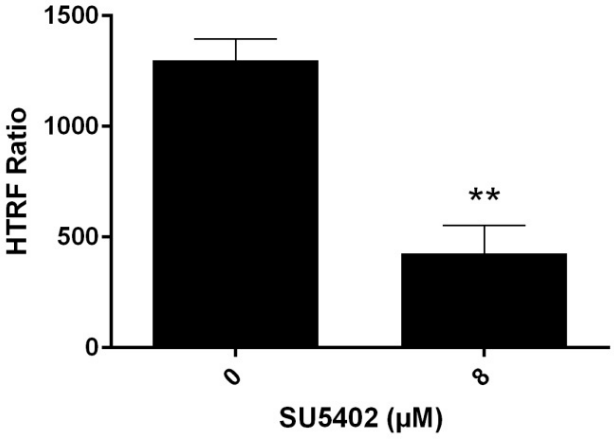

Figure 39: Effect of the FGFR1 inhibitor SU5402 on the phosphorylation of ERK1/2 in HEK293-KL cells after the induction with FGF23 (100 ng/ml) for 20 min. Data are shown as the mean of the HTRF Ratio ± SD (n = 3). Significance was determined with the unpaired Student's *t*-test (** $p < 0.01$).

For the secondary assay, no transfer to automation was required, since the assay format was only needed for the validation of some single candidate hits from the primary screening and not for entire compound libraries.

3.3.3. Pilot Screen of Small-Molecule Compounds and Hit Validation

In a pilot screen, we intended to yield important information about the anticipated number of hits and robustness of the established assays on the one hand, and to identify first compound candidates that interact with FGF23/FGFR1c/Klotho signalling in HEK293-KL cells on the other hand. Since serum levels of the phosphaturic factor FGF23 are elevated in most inherited hypophosphatemic disorders (Gattineni and Baum, 2012; Wagner et al., 2014b), we were highly interested in the identification of small-molecule compounds with an inhibitory action on FGF23 signalling.

As a small set of compounds, the Prestwick Chemical Library was analysed. This library contains 1,280 small molecules, which are 100% approved drugs (Food and Drug Administration (FDA), European Medicines Agency (EMA) and other agencies). Consequently, it presents a great degree of drug-likeliness. The active compounds were selected for their high chemical and pharmacological diversity as well as for their known bioavailability and safety in humans.

We conducted the screening using our developed primary AlphaScreen SureFire cell-reporter assay. HEK293-KL cells were incubated with the small-molecule compounds at a final concentration of 8 µM (n = 1) for 1 h and were then induced with FGF23R179Q (100 ng/ml) for 20 min followed by automated assay performance. During the screening process, the assay fulfilled all appropriate quality criteria (Z' > 0.5, SW > 2 and CV < 20%) indicating an excellent assay performance and robustness. Additionally, toxicity of all 1,280 compounds on HEK293-KL cells was examined with the CellTiter-Blue cell viability assay from Promega. Small-molecule compounds were nominated as candidate hits, if they fulfilled following conditions: (1) reduction of the Alpha signal by more than 40%, (2) low toxicity and (3) no frequent hitter in other AlphaScreens performed at ADSP. Frequent hitters are false positive hits ("inactives"), which are produced e.g. by optical interference with or inhibition of the detection system (Schorpp et al., 2013). After data analysis, 25 primary hits were nominated representing a hit rate of 2%. The identified compounds were reordered as powder at Prestwick Chemical. Selected compounds were prepared for serial dilutions and retested in 10-point-titrations (0.2 - 80 µM) on the primary AlphaScreen SureFire assay in triplicates to get a first idea about required concentrations of individual hit compounds (Figure 40).

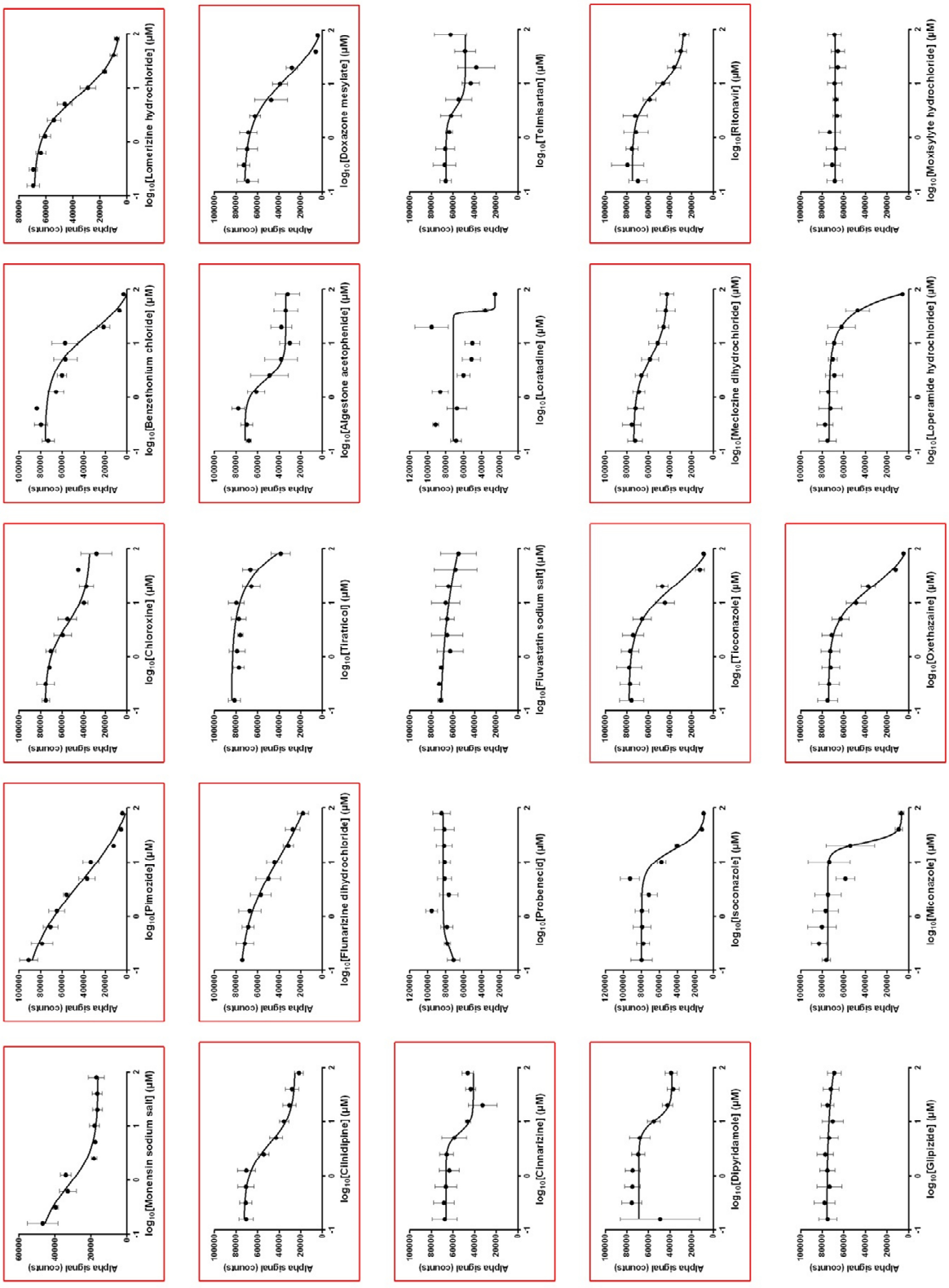

Figure 40: 10-point-titrations of the 25 candidate hits selected from Prestwick Chemical Library in the primary HTS using AlphaScreen SureFire technology. The data are expressed as the mean ± SD (n = 3). Shown are inhibition curves. Selected candidate hits are marked in red.

Thereof, we chose 15 compounds representing sigmoid inhibition curves and giving results with sufficient IC_{50} values in a micromolar range (Table 7). The selected compounds are designated in red in Figure 40 and are shown in higher magnification in Figure 41 .

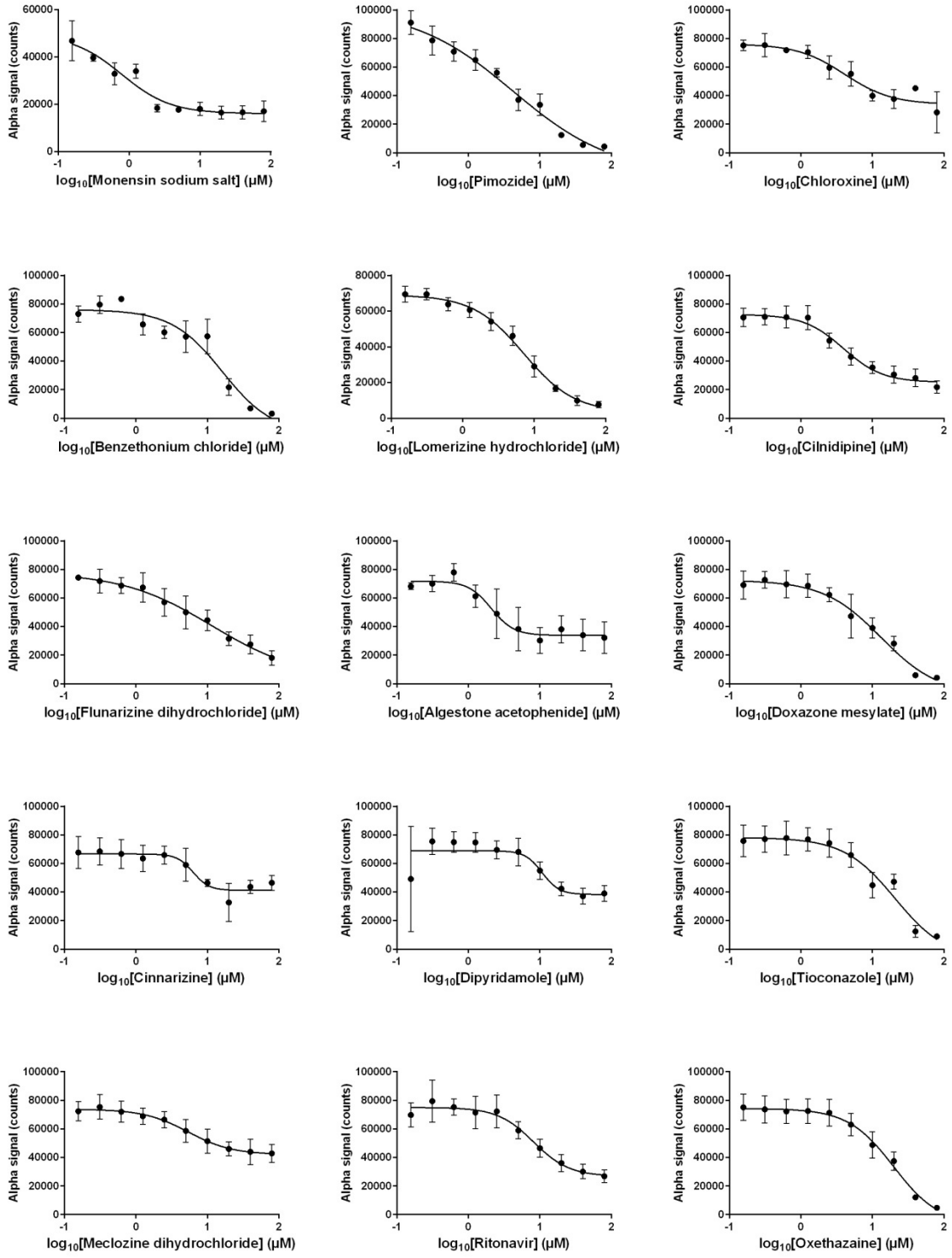

Figure 41: Selected candidate compounds from the retesting process on the primary screening assay.

The potential 15 candidate hits of the primary assay were then investigated with the secondary assay based on the Cisbio HTRF Cellul'erk technology. IC_{50} values were again determined by 10-point-titrations using the compound solutions of the freshly reordered solid samples (n = 1, Figure 42).

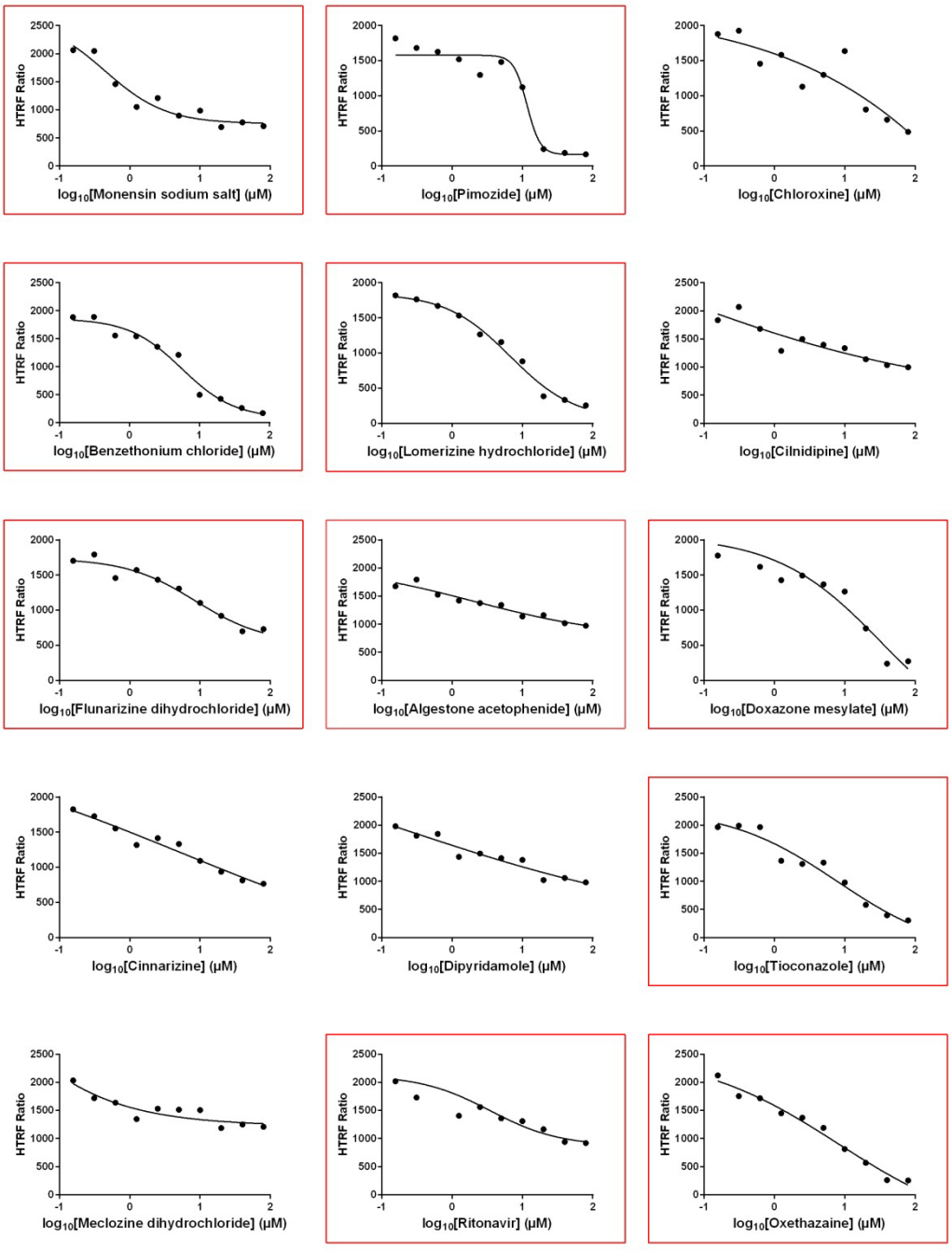

Figure 42: Retesting of 15 candidate small-molecule compounds on the secondary HTRF Cellul'erk cell-reporter assay. Shown are 10-point-titrations as inhibition curves (n = 1). The HTRF Ratio is proportional to the phosphorylation status of ERK1/2 in HEK293-KL cells after the induction with FGF23R179Q (100 ng/ml). Candidate hits chosen for further validation are marked in red.

Specific inhibitors should give similar inhibition curves for the primary and the secondary assay. This was true for ten compounds (Figure 42; marked in red). They represented sigmoid inhibition curves. The IC_{50} values ranged between 0.44 µM and 33.63 µM (Table 7).

Lastly, the modulatory action of the remaining ten compounds on FGF23/FGFR1c/Klotho signalling was tested in Western blot analysis (Figure 43). No effect was detectable for Monensin sodium salt, Benzethonium chloride, Algestone acetophenide, Doxazosin mesylate, Ritonavir and Oxethazaine. The results are exemplarily illustrated for two of the six compounds (Figure 43 A).

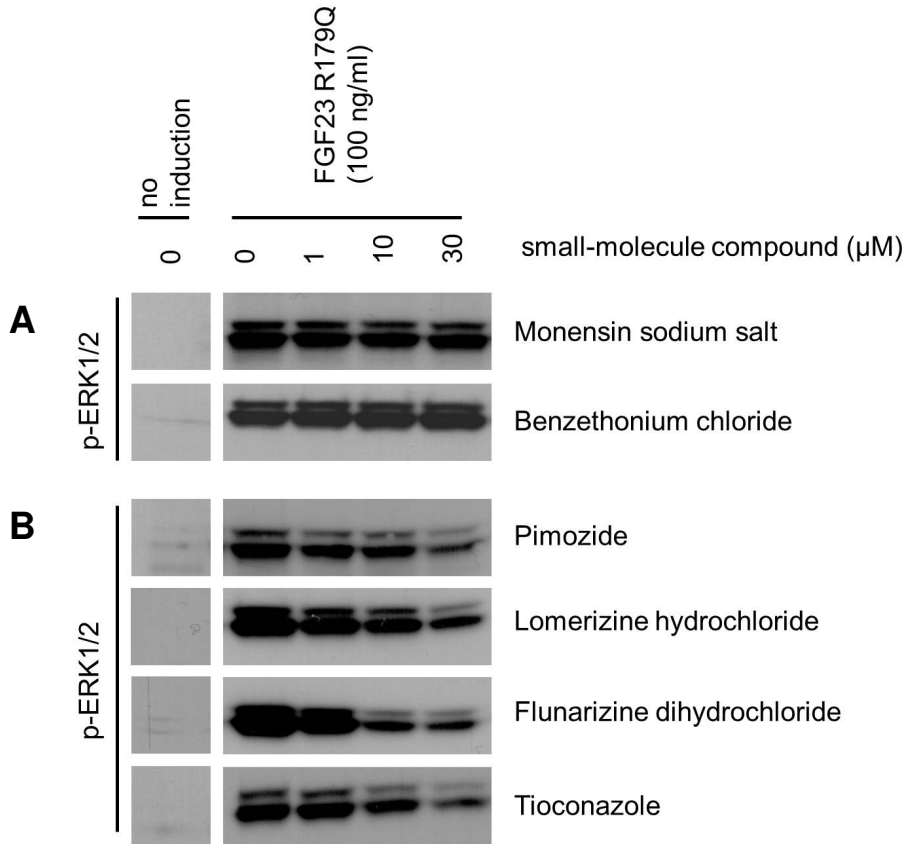

Figure 43: Validation of possible hits from the pilot HTS of the Prestwick Chemical Library. HEK293-KL cells were incubated with increasing concentrations of different small-molecule compounds of the Prestwick Chemical Library for 1 h and were then induced with FGF23R179Q (100 ng/ml) for 20 min. Cell lysates were analysed by Western blot using an antibody against p-ERK1/2. (A) For six compounds of the selected ten candidate hits, no effect could be detected. Exemplarily, Monensin sodium salt and Benzethonium chloride are shown. (B) For four compounds, a reduction of the phosphorylation level of ERK1/2 in induced HEK293-KL cells was noticeable.

Nevertheless, we were able to reproduce the results from the screening assays for four compounds of the Prestwick Chemical Library (Pimozide, Lomerizine hydrochloride, Flunarizine dihydrochloride and Tioconazole) (Figure 43 B). Here, increasing compound

concentrations (0 - 30 µM) led to a reduction of p-ERK1/2 in lysates of HEK293-KL cells after the stimulation with FGF23R179Q. Detection of total ERK1/2 served as a loading control (data not shown).

Taking into consideration that 1,280 small molecules were investigated in the pilot screen, the validated hit nomination of four compounds denotes a final hit rate of 0.3%.

Our results of the pilot screen are summarised in Table 7.

Table 7: 25 candidate hits nominated from the Prestwick Chemical Library.

	Small-molecule compound	**ID**	**Molecular formula**	**Molar mass (g/mol)**	**IC_{50} primary assay**	**IC_{50} secondary assay**	**Western blot**
1	Monensin sodium salt	748	$C_{36}H_{61}NaO_{11}$	692.85	0.78 µM	0.44 µM	no effect
2	***Pimozide***	***308***	***$C_{28}H_{29}F_2N_3O$***	***461.55***	***4.21 µM***	***11.62 µM***	***effect***
3	Chloroxine	1474	$C_9H_5Cl_2NO$	214.05	4.08 µM	-	-
4	Benzethonium chloride	708	$C_{27}H_{42}ClNO_2$	448.08	16.26 µM	5.54 µM	no effect
5	***Lomerizine hydrochloride***	***1775***	***$C_{27}H_{31}ClF_2N_2O_3$***	***505.00***	***7.18 µM***	***6.74 µM***	***effect***
6	Cilnidipine	1376	$C_{27}H_{28}N_2O_7$	492.52	3.92 µM	-	-
7	***Flunarizine dihydrochloride***	***312***	***$C_{26}H_{28}Cl_2F_2N_2$***	***477.42***	***11.50 µM***	***8.56 µM***	***effect***
8	Tiratricol	202	$C1_4H_9I_3O_4$	621.93	-	-	-
9	Algestone acetophenide	1715	$C_{29}H_{36}O_4$	448.59	2.08 µM	2.04 µM	no effect
10	Doxazosin mesylate	858	$C_{24}H_{29}N_5O_8S$	547.58	13.23 µM	33.63 µM	no effect
11	Cinnarizine	278	$C_{26}H_{28}N_2$	368.51	6.32 µM	-	-
12	Probenecid	542	$C_{13}H_{19}NO_4S$	285.36	-	-	-
13	Fluvastatin sodium salt	859	$C_{24}H_{25}FNNaO_4$	433.45	-	-	-
14	Loratadine	1432	$C_{22}H_{23}ClN_2O_2$	382.88	-	-	-
15	Telmisartan	1350	$C_{33}H_{30}N_4O_2$	514.62	-	-	-

16	Dipyridamole	142	$C_{24}H_{40}N_8O_4$	504.63	10.76 µM	-	-
17	Isoconazole	127	$C_{18}H_{14}C_{l4}N_2O$	416.13	-	-	-
18	***Tioconazole***	***1184***	***$C_{16}H_{13}Cl_3N_2OS$***	***387.71***	***20.75 µM***	***7.91µM***	***effect***
19	Meclozine dihydrochloride	457	$C_{25}H_{29}Cl_3N_2$	463.87	5.37 µM	-	-
20	Ritonavir	1782	$C_{37}H_{48}N_6O_5S_2$	720.94	8.16 µM	3.45µM	no effect
21	Glipizide	131	$C_{21}H_{27}N_5O_4S$	445.54	-	-	-
22	Miconazole	67	$C_{18}H_{14}Cl_4N_2O$	416.13	-	-	-
23	Oxethazaine	58	$C_{28}H_{41}N_3O_3$	467.64	19.85 µM	8.08 µM	no effect
24	Loperamide hydrochloride	144	$C_{29}H_{34}Cl_2N_2O_2$	513.50	-	-	-
25	Moxisylyte hydrochoride	42	$C_{16}H_{26}ClNO_3$	315.84	-	-	-

Final nominated hits are marked in bold and italics. ID = identification number at Prestwick Chemical

4. DISCUSSION

4.1. KEY REGULATORS OF PHOSPHATE HOMEOSTASIS

Over the last two decades, our understanding of human phosphate metabolism including genes and mechanisms involved has greatly increased. Of particular importance is the characterisation of a bone-kidney axis that comprises a group of phosphate regulating molecules (Figure 2). Among them, FGF23 has emerged as the major phosphaturic hormone. It controls renal phosphate handling and vitamin D metabolism (Quarles, 2003; Strom and Juppner, 2008).

FGF23 is a 32 kDa protein that is mainly produced by osteoblasts and osteocytes, circulates in the blood and primarily targets the FGFR/Klotho complex in the kidney. Excess FGF23 production results in hypophosphatemia, suppressed $1,25(OH)_2D_3$ levels and impaired bone and cartilage mineralisation. FGF23 deficiency, contrariwise, results in hyperphosphatemia, elevated $1,25(OH)_2D_3$ levels and soft tissue calcification (Liu and Quarles, 2007). There is a major gap, however, in our knowledge of the molecular mechanisms whereby FGF23 expression is controlled in the bone, and the interplay of different regulators of phosphate balance is far from fully understood.

$1,25(OH)_2D_3$ appears to be the principal regulator of FGF23, which stimulates FGF23 production in bone cells in an endocrine feedback loop (Liu et al., 2006a; Saito et al., 2005; Yu et al., 2005). As FGF23 is believed to be expressed predominantly in the skeleton, many of the factors regulating bone metabolism and mineralisation could also impact upon FGF23 synthesis. Here, PHEX, DMP1, ENPP1 and FAM20C seem to play a central role as local regulators that may allow FGF23 to control renal phosphate handling according to the actual influx/efflux of phosphate and calcium to and from the bone. PHEX is a member of the endothelin-converting enzyme family expressed by bone cells. Inactivating mutations of *Phex* lead to increased *Fgf23* gene transcription in *Hyp* mice (Liu et al., 2006b). Even though an initial study proposed that PHEX processes FGF23 (Bowe et al., 2001), we and others could determine that FGF23 is no substrate of PHEX (Benet-Pages et al., 2004; Liu et al., 2003). PHEX regulation of FGF23 must rather involve an as yet unidentified factor. DMP1 is a glycoprotein that belongs to the SIBLING (small integrin-binding ligand N-linked

glycoprotein) family of extracellular matrix proteins. Similar to PHEX, DMP1 is primarily produced by osteoblasts and osteocytes. Moreover, inactivation of Dmp1 also leads to increased skeletal *Fgf23* gene expression (Feng et al., 2006). The breakthrough in understanding *Fgf23* transcriptional regulation in the bone came by comparative analysis of *Hyp* and *Dmp1* null mice (Martin et al., 2011). The discovery that both mutations induce identical intrinsic abnormalities of mineralisation and result in an increase of Fgf23 that cause Fgf23-dependent hypophosphatemia provided the initial insights into the aforementioned bone-kidney axis that coordinates bone mineralisation and systemic phosphate homeostasis (Martin et al., 2012; Qiu et al., 2012; Quarles, 2003; Strom and Juppner, 2008). In humans, loss-of-function mutations in PHEX and DMP1 cause FGF23-dependent hypophosphatemic rickets (Lorenz-Depiereux et al., 2006a; The HYP Consortium, 1995). Inactivating mutations in the *ENPP1* gene were reported to cause both generalised arterial calcification of infancy (GACI), a severe autosomal-recessive disorder with a hypermineralising phenotype (Rutsch et al., 2003), and hypophosphatemic rickets with elevated levels of FGF23 (Lorenz-Depiereux et al., 2010). This suggests an as yet elusive mechanism that balances arterial calcification with bone mineralisation. Similarly, *Enpp1* knockout mice were characterised by severe disruption of the architecture and mineralisation of long bones, dysregulation of calcium/phosphate homeostasis and changes in Fgf23 expression (Mackenzie et al., 2012). However, the molecular mechanism underlying the transcriptional regulation of *FGF23* has not been defined up to now. The Golgi casein kinase FAM20C phosphorylates secretory pathway proteins. A recent publication suggests the SIBLING proteins to be substrates for FAM20C and demonstrates osteopontin (OPN), DMP1 and MEPE to be phosphorylated by FAM20C *in vitro* (Tagliabracci et al., 2012). Actually, the *Fam20c* knockout model has a phenotype resembling the *Dmp1* null mouse phenotype. Furthermore, the loss of function of Fam20c resulted in a significant downregulation of Dmp1 and a significant increase in Fgf23 (Wang et al., 2012b). In addition, humans with FAM20C loss-of-function mutations also show higher FGF23 levels (Rafaelsen et al., 2013) indicating a potential role of FAM20C as an upstream regulator of FGF23. Tagliabracci and co-workers lately described that FAM20C directly phosphorylates FGF23 on S^{180} next to the $^{176}RXXR^{179}$ motif, and such phosphorylation promotes FGF23 proteolysis into metabolically inactive fragments by furin, a member of the SPC family, through blocking O-glycosylation via GALNT3 (Tagliabracci et al., 2014). This would suggest that secretion of intact FGF23 is regulated in a cross-talk between phosphorylation and O-glycosylation (Figure 44). Therefore, FAM20C as a negative regulator

of FGF23 activity is supposed to rather facilitate its posttranslational degradation than control its transcription.

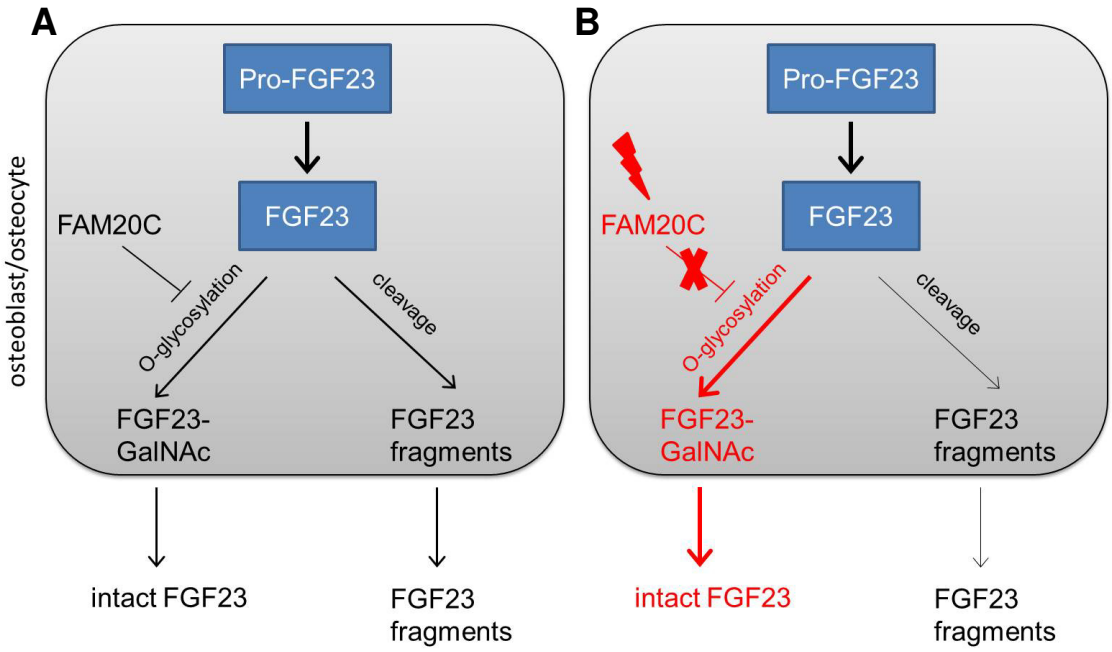

Figure 44: Scheme to illustrate the hypothetical role of FAM20C in controlling levels of circulating intact FGF23. (A) FGF23 undergoes O-linked glycosylation to FGF23-GalNAc and is secreted intact into blood circulation. Non-glycosylated FGF23 is degraded into metabolically inactive FGF23 fragments. FAM20C appears to block this O-glycosylation through phosphorylation of FGF23 on S^{180} next to the ^{176}RXXR^{179} motif, thus facilitating its cleavage into fragments by SPCs. (B) Loss of function of FAM20C is speculated to cause inappropriately high levels of circulating intact, bioactive FGF23 due to a cellular shift towards increased O-glycosylation (marked in red).

The role of other regulators of FGF23 is discussed controversially. Stimulation of FGF23 by PTH was demonstrated in some (Kawata et al., 2007; Lavi-Moshayoff et al., 2010; Rhee et al., 2011; Sato et al., 2004) but not all studies (Liu et al., 2006a; Saji et al., 2010). It is hypothesised that FGF23 and PTH mutually regulate each other in a negative feedback loop, where PTH stimulates FGF23 production and FGF23 in turn suppresses PTH synthesis (Lanske and Razzaque, 2014). Currently, Meir et al. claimed that PTH can increase the transcription of the *FGF23* gene in bone cells by activating the nuclear orphan receptor Nurr1 (nuclear receptor-associated protein 1) (Meir et al., 2014). Additionally, leptin, estrogen, glucocorticoids, iron and circulating Klotho may control FGF23 production (Carrillo-Lopez et al., 2009; Smith et al., 2012; Tsuji et al., 2010). As of today, the effects of phosphate on FGF23 are not understood. Unlike calcium, which has a calcium sensing receptor (CaSR) that permits the sensing and tight control of calcium levels (Brown et al., 1994), a phosphate sensor has not been identified, and the regulation of serum phosphate levels is not so tightly

controlled. Studies that examined the effects of oral phosphate intake on FGF23 levels have detected either no effect (Isakova et al., 2011; Larsson et al., 2003; Nishida et al., 2006) or showed changes in FGF23 production in response to alterations in dietary phosphate intake after a lag time of up to one week (Antoniucci et al., 2006; Ferrari et al., 2005; Perwad et al., 2005). This would rather suggest that phosphate may affect FGF23 indirectly via active vitamin D or other regulators.

4.1.1. Novel Regulators of Phosphate Homeostasis

Remarkably, there are patients afflicted with phosphate balance disorders without mutations in the abovementioned known genes contributing to phosphate balance. Our patient population contains overall 50 index cases showing alterations in phosphate handling without clear genetic reason. During this thesis, 22 exomes of 11 unrelated families with diagnosed hypophosphatemia were investigated. To this point, no novel genetic variants which seem to be disease-causing in at least two unrelated patients could be detected. Maybe the number of investigated exomes has to be strongly increased. Many of the investigated patients were single cases with unknown medical family history. Moreover, it could be possible that causal genetic variants reside within non-coding, regulatory regions or within exonic regions uncovered by the current capture technique used in this study.

In one German multiplex-family with several affected members (Figure 14), mutations in the *PHEX* gene and its regulatory regions could be excluded by Sanger sequencing of DNA from patient #10 and by genome sequencing of DNA from patient #6 (data not shown). Instead, a mutation in the *COL24A1* gene, which is located in the exon-intron-boundary 1 bp upstream of exon 40 in the donor splice site (NM_152890.5:c.3558+1G>T), was revealed by exome sequencing. All affected family members showed a heterozygous G/T genotype. Whether this potential loss-of-function mutation is causative for the diagnosed hypophosphatemia, is unclear up to now. A screening for this mutation in our patient collective with phosphate balance disorders did not provide any new findings. In addition, this variant has not yet been described in the ExAc Browser (Beta) (Cambridge, MA, USA; http://exac.broadinstitute.org; January 2015), a website of the Exome Aggregation Consortium (ExAc) spanning exome sequencing data of more than 60,000 unrelated individuals as part of various disease-specific and population genetic studies. In family member #15 without clinical manifestation of hypophosphatemia, the aforesaid heterozygous genotype was also observed suggesting a phenotype of incomplete penetrance. DNA from additional family members (e.g. #3 and #8)

has to be analysed. Furthermore, it is problematic to investigate aberrant splicing as expected by online splice site prediction tools for the discovered SNV, since mRNA of bone biopsies would presumably be the material of choice. Additionally, FGF23 levels in serum of affected and unaffected family members could be examined by ELISA measurement to verify whether hypophosphatemia is FGF23-mediated in this family.

Collagen XXIV is a newly discovered and poorly characterised member of the fibril-forming family of collagen molecules, which displays unique structural features of invertebrate fibrillar collagens and is expressed predominantly in bone tissue (Matsuo et al., 2006). Vertebrate collagens represent a large family of extracellular proteins that provide specific physical properties to the connective tissue of almost every organ system. There are at least 40 collagen chains that trimerise into 27 types that give rise to a large variety of specialised macroaggregates. Fibril-forming collagens are the most abundant and ubiquitously distributed members of the collagen family. They share a common primary structure that consists of a long collagenous domain made of Gly-X-Y triplets flanked at both ends by non-collagenous propetides. They are widely expressed in soft and hard tissues (type I, III and V) or in cartilage (type II and XI) (Buehler, 2006). Gene expression analyses in the mouse have shown that *Col24a1,* together with *Col27a1,* displays mutually exclusive patterns in the developing and adult skeleton. Here, collagen XXIV and XXVII form homotrimers (Boot-Handford et al., 2003; Koch et al., 2003), which might play comparable roles in cartilage and bone tissue, respectively, by regulating collagen I and II fibrillogenesis and/or matrix calcification and mineralisation (Koch et al., 2003). This hypothesis was strengthened by Matuso and co-workers, who demonstrated that *Col24a1* gene expression gradually increased concomitant with the progression of osteoblast differentiation and might be implicated in the emergence of calcium and phosphate deposits leading to the formation of a mineralisation-competent bone matrix (Matsuo et al., 2008). Inhibition of *Col24a1* expression in murine preosteoblastic cells resulted in significant decrease of ALP, cell mineralisation and expression of osteoblast marker genes such as *Runx2* (runt-related transcription factor 2), *OCN* (osteocalcin) and *Col1* (collagen I) (Wang et al., 2012a). On the other hand, overexpression not only rescued the deficiency in osteoblast differentiation from *Col24a1* silenced cells but also enhanced osteoblastic differentiation in control cells (Wang et al., 2012a). It is assumed that Col24a1 imparts some of its regulatory control on osteoblast differentiation and mineralisation at least partially through interaction with integrin β3 and the transforming growth factor β (TGF-β)/Smad signalling pathway (Wang et al., 2012a). The importance of this signalling

pathway in bone development and homeostasis is discussed in detail in section 4.2.2. Preliminary data showed that the otherwise normal *Col24a1* null mice can be characterised by osteopenia with lower bone mineral density (Matsuo et al., 2008).

Taken together, these results would indicate that *COL24A1* might be a new candidate disease gene involved in bone mineralisation defects and skeletal deformities diagnosed in the German multiplex-family. Nevertheless, to regard *COL24A1* as confidently implicated, further variants within this gene have to be identified in more unrelated individuals with hypophosphatemia and similar clinical presentations. In addition, the molecular mechanism by which COL24A1 could regulate phosphate homeostasis has to be clarified.

4.2. MOUSE MODELS RESEMBLING PHENOTYPES OF METABOLIC BONE DISEASE AND DEVELOPMENTAL SKELETAL DISORDERS

Maintaining physiological phosphate balance is of crucial importance for bone health. The presence of adequate amounts of phosphate is involved in the process of apoptosis of mature chondrocytes in the growth plate of the bone. Without phosphate in high enough quantities, chondrocytes will not go into apoptosis (Miedlich et al., 2010) and the normal physiological chain of events like invasion of blood vessels and the generation of new bone will be blocked. This results in rickets and delayed growth (Tiosano and Hochberg, 2009). In the rest of the skeleton, hypophosphatemia will result in osteomalacia due to an insufficient formation of hydroxyapatite. In the child, both rickets and osteomalacia will be manifested, whereas the adult will have only osteomalacia (Penido and Alon, 2012). Mouse models of bone mineralisation defects could help to examine the causal molecular pathways that may have a regulatory impact on phosphate homeostasis. However, a large number of rare hereditary metabolic bone diseases and skeletal abnormalities are still lacking sufficient mouse models (Faruqi et al., 2014; Vanhoenacker et al., 2001).

4.2.1. Exome Sequencing as a Method of Choice for Mutation Discovery in ENU-Derived Mice

Within the Munich ENU Mutagenesis Project, exome sequencing was performed for a panel of ENU-derived mouse models (n = 18) showing metabolic bone disease and phenotypic

changes in bone development. In contrast to radiation or mutagenic agents like chlorambucil that induce deletions or inversions and often involve more than one gene, ENU is an alkylating chemical agent that primarily induces single nucleotide substitutions (point mutations) with a frequency of approximately one nucleotide substitution per Mb (Andrews et al., 2012; Bull et al., 2013). The use of ENU seems to be a powerful tool for phenotype-driven mutagenesis, where the function of a gene is defined by its gain-of-function or loss-of-function phenotype. Sequentially, a large number of animals are screened in a systemic way to detect individuals which show the specific phenotype of interest. Following the isolation of such an animal, test breeding is performed to confirm the genetic nature of the trait (Balling, 2001). Until the causative mutation is identified, mouse mutants with clinically relevant phenotypes are not maximally valuable as models for human diseases.

Fairfield et al. demonstrated the utility of exome sequencing for mutation discovery in ENU-derived mice. However, the study relied on coarse genetic mapping information, and it was recommended that an exome sequence as a sole source of information may not be enough to detect disease-causing mutations without extensive validation burden (Fairfield et al., 2011). In contrast, in this work, two different exome sequencing strategies were tested even without any additional genetic mapping data: (1) sequencing of a single mutant per trait and comparison with one wild-type C3HeB/FeJ mouse sequence and (2) sequencing of two mutants per trait and comparison with one wild-type C3HeB/FeJ mouse sequence. From 18 different mouse lines investigated, a new candidate mutation could be identified in 14 mouse lines representing an overall success rate of 78% (Table 5). The second setup reduced the validation effort by decreasing the number of nominated candidate variants to be validated by co-segregation of genotype and phenotype (Table 4). Furthermore, the success rate of discovering the putative causative mutation could be increased from 67% (first setup) to 100% (second setup). Nonetheless, the number of investigated ENU-derived mutant mouse lines has to be increased to make a well-founded statement.

Exemplarily, within our cohort of mutant mice, we could detect possible candidate genes in two mouse lines showing aberrations of phosphate homeostasis, BPL010 (Bone screen Pi low #10; mutant 60355 (Table 5)) and KTA041 (Kinky tail alkaline phosphatase #41; mutant 60358 (Table 5)). Exome sequencing revealed a stop mutation in exon 6 of the *Trp63* (transformation-related protein 63) gene (NM_001127259.1:c.1350T>A, NP_001120731.1:p.Tyr450*) in mouse line BPL010, which was initially identified through its low serum Pi levels. The *Trp63* gene encodes tumour protein p63, a member of the p53

family of transcription factors involved in cellular responses to stress and development (Vanbokhoven et al., 2011). Mutations in the human *TP63* gene underlie several malformation syndromes that include various degrees of limb abnormalities, ectodermal dysplasia and facial clefts (van Bokhoven and Brunner, 2002), e.g. ankyloblepharon-ectodermal dysplasia-cleft lip/palate (AEC) syndrome (Dianzani et al., 2003), split-hand/foot malformation 4 (SHFM4) (van Bokhoven et al., 2001) and acro–dermato–ungual–lacrimal–tooth (ADULT) syndrome (Amiel et al., 2001). The identified stop mutation is the first described point mutation within in the mouse *Trp63* gene. *Trp63* knockout mice show several developmental defects which include the lack of limbs and other tissues such as teeth and mammary glands (Crum and McKeon, 2010; Vanbokhoven et al., 2011). Mouse line KTA041 with autosomal recessive inheritance has reduced Pi and elevated Ca serum levels and shows several skeletal abnormalities, e.g. kinky tail as well as rib and vertebrae fusion. Mutants are smaller and exhibit a reduced bone mineral density. We could identify a mutation in exon 8 of the *Scube3* (signal peptide CUB EGF domain-containing protein 3) gene (NM_001004366.1:c.882C>A, NP_001004366.1:p.Asn294Lys) as potentially causative. Scube3 is a secreted, plasma membrane-associated, extracellular protein with multiple EGF-like domains. In mice, a strong expression of Scube3 in the cartilaginous primordia of the skeleton and regions of intramembranous bone formation in the developing craniofacial region as well as in the developing kidney was demonstrated (Haworth et al., 2007). Wu et al. described a high expression of SCUBE3 also in human primary osteoblasts (Wu et al., 2004). Moreover, the human *SCUBE3* gene maps to human chromosome 6p21.31, a region that has been linked with a locus for a rare form of metabolic bone disease known as Paget's disease of bone (Jacobs et al., 1999).

Nonetheless, it remains a possibility that the identified candidate variants in our ENU-derived mutant mouse line cohort are simply linked markers and not causative for the observed phenotype. Segregation analysis in mouse cohorts is the first choice to confirm putative candidate mutations, but other methods like functional analysis and/or further breeding experiments, e.g. mating heterozygous animals to generate homozygous mutant mice, are desired to verify the hypothesised results. Especially in mouse lines with candidate variants in genes with unknown function and no additional information from other mouse models (MGI, Jackson Laboratory), further investigation is necessary to clarify the role of the nominated genes for the molecular mechanisms of phosphate and bone metabolism. In addition, the

analysis of the corresponding syntenic human regions could give first hints about possible human candidate diseases.

In four mutant mouse lines, no causative mutation was identified (Table 5). This failure most likely indicates that these mutations may reside in non-coding, regulatory regions or are localised within exonic regions which are uncovered in the current exome capture design. An additional possibility is that the underlying mutations like larger insertions and deletions and/or translocations do reside in the targeted regions, but are simply not detected using standard mapping and SNV calling, which is clearly biased towards the discovery of single nucleotide substitutions and small indels. Nonetheless, taking into consideration that the major mutation type induced by ENU mutagenesis is a point mutation, this possibility may be of minor significance.

4.2.2. Detection of a Nonsense Mutation in the *Fam46a* Gene Causing Bone Development Abnormalities in a New Mouse Model for Skeletal Dysplasia

One ENU-derived mouse model with significant changes in bone metabolism, content and structure was further investigated. Several observations substantiate the causal role of the detected *Fam46a* candidate mutation within this mouse line. First, we identified a heterozygous *Fam46a* nonsense mutation in the exome data of the mutant mouse which was not present in the C3HeB/FeJ wild-type mouse and in four inbred strains analysed (BALB/c, DBA/2, FVB, SJL). Furthermore, available published resequencing data (Ensembl Genome Browser 72: *Mus musculus*) at the corresponding position (mm9_chr9:85,219,964) revealed that 18 other mouse strains were homozygous for the reference allele. Second, *Fam46a* is located within the candidate linkage interval of the mouse line on mouse chromosome 9. Third, segregation of the phenotype with the corresponding genotype was observed in a first mouse cohort of eight phenotypically mutant mice. Fourth, the mutation type found (NM_001160378.1:c.469G>T, NP_001153850.1:p.Glu157*) is expected to result in a truncation and a consequential loss of function of the Fam46a protein. Fifth, *Fam46a*$^{E157*/-}$ mice exhibited a severe skeletal phenotype possibly resembling the knockout phenotype of the *Fam46a* gene (Figure 19 J).

Fam46a$^{E157*/+}$ mice had significantly high ALP activities (data not shown). ALP is a long known bone formation marker (Etokebe et al., 2009) expressed early in development of bone

and calcified tissues (Rosati et al., 1994). However, serum levels of other bone turnover parameters like Ca and Pi (data not shown) as well as serum levels of FGF23 (Figure 17) were unchanged. We additionally analysed the bone degradation marker CTX-1 (C-telopeptide cross-linked collagen type 1) in *Fam46a*$^{E157*/+}$ and *Fam46a*^{WT} mice, but found no differences between the genotypes (data not shown). More studies are warranted to investigate a possible mineralisation defect in *Fam46a*^{E157*} mice. The intermediate mild phenotype of these mice encompassed significant differences in bone content and structure as measured by pQCT (data not shown). The phenotype became more profound in *Fam46a*$^{E157*/-}$ mice, which displayed ALP activity values even twice as high as in *Fam46a*$^{E157*/+}$ mice. Comparison of whole skeleton preparations of *Fam46a*^{WT} (Figure 19 I), heterozygous *Fam46a*^{E157*} (data not shown) and homozygous *Fam46a*^{E157*} mice (Figure 19 J) by SkyScan analysis clearly exhibited a dramatic increase in skeletal abnormalities including kyphosis of the vertebral column, shortened ribs and compression of the rib cage in the *Fam46a*$^{E157*/-}$ mouse. In contrast, no obvious skeletal abnormalities were seen in *Fam46a*^{WT} and *Fam46a*$^{E157*/+}$ mice. The distinct phenotype in *Fam46a*$^{E157*/+}$ mice seems to be caused by a classical gene dosage effect resulting from the loss-of-function mutation in *Fam46a*.

Long bone malformations as observed in *Fam46a*$^{E157*/-}$ mice may originate early in development (Klempt et al., 2006). It is unknown whether Fam46a is directly involved in embryogenesis, although embryonic expression of *Fam46a* was shown (Etokebe et al., 2009; McGrath et al., 2001). Nevertheless, the low number of delivered *Fam46a*$^{E157*/-}$ mice suggests that Fam46a may have a strong developmental effect and that most of the homozygous mice may die embryonically or perinatally. Further analysis of mouse embryos is necessary to elucidate its specific role in embryonic development and early bone formation. *Fam46a* is also expressed in the bone tissue of adult mice (Figure 21). Besides its potential importance during embryogenesis, this would point to a further role of Fam46a in bone formation and turnover at later, postnatal developmental stages. There are two major modes of osteogenesis: endochondral ossification, in which mesenchymal cells differentiate into cartilage that is later replaced by bone, and intramembranous ossification, which is the direct conversion of mesenchymal tissue into bone (Gilbert, 2000). Interestingly, in homozygous *Fam46a*^{E157*} mice, defects were found in these two modes of bone formation (Figure 20). Comparison to another previously described ENU-derived mouse line, *Col1a1*^{Aga2} (Aga2, Abnormal gait #2), discloses similarity in clinical chemical, skeletal and growth phenotypes (Lisse et al., 2008). As *Fam46a*^{E157*} mice, *Col1a1*^{Aga2} mice exhibited phenotypic variability with reduced body

size, dystrophic limb(s), severe brittleness of bones, thin calvaria and early lethality. ALP levels were significantly increased. Due to the multiple fractures and provisional rib and long bone calluses and deformities, heterozygous *Col1a1*^{Aga2} mice represent an animal model for Osteogenesis imperfecta type II (Lisse et al., 2008). Up to now, we have identified a possible facture of the femur (Figure 19 F) only in one *Fam46a*$^{E157*/-}$ mouse and rib calluses (Figure 19 J) in another homozygous mutant.

Little is known about the function of FAM46A in humans. *In silico* studies have illustrated that FAM46 proteins share all critical catalytic amino acids with the superfamily of nucleotidyltransferase (NTase) fold proteins, and thus might be active NTases, which carry out reactions potentially crucial for cellular signalling (Kuchta et al., 2009). Moreover, it has been depicted that FAM46A is a SMAD signalling pathway-related protein. SMADs are intracellular effectors of TGF-β (Barragan et al., 2008). The importance of TGF-β in bone development and homeostasis has been extensively demonstrated *in vitro* and *in vivo* with strong evidence for profound effects on bone formation, bone resorption and the interplay between these two processes (Janssens et al., 2005). TGF-β signalling promotes osteoprogenitor proliferation, early differentiation and commitment to the osteoblastic lineage through selective MAPK and SMAD2/3 pathways and through the cooperation between TGF-β and PTH, WNT, BMP (bone morphogenetic protein) as well as FGF signalling (Chen et al., 2012). In humans, mutations within the TGF-β/SMAD pathway are associated with skeletal abnormalities like thickened cortices, sclerosis of skull base and vertebrae as well as limb deformity in Camurati-Engelmann disease (OMIM #131300), a rare dominant type of bone dysplasia resulting from domain-specific heterozygous mutations within the *TGFB1* gene (Kinoshita et al., 2000). Interestingly, Loeys-Dietz syndrome (LDS) type 1 - 4 is associated, besides other mainly cardiovascular symptoms, with more or less profound and diverse skeletal abnormalities as osteoarthritis, osteoporosis and craniosynostosis. The syndrome results from mutations within the *TGFBR1* (TGF-β receptor 1) gene (LDS1, OMIM #609192), *TGFBR2* (TGF-β receptor 2) gene (LDS2, OMIM #610168), *SMAD3* gene (LDS3, OMIM #613795) and *TGFB2* gene (LDS4, OMIM #614816) (Lindsay et al., 2012; Loeys et al., 2005; van de Laar et al., 2011). Whether FAM46A has a regulatory role in TGF-β signalling during osteoblast development and/or ossification, is unknown.

By comparing the syntenic regions between mice and humans, *FAM46A* was located within a susceptibility locus for split-hand/foot malformation with long-bone deficiency (SHFLD) on human chromosome 6q14.1 (Naveed et al., 2007). SHFLD (SHFLD1, OMIM %119100;

SHFLD2, OMIM %610685) is a rare, severe limb deformity characterised by tibia aplasia with or without split-hand/split-foot deformity. *Fam46a*$^{E157*/-}$ mice showed severe unilateral or bilateral limb deformities but without tibia aplasia and split-hand/split-foot deformity. Comparison of the dysmorphological phenotypes of *Fam46a*$^{E157*/-}$ mice revealed variably affected long bones, suggesting that the phenotype of bone abnormalities in *Fam46a*$^{E157*/-}$ mice is diverse as observed in SHFLD.

4.3. MODULATION OF FGF23 SIGNALLING BY SMALL-MOLECULE COMPOUNDS

4.3.1. FGF23 as an Attractive Novel Target for Small Molecules

The molecular identification and characterisation of genetic defects leading to a number of rare hereditary and acquired disorders affecting phosphate balance has added tremendous detail to the discovery of the key phosphate regulating factor, FGF23. Several hypophosphatemic disorders caused by the excess actions of FGF23, e.g. XLH, ADHR, ARHR1 and ARHR2 (Table 1), have been described. It is hoped these insights into the pathophysiological mechanism of disorders may guide future treatment strategies that may lead to greater effectiveness, fewer side effects and improvements in the patient's long-term quality of life (Lee and Imel, 2013). Attempts to directly target and inhibit FGF23 activity make sense from a pathophysiological standpoint and have a great potential as novel therapeutic approaches due to the following points. Firstly, the obligatory co-receptor Klotho converts the canonical FGFR1c into a highly specific receptor for circulating FGF23 (Urakawa et al., 2006). Klotho itself is not ubiquitously expressed, but shows a tissue-specific abundance with highest expression in the kidney and lower expression in the brain, parathyroid gland, heart, pancreatic β-islet cells and placenta (Ben-Dov et al., 2007; Huang and Moe, 2011; Li et al., 2004). The strict requirement of Klotho to signal limits the site of action for FGF23 to these tissues despite the widespread expression of FGFRs. Secondly, no causative treatment strategy is available for patients with FGF23-mediated hypophosphatemic disorders. Current medical therapies have mostly been evaluated in children. Although they have efficacy in managing and treating clinical symptoms, renal phosphate wasting persists and the risk of side effects is high. Two major issues remain: (1) growth retardation and recurrent dental infections in children and (2) the necessity of adequate treatment in adults (Linglart et al., 2014). Thirdly, a successful direct targeting and decrease of FGF23 signalling

has already been demonstrated for some small-molecule inhibitors (Wohrle et al., 2013; Zhang et al., 2012), for the isolated C-terminal tail of FGF23 (Goetz et al., 2010) and for monoclonal neutralising anti-FGF23 antibodies (Carpenter et al., 2014).

4.3.2. Establishment of a Method to Identify Regulators of FGF23 Signalling

In this work, a highly specific cell-based *in vitro* system using a modified human embryonic kidney cell line (HEK293-KL) has been successfully established to perform small-molecule compound screens including primary and secondary assays to identify new regulators of FGF23 signalling by monitoring the phosphorylation status of ERK1/2 in a HTS approach.

Initially, in induction experiments followed by Western blot analysis, it was shown that MAPK signalling pathway is activated after the binding of FGF23 to its cognate receptor complex. FGF23 leads to phosphorylation of ERK1/2 and increased expression of EGR1 in HEK293-KL cells (Figure 25, Figure 26). Many biological roles have been attributed to EGR1 ranging from controlling synaptic plasticity (Jones et al., 2001), neurite outgrowth (Harada et al., 2001), wound repair (Khachigian et al., 1996), female reproductive capacity (Lee et al., 1996) as well as growth control and apoptosis (Thiel and Cibelli, 2002). Indeed, induction of *EGR1* gene transcription was monitored in many cell types in response to mitogens (Gashler and Sukhatme, 1995; Guha et al., 2001; Kaufmann and Thiel, 2001), and a direct role of EGR1 in regulating proliferation has been proposed for several cell types like T cells, astrocytes, glioma cells, glomerular mesangial cells and keratinocytes (Biesiada et al., 1996; Hofer et al., 1996; Kaufmann and Thiel, 2001; Perez-Castillo et al., 1993; Thiel and Cibelli, 2002). Likewise, Kaufmann et al. showed that EGR1 biosynthesis is strongly stimulated by activation of ERK1/2 (Kaufmann et al., 2001). As discovered in our cell model, this is also true for FGF23-dependent MAPK signalling. Besides elevated EGR1 protein levels, we detected higher *EGR1* gene expression levels after the stimulation with FGF23 by comparative transcriptome analysis using RNA-Seq. Among the 17 significantly upregulated FGF23-responsive target genes that might belong to a network of factors involved in the regulation of phosphate homeostasis, *EGR1* was the most upregulated one (Table 6). In addition, pathway analysis highlighted *EGR1* to be of central importance (Figure 30). Remarkably, physiological studies in *Hyp* mice have revealed both increased Fgf23 serum levels and increased levels of *Egr1* mRNA (Miyagawa et al., 2014; Ranch et al., 2011).

Taking this into consideration, it is tempting to speculate that EGR1 plays a major role in the FGF23-mediated regulation of phosphate metabolism.

Based on the established cell model, primary and secondary assays suited for HTS were developed on the AlphaScreen SureFire p-ERK1/2 technology from PerkinElmer and the HTRF Cellul'erk p-ERK1/2 platform from Cisbio. In a pilot screen of the Prestwick Chemical Library containing 1,280 small molecules, it was verified that the assay system is robust and suitable for HTS. Moreover, we focused on the identification of inhibitory small molecules that reduce FGF23 action. In a primary screen, 25 hits were nominated for further investigation representing a hit rate of 2%. The compounds were reordered and analysed in 10-point-titrations (0.2 - 80 µM) by use of the primary assay (Figure 40). Toxicity of all primary hit compounds was tested in HEK293-KL cells, and their activity was validated in the secondary assay (Figure 42). Ten compounds could be nominated for further investigation in our established cell system via Western blot analysis. Thereof, four compounds reduced the phosphorylation of ERK1/2 as summarised in Figure 45.

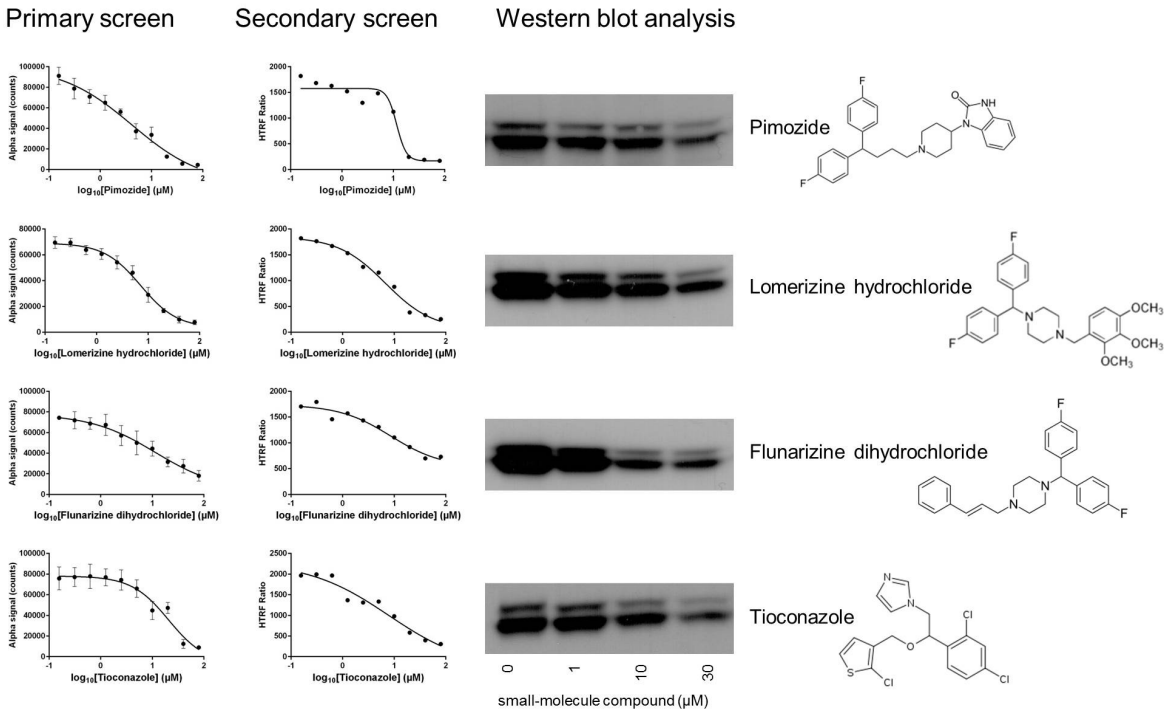

Figure 45: Validated candidate hits of the pilot screen using the Prestwick Chemical Library of 100% approved drugs. All candidate compounds reduced p-ERK1/2 levels in a concentration-dependent manner. Results from the primary and secondary screen as well as from Western blot analysis are summarised.

The reason why the remaining six compounds showed no effect in Western blot analysis (Figure 43 A) is unclear to this point. Maybe the reduction of the phosphorylation status of ERK1/2 was too small to be detected in Western blot analysis, a method that is less sensitive than the detection systems used for the primary and secondary screen. However, only compounds that show an effect in each validation step are usually regarded for further analysis (Schorpp and Hadian, 2014).

The Prestwick Chemical Library contains only 100% approved drugs. This library was designed to reduce the risk of low quality hits, to diminish the cost of the initial screening and to accelerate lead discovery. The strategy behind is the so-called "selective optimisation of side activities (SOSA)" approach (Wermuth, 2004). Only a limited number of highly diverse drug molecules for which bioavailability and toxicity studies have already been performed and which have proven usefulness in humans is submitted. If an initial screening provides hits, they could then be used as starting points for a drug optimisation programme. It can be noticed that, if the initial hit has sufficient affinity for the target, it could be immediately tested in patients.

For that reason, all of the identified hit compounds modulating FGF23 signalling (Figure 45) are presently used drugs within clinics:

- Pimozide (drug name: i.a. Orap; company: i.a. Teva) is an antipsychotic drug of the diphenylbutylpiperidine class that is used in its oral preparation in schizophrenia (Mothi and Sampson, 2013), chronic psychosis and Tourette syndrome (Rose and Moldofsky, 1977). An antimicrobial effect against *Listeria monocytogenes* has also been described (Lieberman and Higgins, 2009). The precise molecular mechanism of its action is unknown. Pimozide blocks dopamine D_2 receptors (Seeman, 2002) and hERG cardiac potassium channels (Kang et al., 2000). Additionally, it is hypothesised that the inhibitory action of Pimozide against STAT5 is a novel potential treatment strategy in myeloproliferative neoplasms (Bar-Natan et al., 2012; Nelson et al., 2011). Side effects like akinesia, dizziness and speech disorder can arise (Teva Select Brands, 2012).
- Lomerizine hydrochloride (drug name: i.a. Terranas; company: i.a. Atomole) is an oral calcium channel blocker with antimigraine properties (Selt et al., 2010). In a case of cerebral autosomal dominant arteriopathy with subcortical infarcts and leukoencephalopathy (CADASIL), Lomerizine hydrochloride was suggested to

prevent recurrent stroke (Shimizu et al., 2014). Molecular mechanisms underlying the action of this drug remain unclear.

- Flunarizine dihydrochloride (drug name: i.a. Sibelium; company: i.a. Janssen Pharmaceutica) is a drug classified as non-selective calcium channel blocker with additional actions including histamine H_1 receptor blocking activity (Taylor and Defeudis, 1986). It is effective in prophylaxis of migraine and vertigo (de Bock et al., 1997; Lepcha et al., 2014) and as an adjuvant in the therapy of epilepsy (Moglia et al., 1986). Weight gain, somnolence and depression were reported to be the most frequent side effects (Leone et al., 1991).
- Tioconazole (drug name: i.a. Trosyd, Gyno-Trosyd; company: i.a. Pfizer) is an antifungal medication of the imidazole class. It is utilised to treat infections caused by fungus or yeast (Marriott et al., 1983). Tioconazole interacts with 14α-demethylase (CYP51A1), a cytochrome P450 enzyme that converts lanosterol to ergosterol, resulting in increased cellular permeability (Ballard et al., 1988). Headache, drowsiness and contact dermatitis have been described as possible side effects (Jones and Kennedy, 1990).

Up till now, no interaction of the identified hit compounds with FGF23/FGFR1c/Klotho signalling or MAPK signalling in general has been described. Functional studies are now warranted to determine whether the identified candidate compounds are FGF23-specific without affecting other FGFs and whether they directly interact with the FGFR1c/Klotho receptor complex or downstream within the intracellular MAPK signalling pathway. Previous studies have revealed that small molecules which target either FGFR tyrosine kinase activity (NVP-BGJ398) (Wohrle et al., 2013) or inhibit downstream FGF23 signalling (PD0325901) (Zhang et al., 2012) can ameliorate hypophosphatemia in animal models. Both types of interaction are interesting, but interaction with the unique FGF23 receptor complex is expected to be more specific than inhibition of MAPK pathway as a major signal cascade from the cell surface to the nucleus involved in miscellaneous biological functions (English and Cobb, 2002).

A precise model for receptor activation has previously been proposed for FGF21, another secreted FGF that binds to receptor complexes composed of FGFR1c and β-Klotho. When β-Klotho or FGF21 is alone, the inhibitory domain (D1/linker region) of FGFR1c effectively inhibits their interactions with the D2/D3 region of the receptor. Once FGF21 binds to β-Klotho, FGF21 and β-Klotho can synergistically overcome the inhibitory effect of the

D1/linker region and bind to the D2/D3 region, which in turn could lead to following receptor dimerisation and activation (Mohammadi et al., 2005; Yie et al., 2012). Taking this into account, similar mechanisms might also be involved for FGF23 receptor binding and receptor complex activation. Small molecules that inhibit this process could be greatly specific candidates for reducing FGF23 signalling. Furthermore, not only FGFR1c but also FGFR3c and FGFR4 are expressed in HEK293-KL cells (data not shown). Accordingly, the nominated candidate hits from Prestwick Chemical Library might reduce elevated actions of FGF23 on both phosphate homeostasis via FGFR1c (Gattineni et al., 2009) and vitamin D metabolism via FGFR3c and FGFR4 (Gattineni et al., 2011) under hypophosphatemic conditions *in vivo*.

As illustrated in Figure 7, in the progression from basic research to hit-to-lead validation, the screening process of the Prestwick Chemical Library has been successfully finished at ADSP. Nonetheless, the Prestwick Chemical Library consists of a comparably small number of well-established small-molecule compounds. In a pilot screen, this library was utilised to evaluate the robustness and appropriateness of our method to perform HTS and to possibly identify first candidate hits. However, screens of larger libraries, e.g. Helmholtz Zentrum München Library, would be necessary to find novel unknown small-molecule compounds interacting with FGF23 signalling.

REFERENCES

Alizadeh Naderi, A.S., and Reilly, R.F. (2010). Hereditary disorders of renal phosphate wasting. Nature reviews. Nephrology *6*, 657-665.

Alkhatib, A., Burton, L.E., and Carachi, R. (2014). Familial tumoral calcinosis. Scottish medical journal *59*, e17-20.

Alon, U.S., Monzavi, R., Lilien, M., Rasoulpour, M., Geffner, M.E., and Yadin, O. (2003). Hypertension in hypophosphatemic rickets--role of secondary hyperparathyroidism. Pediatric nephrology *18*, 155-158.

Amanzadeh, J., and Reilly, R.F., Jr. (2006). Hypophosphatemia: an evidence-based approach to its clinical consequences and management. Nature clinical practice. Nephrology *2*, 136-148.

Amiel, J., Bougeard, G., Francannet, C., Raclin, V., Munnich, A., Lyonnet, S., and Frebourg, T. (2001). TP63 gene mutation in ADULT syndrome. European journal of human genetics : EJHG *9*, 642-645.

Anders, S., and Huber, W. (2010). Differential expression analysis for sequence count data. Genome biology *11*, R106.

Andrews, T.D., Whittle, B., Field, M.A., Balakishnan, B., Zhang, Y., Shao, Y., Cho, V., Kirk, M., Singh, M., Xia, Y., et al. (2012). Massively parallel sequencing of the mouse exome to accurately identify rare, induced mutations: an immediate source for thousands of new mouse models. Open biology *2*, 120061.

Andrukhova, O., Zeitz, U., Goetz, R., Mohammadi, M., Lanske, B., and Erben, R.G. (2012). FGF23 acts directly on renal proximal tubules to induce phosphaturia through activation of the ERK1/2-SGK1 signaling pathway. Bone *51*, 621-628.

Antoniucci, D.M., Yamashita, T., and Portale, A.A. (2006). Dietary phosphorus regulates serum fibroblast growth factor-23 concentrations in healthy men. The Journal of clinical endocrinology and metabolism *91*, 3144-3149.

Arking, D.E., Krebsova, A., Macek, M., Sr., Macek, M., Jr., Arking, A., Mian, I.S., Fried, L., Hamosh, A., Dey, S., McIntosh, I., et al. (2002). Association of human aging with a functional variant of klotho. Proceedings of the National Academy of Sciences of the United States of America *99*, 856-861.

Arnold, C.N., Xia, Y., Lin, P., Ross, C., Schwander, M., Smart, N.G., Muller, U., and Beutler, B. (2011). Rapid identification of a disease allele in mouse through whole genome sequencing and bulk segregation analysis. Genetics *187*, 633-641.

Backstrom, M.C., Kouri, T., Kuusela, A.L., Sievanen, H., Koivisto, A.M., Ikonen, R.S., and Maki, M. (2000). Bone isoenzyme of serum alkaline phosphatase and serum inorganic phosphate in metabolic bone disease of prematurity. Acta paediatrica *89*, 867-873.

Ballard, S.A., Lodola, A., and Tarbit, M.H. (1988). A comparative study of 1-substituted imidazole and 1,2,4-triazole antifungal compounds as inhibitors of testosterone hydroxylations catalysed by mouse hepatic microsomal cytochromes P-450. Biochemical pharmacology *37*, 4643-4651.

Balling, R. (2001). ENU mutagenesis: analyzing gene function in mice. Annual review of genomics and human genetics *2*, 463-492.

Bamshad, M.J., Ng, S.B., Bigham, A.W., Tabor, H.K., Emond, M.J., Nickerson, D.A., and Shendure, J. (2011). Exome sequencing as a tool for Mendelian disease gene discovery. Nature reviews. Genetics *12*, 745-755.

Bar-Natan, M., Nelson, E.A., Walker, S.R., Kuang, Y., Distel, R.J., and Frank, D.A. (2012). Dual inhibition of Jak2 and STAT5 enhances killing of myeloproliferative neoplasia cells. Leukemia *26*, 1407-1410.

Barragan, I., Borrego, S., Abd El-Aziz, M.M., El-Ashry, M.F., Abu-Safieh, L., Bhattacharya, S.S., and Antinolo, G. (2008). Genetic analysis of FAM46A in Spanish families with autosomal recessive retinitis pigmentosa: characterisation of novel VNTRs. Annals of human genetics *72*, 26-34.

Baum, M., Schiavi, S., Dwarakanath, V., and Quigley, R. (2005). Effect of fibroblast growth factor-23 on phosphate transport in proximal tubules. Kidney international *68*, 1148-1153.

Baumann, K., de Rouffignac, C., Roinel, N., Rumrich, G., and Ullrich, K.J. (1975). Renal phosphate transport: inhomogeneity of local proximal transport rates and sodium dependence. Pflugers Archiv : European journal of physiology *356*, 287-298.

Beck, L., Karaplis, A.C., Amizuka, N., Hewson, A.S., Ozawa, H., and Tenenhouse, H.S. (1998). Targeted inactivation of Npt2 in mice leads to severe renal phosphate wasting, hypercalciuria, and skeletal abnormalities. Proceedings of the National Academy of Sciences of the United States of America *95*, 5372-5377.

Ben-Dov, I.Z., Galitzer, H., Lavi-Moshayoff, V., Goetz, R., Kuro-o, M., Mohammadi, M., Sirkis, R., Naveh-Many, T., and Silver, J. (2007). The parathyroid is a target organ for FGF23 in rats. The Journal of clinical investigation *117*, 4003-4008.

Benet-Pages, A., Lorenz-Depiereux, B., Zischka, H., White, K.E., Econs, M.J., and Strom, T.M. (2004). FGF23 is processed by proprotein convertases but not by PHEX. Bone *35*, 455-462.

Benet-Pages, A., Orlik, P., Strom, T.M., and Lorenz-Depiereux, B. (2005). An FGF23 missense mutation causes familial tumoral calcinosis with hyperphosphatemia. Human molecular genetics *14*, 385-390.

Bergwitz, C., and Juppner, H. (2010). Regulation of phosphate homeostasis by PTH, vitamin D, and FGF23. Annu Rev Med *61*, 91-104.

Bergwitz, C., Roslin, N.M., Tieder, M., Loredo-Osti, J.C., Bastepe, M., Abu-Zahra, H., Frappier, D., Burkett, K., Carpenter, T.O., Anderson, D., et al. (2006). SLC34A3 mutations in patients with hereditary hypophosphatemic rickets with hypercalciuria predict a key role for

the sodium-phosphate cotransporter NaPi-IIc in maintaining phosphate homeostasis. American journal of human genetics *78*, 179-192.

Biber, J., Hernando, N., and Forster, I. (2013). Phosphate transporters and their function. Annual review of physiology *75*, 535-550.

Bickle, M. (2010). The beautiful cell: high-content screening in drug discovery. Analytical and bioanalytical chemistry *398*, 219-226.

Biesiada, E., Razandi, M., and Levin, E.R. (1996). Egr-1 activates basic fibroblast growth factor transcription. Mechanistic implications for astrocyte proliferation. The Journal of biological chemistry *271*, 18576-18581.

Bloch, L., Sineshchekova, O., Reichenbach, D., Reiss, K., Saftig, P., Kuro-o, M., and Kaether, C. (2009). Klotho is a substrate for alpha-, beta- and gamma-secretase. FEBS letters *583*, 3221-3224.

Boles, M.K., Wilkinson, B.M., Wilming, L.G., Liu, B., Probst, F.J., Harrow, J., Grafham, D., Hentges, K.E., Woodward, L.P., Maxwell, A., et al. (2009). Discovery of candidate disease genes in ENU-induced mouse mutants by large-scale sequencing, including a splice-site mutation in nucleoredoxin. PLoS genetics *5*, e1000759.

Boot-Handford, R.P., Tuckwell, D.S., Plumb, D.A., Rock, C.F., and Poulsom, R. (2003). A novel and highly conserved collagen (pro(alpha)1(XXVII)) with a unique expression pattern and unusual molecular characteristics establishes a new clade within the vertebrate fibrillar collagen family. The Journal of biological chemistry *278*, 31067-31077.

Bowe, A.E., Finnegan, R., Jan de Beur, S.M., Cho, J., Levine, M.A., Kumar, R., and Schiavi, S.C. (2001). FGF-23 inhibits renal tubular phosphate transport and is a PHEX substrate. Biochemical and biophysical research communications *284*, 977-981.

Boycott, K.M., Vanstone, M.R., Bulman, D.E., and MacKenzie, A.E. (2013). Rare-disease genetics in the era of next-generation sequencing: discovery to translation. Nature reviews. Genetics *14*, 681-691.

Bradford, M.M. (1976). A rapid and sensitive method for the quantitation of microgram quantities of protein utilizing the principle of protein-dye binding. Anal Biochem *72*, 248-254.

Brown, E.M., Pollak, M., Riccardi, D., and Hebert, S.C. (1994). Cloning and characterization of an extracellular Ca(2+)-sensing receptor from parathyroid and kidney: new insights into the physiology and pathophysiology of calcium metabolism. Nephrology, dialysis, transplantation : official publication of the European Dialysis and Transplant Association - European Renal Association *9*, 1703-1706.

Brownstein, C.A., Adler, F., Nelson-Williams, C., Iijima, J., Li, P., Imura, A., Nabeshima, Y., Reyes-Mugica, M., Carpenter, T.O., and Lifton, R.P. (2008). A translocation causing increased alpha-klotho level results in hypophosphatemic rickets and hyperparathyroidism. Proceedings of the National Academy of Sciences of the United States of America *105*, 3455-3460.

Brunette, M.G., Chan, M., Ferriere, C., and Roberts, K.D. (1978). Site of 1,25(OH)2 vitamin D3 synthesis in the kidney. Nature *276*, 287-289.

Buehler, M.J. (2006). Nature designs tough collagen: explaining the nanostructure of collagen fibrils. Proceedings of the National Academy of Sciences of the United States of America *103*, 12285-12290.

Bull, K.R., Rimmer, A.J., Siggs, O.M., Miosge, L.A., Roots, C.M., Enders, A., Bertram, E.M., Crockford, T.L., Whittle, B., Potter, P.K., et al. (2013). Unlocking the bottleneck in forward genetics using whole-genome sequencing and identity by descent to isolate causative mutations. PLoS genetics *9*, e1003219.

Busch, A.E., Wagner, C.A., Schuster, A., Waldegger, S., Biber, J., Murer, H., and Lang, F. (1995). Properties of electrogenic Pi transport by a human renal brush border Na+/Pi transporter. Journal of the American Society of Nephrology : JASN *6*, 1547-1551.

Carmichael, K.D., Bynum, J.A., and Evans, E.B. (2009). Familial tumoral calcinosis: a forty-year follow-up on one family. The Journal of bone and joint surgery. American volume *91*, 664-671.

Carpenter, T.O. (2014). Management of hypophosphatemic rickets. Endocrine Abstracts *DOI:10.1530/endoabs.34.S4.3*.

Carpenter, T.O., Ellis, B.K., Insogna, K.L., Philbrick, W.M., Sterpka, J., and Shimkets, R. (2005). Fibroblast growth factor 7: an inhibitor of phosphate transport derived from oncogenic osteomalacia-causing tumors. The Journal of clinical endocrinology and metabolism *90*, 1012-1020.

Carpenter, T.O., Imel, E.A., Ruppe, M.D., Weber, T.J., Klausner, M.A., Wooddell, M.M., Kawakami, T., Ito, T., Zhang, X., Humphrey, J., et al. (2014). Randomized trial of the anti-FGF23 antibody KRN23 in X-linked hypophosphatemia. The Journal of clinical investigation *124*, 1587-1597.

Carrillo-Lopez, N., Roman-Garcia, P., Rodriguez-Rebollar, A., Fernandez-Martin, J.L., Naves-Diaz, M., and Cannata-Andia, J.B. (2009). Indirect regulation of PTH by estrogens may require FGF23. Journal of the American Society of Nephrology : JASN *20*, 2009-2017.

Carter, C.O. (1977). Monogenic disorders. Journal of medical genetics *14*, 316-320.

Chang, Q., Hoefs, S., van der Kemp, A.W., Topala, C.N., Bindels, R.J., and Hoenderop, J.G. (2005). The beta-glucuronidase klotho hydrolyzes and activates the TRPV5 channel. Science *310*, 490-493.

Chen, C.D., Podvin, S., Gillespie, E., Leeman, S.E., and Abraham, C.R. (2007). Insulin stimulates the cleavage and release of the extracellular domain of Klotho by ADAM10 and ADAM17. Proceedings of the National Academy of Sciences of the United States of America *104*, 19796-19801.

Chen, G., Deng, C., and Li, Y.P. (2012). TGF-beta and BMP signaling in osteoblast differentiation and bone formation. International journal of biological sciences *8*, 272-288.

Chen, H., Xu, C.F., Ma, J., Eliseenkova, A.V., Li, W., Pollock, P.M., Pitteloud, N., Miller, W.T., Neubert, T.A., and Mohammadi, M. (2008). A crystallographic snapshot of tyrosine trans-phosphorylation in action. Proceedings of the National Academy of Sciences of the United States of America *105*, 19660-19665.

Courbebaisse, M., Leroy, C., Bakouh, N., Salaun, C., Beck, L., Grandchamp, B., Planelles, G., Hall, R.A., Friedlander, G., and Prie, D. (2012). A new human NHERF1 mutation decreases renal phosphate transporter NPT2a expression by a PTH-independent mechanism. PloS one *7*, e34764.

Crum, C.P., and McKeon, F.D. (2010). p63 in epithelial survival, germ cell surveillance, and neoplasia. Annual review of pathology *5*, 349-371.

Cunningham, R., Biswas, R., Steplock, D., Shenolikar, S., and Weinman, E. (2010). Role of NHERF and scaffolding proteins in proximal tubule transport. Urological research *38*, 257-262.

Danisi, G., Bonjour, J.P., and Straub, R.W. (1980). Regulation of Na-dependent phosphate influx across the mucosal border of duodenum by 1,25-dihydroxycholecalciferol. Pflugers Archiv : European journal of physiology *388*, 227-232.

De Beur, S.M., Finnegan, R.B., Vassiliadis, J., Cook, B., Barberio, D., Estes, S., Manavalan, P., Petroziello, J., Madden, S.L., Cho, J.Y., et al. (2002). Tumors associated with oncogenic osteomalacia express genes important in bone and mineral metabolism. Journal of bone and mineral research : the official journal of the American Society for Bone and Mineral Research *17*, 1102-1110.

de Bock, G.H., Eelhart, J., van Marwijk, H.W., Tromp, T.P., and Springer, M.P. (1997). A postmarketing study of flunarizine in migraine and vertigo. Pharmacy world & science : PWS *19*, 269-274.

Dianzani, I., Garelli, E., Gustavsson, P., Carando, A., Gustafsson, B., Dahl, N., and Anneren, G. (2003). Rapp-Hodgkin and AEC syndromes due to a new frameshift mutation in the TP63 gene. Journal of medical genetics *40*, e133.

Dubal, D.B., Yokoyama, J.S., Zhu, L., Broestl, L., Worden, K., Wang, D., Sturm, V.E., Kim, D., Klein, E., Yu, G.Q., et al. (2014). Life extension factor klotho enhances cognition. Cell reports *7*, 1065-1076.

Duursma, S.A., Visser, W.J., Mees, E.J., and Njio, L. (1974). Serum calcium, phosphate and alkaline phosphatase and morphometric bone examinations in 30 patients with renal insufficiency. Calcified tissue research *16*, 129-138.

Econs, M.J., and Drezner, M.K. (1994). Tumor-induced osteomalacia--unveiling a new hormone. The New England journal of medicine *330*, 1679-1681.

Eggert, U.S. (2013). The why and how of phenotypic small-molecule screens. Nature chemical biology *9*, 206-209.

Eicher, E.M., Southard, J.L., Scriver, C.R., and Glorieux, F.H. (1976). Hypophosphatemia: mouse model for human familial hypophosphatemic (vitamin D-resistant) rickets.

Proceedings of the National Academy of Sciences of the United States of America *73*, 4667-4671.

English, J.M., and Cobb, M.H. (2002). Pharmacological inhibitors of MAPK pathways. Trends in pharmacological sciences *23*, 40-45.

Etokebe, G.E., Bulat-Kardum, L., Munthe, L.A., Balen, S., and Dembic, Z. (2014). Association of variable number of tandem repeats in the coding region of the FAM46A gene, FAM46A rs11040 SNP and BAG6 rs3117582 SNP with susceptibility to tuberculosis. PloS one *9*, e91385.

Etokebe, G.E., Kuchler, A.M., Haraldsen, G., Landin, M., Osmundsen, H., and Dembic, Z. (2009). Family-with-sequence-similarity-46, member A (Fam46a) gene is expressed in developing tooth buds. Archives of oral biology *54*, 1002-1007.

European Organisation for Rare Diseases, E. (2005). Rare Diseases: Understanding This Public Health Priority.

Fairfield, H., Gilbert, G.J., Barter, M., Corrigan, R.R., Curtain, M., Ding, Y., D'Ascenzo, M., Gerhardt, D.J., He, C., Huang, W., et al. (2011). Mutation discovery in mice by whole exome sequencing. Genome biology *12*, R86.

Farrow, E.G., Imel, E.A., and White, K.E. (2011a). Miscellaneous non-inflammatory musculoskeletal conditions. Hyperphosphatemic familial tumoral calcinosis (FGF23, GALNT3 and alphaKlotho). Best practice & research. Clinical rheumatology *25*, 735-747.

Farrow, E.G., Summers, L.J., Schiavi, S.C., McCormick, J.A., Ellison, D.H., and White, K.E. (2010). Altered renal FGF23-mediated activity involving MAPK and Wnt: effects of the Hyp mutation. The Journal of endocrinology *207*, 67-75.

Farrow, E.G., Yu, X., Summers, L.J., Davis, S.I., Fleet, J.C., Allen, M.R., Robling, A.G., Stayrook, K.R., Jideonwo, V., Magers, M.J., et al. (2011b). Iron deficiency drives an autosomal dominant hypophosphatemic rickets (ADHR) phenotype in fibroblast growth factor-23 (Fgf23) knock-in mice. Proceedings of the National Academy of Sciences of the United States of America *108*, E1146-1155.

Faruqi, T., Dhawan, N., Bahl, J., Gupta, V., Vohra, S., Tu, K., and Abdelmagid, S.M. (2014). Molecular, phenotypic aspects and therapeutic horizons of rare genetic bone disorders. BioMed research international *2014*, 670842.

Favata, M.F., Horiuchi, K.Y., Manos, E.J., Daulerio, A.J., Stradley, D.A., Feeser, W.S., Van Dyk, D.E., Pitts, W.J., Earl, R.A., Hobbs, F., et al. (1998). Identification of a novel inhibitor of mitogen-activated protein kinase kinase. The Journal of biological chemistry *273*, 18623-18632.

Feng, J.Q., Scott, G., Guo, D., Jiang, B., Harris, M., Ward, T., Ray, M., Bonewald, L.F., Harris, S.E., and Mishina, Y. (2008). Generation of a conditional null allele for Dmp1 in mouse. Genesis *46*, 87-91.

Feng, J.Q., Ward, L.M., Liu, S., Lu, Y., Xie, Y., Yuan, B., Yu, X., Rauch, F., Davis, S.I., Zhang, S., et al. (2006). Loss of DMP1 causes rickets and osteomalacia and identifies a role for osteocytes in mineral metabolism. Nature genetics *38*, 1310-1315.

Ferrari, S.L., Bonjour, J.P., and Rizzoli, R. (2005). Fibroblast growth factor-23 relationship to dietary phosphate and renal phosphate handling in healthy young men. The Journal of clinical endocrinology and metabolism *90*, 1519-1524.

Forster, I.C., Hernando, N., Biber, J., and Murer, H. (2006). Proximal tubular handling of phosphate: A molecular perspective. Kidney international *70*, 1548-1559.

Fuchs, H., Gailus-Durner, V., Neschen, S., Adler, T., Afonso, L.C., Aguilar-Pimentel, J.A., Becker, L., Bohla, A., Calzada-Wack, J., Cohrs, C., et al. (2012). Innovations in phenotyping of mouse models in the German Mouse Clinic. Mammalian genome : official journal of the International Mammalian Genome Society *23*, 611-622.

Furdui, C.M., Lew, E.D., Schlessinger, J., and Anderson, K.S. (2006). Autophosphorylation of FGFR1 kinase is mediated by a sequential and precisely ordered reaction. Molecular cell *21*, 711-717.

Gashler, A., and Sukhatme, V.P. (1995). Early growth response protein 1 (Egr-1): prototype of a zinc-finger family of transcription factors. Progress in nucleic acid research and molecular biology *50*, 191-224.

Gattineni, J., Bates, C., Twombley, K., Dwarakanath, V., Robinson, M.L., Goetz, R., Mohammadi, M., and Baum, M. (2009). FGF23 decreases renal NaPi-2a and NaPi-2c expression and induces hypophosphatemia in vivo predominantly via FGF receptor 1. American journal of physiology. Renal physiology *297*, F282-291.

Gattineni, J., and Baum, M. (2012). Genetic disorders of phosphate regulation. Pediatric nephrology *27*, 1477-1487.

Gattineni, J., Twombley, K., Goetz, R., Mohammadi, M., and Baum, M. (2011). Regulation of serum 1,25(OH)2 vitamin D3 levels by fibroblast growth factor 23 is mediated by FGF receptors 3 and 4. American journal of physiology. Renal physiology *301*, F371-377.

Gilbert, S.F. (2000). Osteogenesis: The Development of Bones. Developmental Biology. 6th edition. Sunderland (MA): Sinauer Associates. Available from: http://www.ncbi.nlm.nih.gov/books/NBK10056.

Goetz, R., Beenken, A., Ibrahimi, O.A., Kalinina, J., Olsen, S.K., Eliseenkova, A.V., Xu, C., Neubert, T.A., Zhang, F., Linhardt, R.J., et al. (2007). Molecular insights into the klotho-dependent, endocrine mode of action of fibroblast growth factor 19 subfamily members. Molecular and cellular biology *27*, 3417-3428.

Goetz, R., Nakada, Y., Hu, M.C., Kurosu, H., Wang, L., Nakatani, T., Shi, M., Eliseenkova, A.V., Razzaque, M.S., Moe, O.W., et al. (2010). Isolated C-terminal tail of FGF23 alleviates hypophosphatemia by inhibiting FGF23-FGFR-Klotho complex formation. Proceedings of the National Academy of Sciences of the United States of America *107*, 407-412.

Greenberg, B.G., Winters, R.W., and Graham, J.B. (1960). The normal range of serum inorganic phosphorus and its utility as a discriminant in the diagnosis of congenital hypophosphatemia. The Journal of clinical endocrinology and metabolism *20*, 364-379.

Guha, M., O'Connell, M.A., Pawlinski, R., Hollis, A., McGovern, P., Yan, S.F., Stern, D., and Mackman, N. (2001). Lipopolysaccharide activation of the MEK-ERK1/2 pathway in human

monocytic cells mediates tissue factor and tumor necrosis factor alpha expression by inducing Elk-1 phosphorylation and Egr-1 expression. Blood *98*, 1429-1439.

Harada, T., Morooka, T., Ogawa, S., and Nishida, E. (2001). ERK induces p35, a neuron-specific activator of Cdk5, through induction of Egr1. Nature cell biology *3*, 453-459.

Harris, C.A., Sutton, R.A., and Dirks, J.H. (1977). Effects of hypercalcemia on calcium and phosphate ultrafilterability and tubular reabsorption in the rat. The American journal of physiology *233*, F201-206.

Hattenhauer, O., Traebert, M., Murer, H., and Biber, J. (1999). Regulation of small intestinal Na-P(i) type IIb cotransporter by dietary phosphate intake. The American journal of physiology *277*, G756-762.

Haura, E.B., Ricart, A.D., Larson, T.G., Stella, P.J., Bazhenova, L., Miller, V.A., Cohen, R.B., Eisenberg, P.D., Selaru, P., Wilner, K.D., et al. (2010). A phase II study of PD-0325901, an oral MEK inhibitor, in previously treated patients with advanced non-small cell lung cancer. Clinical cancer research : an official journal of the American Association for Cancer Research *16*, 2450-2457.

Haworth, K., Smith, F., Zoupa, M., Seppala, M., Sharpe, P.T., and Cobourne, M.T. (2007). Expression of the Scube3 epidermal growth factor-related gene during early embryonic development in the mouse. Gene expression patterns : GEP *7*, 630-634.

Hofer, G., Grimmer, C., Sukhatme, V.P., Sterzel, R.B., and Rupprecht, H.D. (1996). Transcription factor Egr-1 regulates glomerular mesangial cell proliferation. The Journal of biological chemistry *271*, 28306-28310.

Horvai, A.E., and Boyce, B.F. (2011). Metabolic bone diseases. Seminars in diagnostic pathology *28*, 13-25.

Hrabe de Angelis, M., and Balling, R. (1998). Large scale ENU screens in the mouse: genetics meets genomics. Mutation research *400*, 25-32.

Hrabe de Angelis, M.H., Flaswinkel, H., Fuchs, H., Rathkolb, B., Soewarto, D., Marschall, S., Heffner, S., Pargent, W., Wuensch, K., Jung, M., et al. (2000). Genome-wide, large-scale production of mutant mice by ENU mutagenesis. Nature genetics *25*, 444-447.

Hu, L., Andersson, G., Jonsson, K.B., Melhus, H., and Lind, T. (2013a). Adamts1 is highly induced in rachitic bones of FGF23 transgenic mice and participates in degradation of non-mineralized bone matrix collagen. Biochemical and biophysical research communications *430*, 901-906.

Hu, M.C., Shiizaki, K., Kuro-o, M., and Moe, O.W. (2013b). Fibroblast growth factor 23 and Klotho: physiology and pathophysiology of an endocrine network of mineral metabolism. Annual review of physiology *75*, 503-533.

Huang, C.L. (2010). Regulation of ion channels by secreted Klotho: mechanisms and implications. Kidney international *77*, 855-860.

Huang, C.L., and Moe, O.W. (2011). Klotho: a novel regulator of calcium and phosphorus homeostasis. Pflugers Archiv : European journal of physiology *462*, 185-193.

Hughes, J.P., Rees, S., Kalindjian, S.B., and Philpott, K.L. (2011). Principles of early drug discovery. British journal of pharmacology *162*, 1239-1249.

Ichikawa, S., Imel, E.A., Kreiter, M.L., Yu, X., Mackenzie, D.S., Sorenson, A.H., Goetz, R., Mohammadi, M., White, K.E., and Econs, M.J. (2007). A homozygous missense mutation in human KLOTHO causes severe tumoral calcinosis. The Journal of clinical investigation *117*, 2684-2691.

Imura, A., Iwano, A., Tohyama, O., Tsuji, Y., Nozaki, K., Hashimoto, N., Fujimori, T., and Nabeshima, Y. (2004). Secreted Klotho protein in sera and CSF: implication for post-translational cleavage in release of Klotho protein from cell membrane. FEBS letters *565*, 143-147.

Isakova, T., Gutierrez, O.M., Smith, K., Epstein, M., Keating, L.K., Juppner, H., and Wolf, M. (2011). Pilot study of dietary phosphorus restriction and phosphorus binders to target fibroblast growth factor 23 in patients with chronic kidney disease. Nephrology, dialysis, transplantation : official publication of the European Dialysis and Transplant Association - European Renal Association *26*, 584-591.

Iversen, P.W., Beck, B., Chen, Y.F., Dere, W., Devanarayan, V., Eastwood, B.J., Farmen, M.W., Iturria, S.J., Montrose, C., Moore, R.A., et al. (2004). HTS Assay Validation. In Assay Guidance Manual. G.S. Sittampalam, N. Gal-Edd, M. Arkin, D. Auld, C. Austin, B. Bejcek, M. Glicksman, J. Inglese, V. Lemmon, Z. Li, et al., eds. (Bethesda (MD)).

Jacobs, J.W., Huisman, A.M., van Paassen, H.C., and Bijlsma, J.W. (1999). [Paget's disease of the bones: diagnosis and treatment]. Nederlands tijdschrift voor geneeskunde *143*, 719-725.

Jakob, F. (2007). [Metabolic bone diseases]. Der Internist *48*, 1101-1117.

Janssens, K., ten Dijke, P., Janssens, S., and Van Hul, W. (2005). Transforming growth factor-beta1 to the bone. Endocrine reviews *26*, 743-774.

Jones, M.W., Errington, M.L., French, P.J., Fine, A., Bliss, T.V., Garel, S., Charnay, P., Bozon, B., Laroche, S., and Davis, S. (2001). A requirement for the immediate early gene Zif268 in the expression of late LTP and long-term memories. Nature neuroscience *4*, 289-296.

Jones, S.K., and Kennedy, C.T. (1990). Contact dermatitis from tioconazole. Contact dermatitis *22*, 122-123.

Kang, J., Wang, L., Cai, F., and Rampe, D. (2000). High affinity blockade of the HERG cardiac K(+) channel by the neuroleptic pimozide. European journal of pharmacology *392*, 137-140.

Karim, Z., Gerard, B., Bakouh, N., Alili, R., Leroy, C., Beck, L., Silve, C., Planelles, G., Urena-Torres, P., Grandchamp, B., et al. (2008). NHERF1 mutations and responsiveness of renal parathyroid hormone. The New England journal of medicine *359*, 1128-1135.

Kato, K., Jeanneau, C., Tarp, M.A., Benet-Pages, A., Lorenz-Depiereux, B., Bennett, E.P., Mandel, U., Strom, T.M., and Clausen, H. (2006). Polypeptide GalNAc-transferase T3 and familial tumoral calcinosis. Secretion of fibroblast growth factor 23 requires O-glycosylation. The Journal of biological chemistry *281*, 18370-18377.

Kaufmann, K., Bach, K., and Thiel, G. (2001). The extracellular signal-regulated protein kinases Erk1/Erk2 stimulate expression and biological activity of the transcriptional regulator Egr-1. Biological chemistry *382*, 1077-1081.

Kaufmann, K., and Thiel, G. (2001). Epidermal growth factor and platelet-derived growth factor induce expression of Egr-1, a zinc finger transcription factor, in human malignant glioma cells. Journal of the neurological sciences *189*, 83-91.

Kawata, T., Imanishi, Y., Kobayashi, K., Miki, T., Arnold, A., Inaba, M., and Nishizawa, Y. (2007). Parathyroid hormone regulates fibroblast growth factor-23 in a mouse model of primary hyperparathyroidism. Journal of the American Society of Nephrology : JASN *18*, 2683-2688.

Keays, D.A., Clark, T.G., and Flint, J. (2006). Estimating the number of coding mutations in genotypic- and phenotypic-driven N-ethyl-N-nitrosourea (ENU) screens. Mammalian genome : official journal of the International Mammalian Genome Society *17*, 230-238.

Khachigian, L.M., Lindner, V., Williams, A.J., and Collins, T. (1996). Egr-1-induced endothelial gene expression: a common theme in vascular injury. Science *271*, 1427-1431.

Kinoshita, A., Saito, T., Tomita, H., Makita, Y., Yoshida, K., Ghadami, M., Yamada, K., Kondo, S., Ikegawa, S., Nishimura, G., et al. (2000). Domain-specific mutations in TGFB1 result in Camurati-Engelmann disease. Nature genetics *26*, 19-20.

Klempt, M., Rathkolb, B., Fuchs, E., de Angelis, M.H., Wolf, E., and Aigner, B. (2006). Genotype-specific environmental impact on the variance of blood values in inbred and F1 hybrid mice. Mammalian genome : official journal of the International Mammalian Genome Society *17*, 93-102.

Koch, M., Laub, F., Zhou, P., Hahn, R.A., Tanaka, S., Burgeson, R.E., Gerecke, D.R., Ramirez, F., and Gordon, M.K. (2003). Collagen XXIV, a vertebrate fibrillar collagen with structural features of invertebrate collagens: selective expression in developing cornea and bone. The Journal of biological chemistry *278*, 43236-43244.

Kuchta, K., Knizewski, L., Wyrwicz, L.S., Rychlewski, L., and Ginalski, K. (2009). Comprehensive classification of nucleotidyltransferase fold proteins: identification of novel families and their representatives in human. Nucleic acids research *37*, 7701-7714.

Kuro-o, M., Matsumura, Y., Aizawa, H., Kawaguchi, H., Suga, T., Utsugi, T., Ohyama, Y., Kurabayashi, M., Kaname, T., Kume, E., et al. (1997). Mutation of the mouse klotho gene leads to a syndrome resembling ageing. Nature *390*, 45-51.

Kurosu, H., Ogawa, Y., Miyoshi, M., Yamamoto, M., Nandi, A., Rosenblatt, K.P., Baum, M.G., Schiavi, S., Hu, M.C., Moe, O.W., et al. (2006). Regulation of fibroblast growth factor-23 signaling by klotho. The Journal of biological chemistry *281*, 6120-6123.

Kurosu, H., Yamamoto, M., Clark, J.D., Pastor, J.V., Nandi, A., Gurnani, P., McGuinness, O.P., Chikuda, H., Yamaguchi, M., Kawaguchi, H., et al. (2005). Suppression of aging in mice by the hormone Klotho. Science *309*, 1829-1833.

Lagali, P.S., Kakuk, L.E., Griesinger, I.B., Wong, P.W., and Ayyagari, R. (2002). Identification and characterization of C6orf37, a novel candidate human retinal disease gene on chromosome 6q14. Biochemical and biophysical research communications *293*, 356-365.

Lanske, B., and Razzaque, M.S. (2014). Molecular interactions of FGF23 and PTH in phosphate regulation. Kidney international *86*, 1072-1074.

Lapointe, J.Y., Tessier, J., Paquette, Y., Wallendorff, B., Coady, M.J., Pichette, V., and Bonnardeaux, A. (2006). NPT2a gene variation in calcium nephrolithiasis with renal phosphate leak. Kidney international *69*, 2261-2267.

Larsson, T., Nisbeth, U., Ljunggren, O., Juppner, H., and Jonsson, K.B. (2003). Circulating concentration of FGF-23 increases as renal function declines in patients with chronic kidney disease, but does not change in response to variation in phosphate intake in healthy volunteers. Kidney international *64*, 2272-2279.

Lavi-Moshayoff, V., Wasserman, G., Meir, T., Silver, J., and Naveh-Many, T. (2010). PTH increases FGF23 gene expression and mediates the high-FGF23 levels of experimental kidney failure: a bone parathyroid feedback loop. American journal of physiology. Renal physiology *299*, F882-889.

Lee, J.Y., and Imel, E.A. (2013). The changing face of hypophosphatemic disorders in the FGF-23 era. Pediatric endocrinology reviews : PER *10 Suppl 2*, 367-379.

Lee, S.L., Sadovsky, Y., Swirnoff, A.H., Polish, J.A., Goda, P., Gavrilina, G., and Milbrandt, J. (1996). Luteinizing hormone deficiency and female infertility in mice lacking the transcription factor NGFI-A (Egr-1). Science *273*, 1219-1221.

Leone, M., Grazzi, L., La Mantia, L., and Bussone, G. (1991). Flunarizine in migraine: a minireview. Headache *31*, 388-391.

Lepcha, A., Amalanathan, S., Augustine, A.M., Tyagi, A.K., and Balraj, A. (2014). Flunarizine in the prophylaxis of migrainous vertigo: a randomized controlled trial. European archives of oto-rhino-laryngology : official journal of the European Federation of Oto-Rhino-Laryngological Societies *271*, 2931-2936.

Li, H., and Durbin, R. (2009). Fast and accurate short read alignment with Burrows-Wheeler transform. Bioinformatics *25*, 1754-1760.

Li, H., and Durbin, R. (2010). Fast and accurate long-read alignment with Burrows-Wheeler transform. Bioinformatics *26*, 589-595.

Li, H., Handsaker, B., Wysoker, A., Fennell, T., Ruan, J., Homer, N., Marth, G., Abecasis, G., Durbin, R., and Genome Project Data Processing, S. (2009). The Sequence Alignment/Map format and SAMtools. Bioinformatics *25*, 2078-2079.

Li, S.A., Watanabe, M., Yamada, H., Nagai, A., Kinuta, M., and Takei, K. (2004). Immunohistochemical localization of Klotho protein in brain, kidney, and reproductive organs of mice. Cell structure and function *29*, 91-99.

Lieberman, L.A., and Higgins, D.E. (2009). A small-molecule screen identifies the antipsychotic drug pimozide as an inhibitor of Listeria monocytogenes infection. Antimicrobial agents and chemotherapy *53*, 756-764.

Lim, Y.H., Ovejero, D., Sugarman, J.S., Deklotz, C.M., Maruri, A., Eichenfield, L.F., Kelley, P.K., Juppner, H., Gottschalk, M., Tifft, C.J., et al. (2014). Multilineage somatic activating mutations in HRAS and NRAS cause mosaic cutaneous and skeletal lesions, elevated FGF23 and hypophosphatemia. Human molecular genetics *23*, 397-407.

Lindsay, M.E., Schepers, D., Bolar, N.A., Doyle, J.J., Gallo, E., Fert-Bober, J., Kempers, M.J., Fishman, E.K., Chen, Y., Myers, L., et al. (2012). Loss-of-function mutations in TGFB2 cause a syndromic presentation of thoracic aortic aneurysm. Nature genetics *44*, 922-927.

Linglart, A., Biosse-Duplan, M., Briot, K., Chaussain, C., Esterle, L., Guillaume-Czitrom, S., Kamenicky, P., Nevoux, J., Prie, D., Rothenbuhler, A., et al. (2014). Therapeutic management of hypophosphatemic rickets from infancy to adulthood. Endocrine connections *3*, R13-30.

Lisse, T.S., Thiele, F., Fuchs, H., Hans, W., Przemeck, G.K., Abe, K., Rathkolb, B., Quintanilla-Martinez, L., Hoelzlwimmer, G., Helfrich, M., et al. (2008). ER stress-mediated apoptosis in a new mouse model of osteogenesis imperfecta. PLoS genetics *4*, e7.

Liu, F., Wu, S., Ren, H., and Gu, J. (2011). Klotho suppresses RIG-I-mediated senescence-associated inflammation. Nature cell biology *13*, 254-262.

Liu, H., Fergusson, M.M., Castilho, R.M., Liu, J., Cao, L., Chen, J., Malide, D., Rovira, II, Schimel, D., Kuo, C.J., et al. (2007). Augmented Wnt signaling in a mammalian model of accelerated aging. Science *317*, 803-806.

Liu, S., Guo, R., Simpson, L.G., Xiao, Z.S., Burnham, C.E., and Quarles, L.D. (2003). Regulation of fibroblastic growth factor 23 expression but not degradation by PHEX. The Journal of biological chemistry *278*, 37419-37426.

Liu, S., and Quarles, L.D. (2007). How fibroblast growth factor 23 works. Journal of the American Society of Nephrology : JASN *18*, 1637-1647.

Liu, S., Tang, W., Zhou, J., Stubbs, J.R., Luo, Q., Pi, M., and Quarles, L.D. (2006a). Fibroblast growth factor 23 is a counter-regulatory phosphaturic hormone for vitamin D. Journal of the American Society of Nephrology : JASN *17*, 1305-1315.

Liu, S., Vierthaler, L., Tang, W., Zhou, J., and Quarles, L.D. (2008). FGFR3 and FGFR4 do not mediate renal effects of FGF23. Journal of the American Society of Nephrology : JASN *19*, 2342-2350.

Liu, S., Zhou, J., Tang, W., Jiang, X., Rowe, D.W., and Quarles, L.D. (2006b). Pathogenic role of Fgf23 in Hyp mice. American journal of physiology. Endocrinology and metabolism *291*, E38-49.

Loeys, B.L., Chen, J., Neptune, E.R., Judge, D.P., Podowski, M., Holm, T., Meyers, J., Leitch, C.C., Katsanis, N., Sharifi, N., et al. (2005). A syndrome of altered cardiovascular, craniofacial, neurocognitive and skeletal development caused by mutations in TGFBR1 or TGFBR2. Nature genetics *37*, 275-281.

Lorenz-Depiereux, B., Bastepe, M., Benet-Pages, A., Amyere, M., Wagenstaller, J., Muller-Barth, U., Badenhoop, K., Kaiser, S.M., Rittmaster, R.S., Shlossberg, A.H., et al. (2006a). DMP1 mutations in autosomal recessive hypophosphatemia implicate a bone matrix protein in the regulation of phosphate homeostasis. Nature genetics *38*, 1248-1250.

Lorenz-Depiereux, B., Benet-Pages, A., Eckstein, G., Tenenbaum-Rakover, Y., Wagenstaller, J., Tiosano, D., Gershoni-Baruch, R., Albers, N., Lichtner, P., Schnabel, D., et al. (2006b). Hereditary hypophosphatemic rickets with hypercalciuria is caused by mutations in the sodium-phosphate cotransporter gene SLC34A3. American journal of human genetics *78*, 193-201.

Lorenz-Depiereux, B., Schnabel, D., Tiosano, D., Hausler, G., and Strom, T.M. (2010). Loss-of-function ENPP1 mutations cause both generalized arterial calcification of infancy and autosomal-recessive hypophosphatemic rickets. American journal of human genetics *86*, 267-272.

Lyon, M.F., Scriver, C.R., Baker, L.R., Tenenhouse, H.S., Kronick, J., and Mandla, S. (1986). The Gy mutation: another cause of X-linked hypophosphatemia in mouse. Proceedings of the National Academy of Sciences of the United States of America *83*, 4899-4903.

Macarron, R., Banks, M.N., Bojanic, D., Burns, D.J., Cirovic, D.A., Garyantes, T., Green, D.V., Hertzberg, R.P., Janzen, W.P., Paslay, J.W., et al. (2011). Impact of high-throughput screening in biomedical research. Nature reviews. Drug discovery *10*, 188-195.

Mackenzie, N.C., Zhu, D., Milne, E.M., van 't Hof, R., Martin, A., Darryl Quarles, L., Millan, J.L., Farquharson, C., and MacRae, V.E. (2012). Altered bone development and an increase in FGF-23 expression in Enpp1(-/-) mice. PloS one *7*, e32177.

Magagnin, S., Werner, A., Markovich, D., Sorribas, V., Stange, G., Biber, J., and Murer, H. (1993). Expression cloning of human and rat renal cortex Na/Pi cotransport. Proceedings of the National Academy of Sciences of the United States of America *90*, 5979-5983.

Magen, D., Berger, L., Coady, M.J., Ilivitzki, A., Militianu, D., Tieder, M., Selig, S., Lapointe, J.Y., Zelikovic, I., and Skorecki, K. (2010). A loss-of-function mutation in NaPi-IIa and renal Fanconi's syndrome. The New England journal of medicine *362*, 1102-1109.

Marriott, M.S., Baird, J.R., Brammer, K.W., Faulkner, J.K., Halliwell, G., Jevons, S., and Tarbit, M.H. (1983). Tioconazole, a new imidazole-antifungal agent for the treatment of dermatomycoses. Antifungal and pharmacologic properties. Dermatologica *166 Suppl 1*, 1-7.

Martin, A., David, V., and Quarles, L.D. (2012). Regulation and function of the FGF23/klotho endocrine pathways. Physiological reviews *92*, 131-155.

Martin, A., Liu, S., David, V., Li, H., Karydis, A., Feng, J.Q., and Quarles, L.D. (2011). Bone proteins PHEX and DMP1 regulate fibroblastic growth factor Fgf23 expression in osteocytes through a common pathway involving FGF receptor (FGFR) signaling. FASEB journal : official publication of the Federation of American Societies for Experimental Biology *25*, 2551-2562.

Matsuo, N., Tanaka, S., Gordon, M.K., Koch, M., Yoshioka, H., and Ramirez, F. (2006). CREB-AP1 protein complexes regulate transcription of the collagen XXIV gene (Col24a1) in osteoblasts. The Journal of biological chemistry *281*, 5445-5452.

Matsuo, N., Tanaka, S., Yoshioka, H., Koch, M., Gordon, M.K., and Ramirez, F. (2008). Collagen XXIV (Col24a1) gene expression is a specific marker of osteoblast differentiation and bone formation. Connective tissue research *49*, 68-75.

McGrath, J.A., Duijf, P.H., Doetsch, V., Irvine, A.D., de Waal, R., Vanmolkot, K.R., Wessagowit, V., Kelly, A., Atherton, D.J., Griffiths, W.A., et al. (2001). Hay-Wells syndrome is caused by heterozygous missense mutations in the SAM domain of p63. Human molecular genetics *10*, 221-229.

Meir, T., Durlacher, K., Pan, Z., Amir, G., Richards, W.G., Silver, J., and Naveh-Many, T. (2014). Parathyroid hormone activates the orphan nuclear receptor Nurr1 to induce FGF23 transcription. Kidney international *86*, 1106-1115.

Metzker, M.L. (2010). Sequencing technologies - the next generation. Nature reviews. Genetics *11*, 31-46.

Meyer, R.A., Jr., Meyer, M.H., and Gray, R.W. (1989). Parabiosis suggests a humoral factor is involved in X-linked hypophosphatemia in mice. Journal of bone and mineral research : the official journal of the American Society for Bone and Mineral Research *4*, 493-500.

Miedlich, S.U., Zalutskaya, A., Zhu, E.D., and Demay, M.B. (2010). Phosphate-induced apoptosis of hypertrophic chondrocytes is associated with a decrease in mitochondrial membrane potential and is dependent upon Erk1/2 phosphorylation. The Journal of biological chemistry *285*, 18270-18275.

Miyagawa, K., Yamazaki, M., Kawai, M., Nishino, J., Koshimizu, T., Ohata, Y., Tachikawa, K., Mikuni-Takagaki, Y., Kogo, M., Ozono, K., et al. (2014). Dysregulated gene expression in the primary osteoblasts and osteocytes isolated from hypophosphatemic Hyp mice. PloS one *9*, e93840.

Moglia, A., Bergamasco, B., Di Perri, R., and Mancia, D. (1986). Flunarizine as add-on therapy in epilepsy. Crossover study vs placebo. Functional neurology *1*, 547-550.

Mohammadi, M., McMahon, G., Sun, L., Tang, C., Hirth, P., Yeh, B.K., Hubbard, S.R., and Schlessinger, J. (1997). Structures of the tyrosine kinase domain of fibroblast growth factor receptor in complex with inhibitors. Science *276*, 955-960.

Mohammadi, M., Olsen, S.K., and Ibrahimi, O.A. (2005). Structural basis for fibroblast growth factor receptor activation. Cytokine & growth factor reviews *16*, 107-137.

Mothi, M., and Sampson, S. (2013). Pimozide for schizophrenia or related psychoses. The Cochrane database of systematic reviews *11*, CD001949.

Naveed, M., Nath, S.K., Gaines, M., Al-Ali, M.T., Al-Khaja, N., Hutchings, D., Golla, J., Deutsch, S., Bottani, A., Antonarakis, S.E., et al. (2007). Genomewide linkage scan for split-hand/foot malformation with long-bone deficiency in a large Arab family identifies two novel susceptibility loci on chromosomes 1q42.2-q43 and 6q14.1. American journal of human genetics *80*, 105-111.

Nehgme, R., Fahey, J.T., Smith, C., and Carpenter, T.O. (1997). Cardiovascular abnormalities in patients with X-linked hypophosphatemia. The Journal of clinical endocrinology and metabolism *82*, 2450-2454.

Nelson, E.A., Walker, S.R., Weisberg, E., Bar-Natan, M., Barrett, R., Gashin, L.B., Terrell, S., Klitgaard, J.L., Santo, L., Addorio, M.R., et al. (2011). The STAT5 inhibitor pimozide decreases survival of chronic myelogenous leukemia cells resistant to kinase inhibitors. Blood *117*, 3421-3429.

Nesbitt, T., Coffman, T.M., Griffiths, R., and Drezner, M.K. (1992). Crosstransplantation of kidneys in normal and Hyp mice. Evidence that the Hyp mouse phenotype is unrelated to an intrinsic renal defect. The Journal of clinical investigation *89*, 1453-1459.

Ng, S.B., Buckingham, K.J., Lee, C., Bigham, A.W., Tabor, H.K., Dent, K.M., Huff, C.D., Shannon, P.T., Jabs, E.W., Nickerson, D.A., et al. (2010). Exome sequencing identifies the cause of a mendelian disorder. Nature genetics *42*, 30-35.

Ng, S.B., Turner, E.H., Robertson, P.D., Flygare, S.D., Bigham, A.W., Lee, C., Shaffer, T., Wong, M., Bhattacharjee, A., Eichler, E.E., et al. (2009). Targeted capture and massively parallel sequencing of 12 human exomes. Nature *461*, 272-276.

Nishida, Y., Taketani, Y., Yamanaka-Okumura, H., Imamura, F., Taniguchi, A., Sato, T., Shuto, E., Nashiki, K., Arai, H., Yamamoto, H., et al. (2006). Acute effect of oral phosphate loading on serum fibroblast growth factor 23 levels in healthy men. Kidney international *70*, 2141-2147.

Ornitz, D.M., and Itoh, N. (2001). Fibroblast growth factors. Genome biology *2*, REVIEWS3005.

Ornitz, D.M., Xu, J., Colvin, J.S., McEwen, D.G., MacArthur, C.A., Coulier, F., Gao, G., and Goldfarb, M. (1996). Receptor specificity of the fibroblast growth factor family. The Journal of biological chemistry *271*, 15292-15297.

Pastoriza-Munoz, E., Colindres, R.E., Lassiter, W.E., and Lechene, C. (1978). Effect of parathyroid hormone on phosphate reabsorption in rat distal convolution. The American journal of physiology *235*, F321-330.

Pearson, G., Robinson, F., Beers Gibson, T., Xu, B.E., Karandikar, M., Berman, K., and Cobb, M.H. (2001). Mitogen-activated protein (MAP) kinase pathways: regulation and physiological functions. Endocrine reviews *22*, 153-183.

Penido, M.G., and Alon, U.S. (2012). Phosphate homeostasis and its role in bone health. Pediatric nephrology *27*, 2039-2048.

Perez-Castillo, A., Pipaon, C., Garcia, I., and Alemany, S. (1993). NGFI-A gene expression is necessary for T lymphocyte proliferation. The Journal of biological chemistry *268*, 19445-19450.

Perwad, F., Azam, N., Zhang, M.Y., Yamashita, T., Tenenhouse, H.S., and Portale, A.A. (2005). Dietary and serum phosphorus regulate fibroblast growth factor 23 expression and 1,25-dihydroxyvitamin D metabolism in mice. Endocrinology *146*, 5358-5364.

Portale, A.A., Halloran, B.P., and Morris, R.C., Jr. (1987). Dietary intake of phosphorus modulates the circadian rhythm in serum concentration of phosphorus. Implications for the renal production of 1,25-dihydroxyvitamin D. The Journal of clinical investigation *80*, 1147-1154.

Prie, D., Huart, V., Bakouh, N., Planelles, G., Dellis, O., Gerard, B., Hulin, P., Benque-Blanchet, F., Silve, C., Grandchamp, B., et al. (2002). Nephrolithiasis and osteoporosis associated with hypophosphatemia caused by mutations in the type 2a sodium-phosphate cotransporter. The New England journal of medicine *347*, 983-991.

Qiu, N., Xiao, Z., Cao, L., Buechel, M.M., David, V., Roan, E., and Quarles, L.D. (2012). Disruption of Kif3a in osteoblasts results in defective bone formation and osteopenia. J Cell Sci *125*, 1945-1957.

Quarles, L.D. (2003). Evidence for a bone-kidney axis regulating phosphate homeostasis. The Journal of clinical investigation *112*, 642-646.

Rafaelsen, S.H., Raeder, H., Fagerheim, A.K., Knappskog, P., Carpenter, T.O., Johansson, S., and Bjerknes, R. (2013). Exome sequencing reveals FAM20c mutations associated with fibroblast growth factor 23-related hypophosphatemia, dental anomalies, and ectopic calcification. Journal of bone and mineral research : the official journal of the American Society for Bone and Mineral Research *28*, 1378-1385.

Ranch, D., Zhang, M.Y., Portale, A.A., and Perwad, F. (2011). Fibroblast growth factor 23 regulates renal 1,25-dihydroxyvitamin D and phosphate metabolism via the MAP kinase signaling pathway in Hyp mice. Journal of bone and mineral research : the official journal of the American Society for Bone and Mineral Research *26*, 1883-1890.

Razzaque, M.S. (2009). The FGF23-Klotho axis: endocrine regulation of phosphate homeostasis. Nature reviews. Endocrinology *5*, 611-619.

Razzaque, M.S., Sitara, D., Taguchi, T., St-Arnaud, R., and Lanske, B. (2006). Premature aging-like phenotype in fibroblast growth factor 23 null mice is a vitamin D-mediated process. FASEB journal : official publication of the Federation of American Societies for Experimental Biology *20*, 720-722.

Reilly, R.F. (2005). Disorders of serum phosphorus. Nephrology in 30 Days, Eds Reilly RF and Perazella MA, McGraw Hill Book Co., New York, 161–176.

Reuss-Borst, M.A. (2014). [Metabolic bone disease osteomalacia]. Zeitschrift fur Rheumatologie *73*, 316-322.

Rhee, Y., Bivi, N., Farrow, E., Lezcano, V., Plotkin, L.I., White, K.E., and Bellido, T. (2011). Parathyroid hormone receptor signaling in osteocytes increases the expression of fibroblast growth factor-23 in vitro and in vivo. Bone *49*, 636-643.

Riminucci, M., Collins, M.T., Fedarko, N.S., Cherman, N., Corsi, A., White, K.E., Waguespack, S., Gupta, A., Hannon, T., Econs, M.J., et al. (2003). FGF-23 in fibrous dysplasia of bone and its relationship to renal phosphate wasting. The Journal of clinical investigation *112*, 683-692.

Robinson, J.T., Thorvaldsdottir, H., Winckler, W., Guttman, M., Lander, E.S., Getz, G., and Mesirov, J.P. (2011). Integrative genomics viewer. Nature biotechnology *29*, 24-26.

Roman-Garcia, P., Carrillo-Lopez, N., Naves-Diaz, M., Rodriguez, I., Ortiz, A., and Cannata-Andia, J.B. (2012). Dual-specificity phosphatases are implicated in severe hyperplasia and

lack of response to FGF23 of uremic parathyroid glands from rats. Endocrinology *153*, 1627-1637.

Rosati, R., Horan, G.S., Pinero, G.J., Garofalo, S., Keene, D.R., Horton, W.A., Vuorio, E., de Crombrugghe, B., and Behringer, R.R. (1994). Normal long bone growth and development in type X collagen-null mice. Nature genetics *8*, 129-135.

Rose, M.S., and Moldofsky, H. (1977). Comparison of pimozide with haloperidol in Gilles de la Tourette syndrome. Lancet *1*, 103.

Rowe, P.S., de Zoysa, P.A., Dong, R., Wang, H.R., White, K.E., Econs, M.J., and Oudet, C.L. (2000). MEPE, a new gene expressed in bone marrow and tumors causing osteomalacia. Genomics *67*, 54-68.

Rutsch, F., Ruf, N., Vaingankar, S., Toliat, M.R., Suk, A., Hohne, W., Schauer, G., Lehmann, M., Roscioli, T., Schnabel, D., et al. (2003). Mutations in ENPP1 are associated with 'idiopathic' infantile arterial calcification. Nature genetics *34*, 379-381.

Sabrautzki, S., Janas, E., Lorenz-Depiereux, B., Calzada-Wack, J., Aguilar-Pimentel, J.A., Rathkolb, B., Adler, T., Cohrs, C., Hans, W., Diener, S., et al. (2013). An ENU mutagenesis-derived mouse model with a dominant Jak1 mutation resembling phenotypes of systemic autoimmune disease. The American journal of pathology *183*, 352-368.

Sabrautzki, S., Rubio-Aliaga, I., Hans, W., Fuchs, H., Rathkolb, B., Calzada-Wack, J., Cohrs, C.M., Klaften, M., Seedorf, H., Eck, S., et al. (2012). New mouse models for metabolic bone diseases generated by genome-wide ENU mutagenesis. Mammalian genome : official journal of the International Mammalian Genome Society *23*, 416-430.

Saito, H., Kusano, K., Kinosaki, M., Ito, H., Hirata, M., Segawa, H., Miyamoto, K., and Fukushima, N. (2003). Human fibroblast growth factor-23 mutants suppress Na+-dependent phosphate co-transport activity and 1alpha,25-dihydroxyvitamin D3 production. The Journal of biological chemistry *278*, 2206-2211.

Saito, H., Maeda, A., Ohtomo, S., Hirata, M., Kusano, K., Kato, S., Ogata, E., Segawa, H., Miyamoto, K., and Fukushima, N. (2005). Circulating FGF-23 is regulated by 1alpha,25-dihydroxyvitamin D3 and phosphorus in vivo. The Journal of biological chemistry *280*, 2543-2549.

Saji, F., Shigematsu, T., Sakaguchi, T., Ohya, M., Orita, H., Maeda, Y., Ooura, M., Mima, T., and Negi, S. (2010). Fibroblast growth factor 23 production in bone is directly regulated by 1{alpha},25-dihydroxyvitamin D, but not PTH. American journal of physiology. Renal physiology *299*, F1212-1217.

Sanger, F., Nicklen, S., and Coulson, A.R. (1977). DNA sequencing with chain-terminating inhibitors. Proceedings of the National Academy of Sciences of the United States of America *74*, 5463-5467.

Sato, T., Tominaga, Y., Ueki, T., Goto, N., Matsuoka, S., Katayama, A., Haba, T., Uchida, K., Nakanishi, S., Kazama, J.J., et al. (2004). Total parathyroidectomy reduces elevated circulating fibroblast growth factor 23 in advanced secondary hyperparathyroidism. American journal of kidney diseases : the official journal of the National Kidney Foundation *44*, 481-487.

Schlessinger, J., Plotnikov, A.N., Ibrahimi, O.A., Eliseenkova, A.V., Yeh, B.K., Yayon, A., Linhardt, R.J., and Mohammadi, M. (2000). Crystal structure of a ternary FGF-FGFR-heparin complex reveals a dual role for heparin in FGFR binding and dimerization. Molecular cell *6*, 743-750.

Schmitt, C.P., and Mehls, O. (2004). The enigma of hyperparathyroidism in hypophosphatemic rickets. Pediatric nephrology *19*, 473-477.

Schorpp, K., and Hadian, K. (2014). Small molecule screening at Helmholtz Zentrum Munchen - from biology to molecules. Combinatorial chemistry & high throughput screening *17*, 266-271.

Schorpp, K., Rothenaigner, I., Salmina, E., Reinshagen, J., Low, T., Brenke, J.K., Gopalakrishnan, J., Tetko, I.V., Gul, S., and Hadian, K. (2013). Identification of Small-Molecule Frequent Hitters from AlphaScreen High-Throughput Screens. Journal of biomolecular screening *19*, 715-726.

Seeman, P. (2002). Atypical antipsychotics: mechanism of action. Canadian journal of psychiatry. Revue canadienne de psychiatrie *47*, 27-38.

Segawa, H., Kawakami, E., Kaneko, I., Kuwahata, M., Ito, M., Kusano, K., Saito, H., Fukushima, N., and Miyamoto, K. (2003). Effect of hydrolysis-resistant FGF23-R179Q on dietary phosphate regulation of the renal type-II Na/Pi transporter. Pflugers Archiv : European journal of physiology *446*, 585-592.

Segawa, H., Onitsuka, A., Furutani, J., Kaneko, I., Aranami, F., Matsumoto, N., Tomoe, Y., Kuwahata, M., Ito, M., Matsumoto, M., et al. (2009). Npt2a and Npt2c in mice play distinct and synergistic roles in inorganic phosphate metabolism and skeletal development. American journal of physiology. Renal physiology *297*, F671-678.

Selt, M., Bartlett, C.A., Harvey, A.R., Dunlop, S.A., and Fitzgerald, M. (2010). Limited restoration of visual function after partial optic nerve injury; a time course study using the calcium channel blocker lomerizine. Brain research bulletin *81*, 467-471.

Shalhoub, V., Ward, S.C., Sun, B., Stevens, J., Renshaw, L., Hawkins, N., and Richards, W.G. (2011). Fibroblast growth factor 23 (FGF23) and alpha-klotho stimulate osteoblastic MC3T3.E1 cell proliferation and inhibit mineralization. Calcified tissue international *89*, 140-150.

Shendure, J., and Ji, H. (2008). Next-generation DNA sequencing. Nature biotechnology *26*, 1135-1145.

Shimada, T., Hasegawa, H., Yamazaki, Y., Muto, T., Hino, R., Takeuchi, Y., Fujita, T., Nakahara, K., Fukumoto, S., and Yamashita, T. (2004a). FGF-23 is a potent regulator of vitamin D metabolism and phosphate homeostasis. Journal of bone and mineral research : the official journal of the American Society for Bone and Mineral Research *19*, 429-435.

Shimada, T., Mizutani, S., Muto, T., Yoneya, T., Hino, R., Takeda, S., Takeuchi, Y., Fujita, T., Fukumoto, S., and Yamashita, T. (2001). Cloning and characterization of FGF23 as a causative factor of tumor-induced osteomalacia. Proceedings of the National Academy of Sciences of the United States of America *98*, 6500-6505.

Shimada, T., Urakawa, I., Yamazaki, Y., Hasegawa, H., Hino, R., Yoneya, T., Takeuchi, Y., Fujita, T., Fukumoto, S., and Yamashita, T. (2004b). FGF-23 transgenic mice demonstrate hypophosphatemic rickets with reduced expression of sodium phosphate cotransporter type IIa. Biochemical and biophysical research communications *314*, 409-414.

Shimizu, H., Nagami, S., and Takahashi, N. (2014). [A case of cerebral autosomal dominant arteriopathy with subcortical infarcts and leukoencephalopathy (CADASIL) in which lomerizine hydrochloride was suggested to prevent recurrent stroke]. Rinsho shinkeigaku = Clinical neurology *54*, 22-26.

Smith, R.C., O'Bryan, L.M., Farrow, E.G., Summers, L.J., Clinkenbeard, E.L., Roberts, J.L., Cass, T.A., Saha, J., Broderick, C., Ma, Y.L., et al. (2012). Circulating alphaKlotho influences phosphate handling by controlling FGF23 production. The Journal of clinical investigation *122*, 4710-4715.

Strom, T.M., Francis, F., Lorenz, B., Boddrich, A., Econs, M.J., Lehrach, H., and Meitinger, T. (1997). Pex gene deletions in Gy and Hyp mice provide mouse models for X-linked hypophosphatemia. Human molecular genetics *6*, 165-171.

Strom, T.M., and Juppner, H. (2008). PHEX, FGF23, DMP1 and beyond. Current opinion in nephrology and hypertension *17*, 357-362.

Sultan, M., Schulz, M.H., Richard, H., Magen, A., Klingenhoff, A., Scherf, M., Seifert, M., Borodina, T., Soldatov, A., Parkhomchuk, D., et al. (2008). A global view of gene activity and alternative splicing by deep sequencing of the human transcriptome. Science *321*, 956-960.

Swinney, D.C., and Anthony, J. (2011). How were new medicines discovered? Nature reviews. Drug discovery *10*, 507-519.

Szebenyi, G., and Fallon, J.F. (1999). Fibroblast growth factors as multifunctional signaling factors. International review of cytology *185*, 45-106.

Tagliabracci, V.S., Engel, J.L., Wen, J., Wiley, S.E., Worby, C.A., Kinch, L.N., Xiao, J., Grishin, N.V., and Dixon, J.E. (2012). Secreted kinase phosphorylates extracellular proteins that regulate biomineralization. Science *336*, 1150-1153.

Tagliabracci, V.S., Engel, J.L., Wiley, S.E., Xiao, J., Gonzalez, D.J., Nidumanda Appaiah, H., Koller, A., Nizet, V., White, K.E., and Dixon, J.E. (2014). Dynamic regulation of FGF23 by Fam20C phosphorylation, GalNAc-T3 glycosylation, and furin proteolysis. Proceedings of the National Academy of Sciences of the United States of America *111*, 5520-5525.

Takahasi, K.R., Sakuraba, Y., and Gondo, Y. (2007). Mutational pattern and frequency of induced nucleotide changes in mouse ENU mutagenesis. BMC molecular biology *8*, 52.

Taylor, J.E., and Defeudis, F.V. (1986). Interactions of verapamil, D 600, flunarizine and nifedipine with cerebral histamine-receptors. Neurochemistry international *9*, 379-381.

Tenenhouse, H.S., and Econs, M.J. (2001). Mendelian hypophosphatemias. 8th ed. edn. McGraw Hill Book Co., New York, 5039-5067.

Teva Select Brands (2012). ORAP (pimozide) tablet [Teva Select Brands]. DailyMed. .

The ADHR Consortium (2000). Autosomal dominant hypophosphataemic rickets is associated with mutations in FGF23. Nature genetics *26*, 345-348.

The HYP Consortium (1995). A gene (PEX) with homologies to endopeptidases is mutated in patients with X-linked hypophosphatemic rickets. The HYP Consortium. Nature genetics *11*, 130-136.

Thiel, G., and Cibelli, G. (2002). Regulation of life and death by the zinc finger transcription factor Egr-1. Journal of cellular physiology *193*, 287-292.

Tiosano, D., and Hochberg, Z. (2009). Hypophosphatemia: the common denominator of all rickets. Journal of bone and mineral metabolism *27*, 392-401.

Tohyama, O., Imura, A., Iwano, A., Freund, J.N., Henrissat, B., Fujimori, T., and Nabeshima, Y. (2004). Klotho is a novel beta-glucuronidase capable of hydrolyzing steroid beta-glucuronides. The Journal of biological chemistry *279*, 9777-9784.

Topaz, O., Shurman, D.L., Bergman, R., Indelman, M., Ratajczak, P., Mizrachi, M., Khamaysi, Z., Behar, D., Petronius, D., Friedman, V., et al. (2004). Mutations in GALNT3, encoding a protein involved in O-linked glycosylation, cause familial tumoral calcinosis. Nature genetics *36*, 579-581.

Tsuji, K., Maeda, T., Kawane, T., Matsunuma, A., and Horiuchi, N. (2010). Leptin stimulates fibroblast growth factor 23 expression in bone and suppresses renal 1alpha,25-dihydroxyvitamin D3 synthesis in leptin-deficient mice. Journal of bone and mineral research : the official journal of the American Society for Bone and Mineral Research *25*, 1711-1723.

Ullrich, K.J., Rumrich, G., and Kloss, S. (1977). Phosphate transport in the proximal convolution of the rat kidney. I. Tubular heterogeneity, effect of parathyroid hormone in acute and chronic parathyroidectomized animals and effect of phosphate diet. Pflugers Archiv : European journal of physiology *372*, 269-274.

Urakawa, I., Yamazaki, Y., Shimada, T., Iijima, K., Hasegawa, H., Okawa, K., Fujita, T., Fukumoto, S., and Yamashita, T. (2006). Klotho converts canonical FGF receptor into a specific receptor for FGF23. Nature *444*, 770-774.

van Bokhoven, H., and Brunner, H.G. (2002). Splitting p63. American journal of human genetics *71*, 1-13.

van Bokhoven, H., Hamel, B.C., Bamshad, M., Sangiorgi, E., Gurrieri, F., Duijf, P.H., Vanmolkot, K.R., van Beusekom, E., van Beersum, S.E., Celli, J., et al. (2001). p63 Gene mutations in eec syndrome, limb-mammary syndrome, and isolated split hand-split foot malformation suggest a genotype-phenotype correlation. American journal of human genetics *69*, 481-492.

van de Laar, I.M., Oldenburg, R.A., Pals, G., Roos-Hesselink, J.W., de Graaf, B.M., Verhagen, J.M., Hoedemaekers, Y.M., Willemsen, R., Severijnen, L.A., Venselaar, H., et al. (2011). Mutations in SMAD3 cause a syndromic form of aortic aneurysms and dissections with early-onset osteoarthritis. Nature genetics *43*, 121-126.

Vanbokhoven, H., Melino, G., Candi, E., and Declercq, W. (2011). p63, a story of mice and men. The Journal of investigative dermatology *131*, 1196-1207.

Vanhoenacker, F.M., Van Hul, W., Gielen, J., and De Schepper, A.M. (2001). Congenital skeletal abnormalities: an introduction to the radiological semiology. European journal of radiology *40*, 168-183.

Verge, C.F., Lam, A., Simpson, J.M., Cowell, C.T., Howard, N.J., and Silink, M. (1991). Effects of therapy in X-linked hypophosphatemic rickets. The New England journal of medicine *325*, 1843-1848.

Villa-Bellosta, R., Barac-Nieto, M., Breusegem, S.Y., Barry, N.P., Levi, M., and Sorribas, V. (2008). Interactions of the growth-related, type IIc renal sodium/phosphate cotransporter with PDZ proteins. Kidney international *73*, 456-464.

Vinals, F., and Pouyssegur, J. (1999). Confluence of vascular endothelial cells induces cell cycle exit by inhibiting p42/p44 mitogen-activated protein kinase activity. Molecular and cellular biology *19*, 2763-2772.

Virkki, L.V., Forster, I.C., Biber, J., and Murer, H. (2005). Substrate interactions in the human type IIa sodium-phosphate cotransporter (NaPi-IIa). American journal of physiology. Renal physiology *288*, F969-981.

Virkki, L.V., Forster, I.C., Hernando, N., Biber, J., and Murer, H. (2003). Functional characterization of two naturally occurring mutations in the human sodium-phosphate cotransporter type IIa. Journal of bone and mineral research : the official journal of the American Society for Bone and Mineral Research *18*, 2135-2141.

Wagner, C.A., Hernando, N., Forster, I.C., and Biber, J. (2014a). The SLC34 family of sodium-dependent phosphate transporters. Pflugers Archiv : European journal of physiology *466*, 139-153.

Wagner, C.A., Rubio-Aliaga, I., Biber, J., and Hernando, N. (2014b). Genetic diseases of renal phosphate handling. Nephrology, dialysis, transplantation : official publication of the European Dialysis and Transplant Association - European Renal Association *29 Suppl 4*, iv45-54.

Wang, W., Olson, D., Liang, G., Franceschi, R.T., Li, C., Wang, B., Wang, S.S., and Yang, S. (2012a). Collagen XXIV (Col24alpha1) promotes osteoblastic differentiation and mineralization through TGF-beta/Smads signaling pathway. International journal of biological sciences *8*, 1310-1322.

Wang, X., Wang, S., Li, C., Gao, T., Liu, Y., Rangiani, A., Sun, Y., Hao, J., George, A., Lu, Y., et al. (2012b). Inactivation of a novel FGF23 regulator, FAM20C, leads to hypophosphatemic rickets in mice. PLoS genetics *8*, e1002708.

Wang, Z., Gerstein, M., and Snyder, M. (2009). RNA-Seq: a revolutionary tool for transcriptomics. Nature reviews. Genetics *10*, 57-63.

Weinstein, L.S., Shenker, A., Gejman, P.V., Merino, M.J., Friedman, E., and Spiegel, A.M. (1991). Activating mutations of the stimulatory G protein in the McCune-Albright syndrome. The New England journal of medicine *325*, 1688-1695.

Wermuth, C.G. (2004). Selective optimization of side activities: another way for drug discovery. Journal of medicinal chemistry *47*, 1303-1314.

White, K.E., Cabral, J.M., Davis, S.I., Fishburn, T., Evans, W.E., Ichikawa, S., Fields, J., Yu, X., Shaw, N.J., McLellan, N.J., et al. (2005). Mutations that cause osteoglophonic dysplasia define novel roles for FGFR1 in bone elongation. American journal of human genetics *76*, 361-367.

White, K.E., Carn, G., Lorenz-Depiereux, B., Benet-Pages, A., Strom, T.M., and Econs, M.J. (2001). Autosomal-dominant hypophosphatemic rickets (ADHR) mutations stabilize FGF-23. Kidney international *60*, 2079-2086.

Wohrle, S., Henninger, C., Bonny, O., Thuery, A., Beluch, N., Hynes, N.E., Guagnano, V., Sellers, W.R., Hofmann, F., Kneissel, M., et al. (2013). Pharmacological inhibition of fibroblast growth factor (FGF) receptor signaling ameliorates FGF23-mediated hypophosphatemic rickets. Journal of bone and mineral research : the official journal of the American Society for Bone and Mineral Research *28*, 899-911.

Wolf, I., Levanon-Cohen, S., Bose, S., Ligumsky, H., Sredni, B., Kanety, H., Kuro-o, M., Karlan, B., Kaufman, B., Koeffler, H.P., et al. (2008). Klotho: a tumor suppressor and a modulator of the IGF-1 and FGF pathways in human breast cancer. Oncogene *27*, 7094-7105.

Wolf, J., LoRusso, P.M., Camidge, R.D., Perez, J.M., Tabernero, J., M., H., and al., e. (2012). A phase I dose escalation study of NVP-BGJ398, a selective pan FGFR inhibitor in genetically preselected advanced solid tumors. Proceedings of the 103rd Annual Meeting of the American Association for Cancer Research *Abstract nr LB-122*. .

Wu, B.T., Su, Y.H., Tsai, M.T., Wasserman, S.M., Topper, J.N., and Yang, R.B. (2004). A novel secreted, cell-surface glycoprotein containing multiple epidermal growth factor-like repeats and one CUB domain is highly expressed in primary osteoblasts and bones. The Journal of biological chemistry *279*, 37485-37490.

Wunder, F., Kalthof, B., Muller, T., and Huser, J. (2008). Functional cell-based assays in microliter volumes for ultra-high throughput screening. Combinatorial chemistry & high throughput screening *11*, 495-504.

Yabas, M., Teh, C.E., Frankenreiter, S., Lal, D., Roots, C.M., Whittle, B., Andrews, D.T., Zhang, Y., Teoh, N.C., Sprent, J., et al. (2011). ATP11C is critical for the internalization of phosphatidylserine and differentiation of B lymphocytes. Nature immunology *12*, 441-449.

Yamashita, T., Konishi, M., Miyake, A., Inui, K., and Itoh, N. (2002). Fibroblast growth factor (FGF)-23 inhibits renal phosphate reabsorption by activation of the mitogen-activated protein kinase pathway. The Journal of biological chemistry *277*, 28265-28270.

Yamazaki, M., Ozono, K., Okada, T., Tachikawa, K., Kondou, H., Ohata, Y., and Michigami, T. (2010). Both FGF23 and extracellular phosphate activate Raf/MEK/ERK pathway via FGF receptors in HEK293 cells. Journal of cellular biochemistry *111*, 1210-1221.

Yamazaki, Y., Tamada, T., Kasai, N., Urakawa, I., Aono, Y., Hasegawa, H., Fujita, T., Kuroki, R., Yamashita, T., Fukumoto, S., et al. (2008). Anti-FGF23 neutralizing antibodies show the physiological role and structural features of FGF23. Journal of bone and mineral research : the official journal of the American Society for Bone and Mineral Research *23*, 1509-1518.

Yie, J., Wang, W., Deng, L., Tam, L.T., Stevens, J., Chen, M.M., Li, Y., Xu, J., Lindberg, R., Hecht, R., et al. (2012). Understanding the physical interactions in the FGF21/FGFR/beta-Klotho complex: structural requirements and implications in FGF21 signaling. Chemical biology & drug design *79*, 398-410.

Yoshiko, Y., Wang, H., Minamizaki, T., Ijuin, C., Yamamoto, R., Suemune, S., Kozai, K., Tanne, K., Aubin, J.E., and Maeda, N. (2007). Mineralized tissue cells are a principal source of FGF23. Bone *40*, 1565-1573.

Yu, X., Sabbagh, Y., Davis, S.I., Demay, M.B., and White, K.E. (2005). Genetic dissection of phosphate- and vitamin D-mediated regulation of circulating Fgf23 concentrations. Bone *36*, 971-977.

Zhang, J.H., Chung, T.D., and Oldenburg, K.R. (1999). A Simple Statistical Parameter for Use in Evaluation and Validation of High Throughput Screening Assays. Journal of biomolecular screening *4*, 67-73.

Zhang, M.Y., Ranch, D., Pereira, R.C., Armbrecht, H.J., Portale, A.A., and Perwad, F. (2012). Chronic inhibition of ERK1/2 signaling improves disordered bone and mineral metabolism in hypophosphatemic (Hyp) mice. Endocrinology *153*, 1806-1816.

Zhang, Z., Alpert, D., Francis, R., Chatterjee, B., Yu, Q., Tansey, T., Sabol, S.L., Cui, C., Bai, Y., Koriabine, M., et al. (2009). Massively parallel sequencing identifies the gene Megf8 with ENU-induced mutation causing heterotaxy. Proceedings of the National Academy of Sciences of the United States of America *106*, 3219-3224.

Zhao, Y., Banerjee, S., Dey, N., LeJeune, W.S., Sarkar, P.S., Brobey, R., Rosenblatt, K.P., Tilton, R.G., and Choudhary, S. (2011). Klotho depletion contributes to increased inflammation in kidney of the db/db mouse model of diabetes via RelA (serine)536 phosphorylation. Diabetes *60*, 1907-1916.

ACKNOWLEDGEMENTS

My sincere thanks go to PD Dr. Tim-Matthias Strom for his valuable and great support, stimulating discussions as well as for the possibility to work in his group. The important comments on this thesis have always been very helpful.

Special thanks to Prof. Dr. Thomas Meitinger for the opportunity to do my thesis in his institute. I would also like to thank him for taking me to several interesting conferences.

I am sincerely thankful to Prof. Dr. Hans-Rudolf Fries for supporting this work at the Technical University Munich.

I deeply thank Prof. Dr. Walter Just for the second opinion of this thesis.

For the brilliant support, advice and guidance during my whole thesis as well as for the proofreading of this work, I am particularly grateful to Dr. Bettina Lorenz-Depiereux. Her enormous enthusiasm helped me a lot to manage challenging situations during the last years.

I would also like to give thanks to my cooperation partners for the excellent and productive cooperation: Dr. Kamyar Hadian and Dr. Kenji Schorpp at ADSP as well as Dr. Sibylle Sabrautzki, Sieglinde Bayer and Andreas Mayer at IEG.

I want to thank Elisabeth Graf for her huge support concerning NGS as well as Thomas Wieland and Thomas Schwarzmayr for their great help in bioinformatic questions.

For technical assistance, I thank Sandy Lösecke and Carola Fischer.

All my colleagues, I would like to thank for the wonderful atmosphere within the institute, for our great conversations not only about science but about everything else, for always being there for me and for the fantastic time we spent together.

This PhD project was supported by a grant of the “Bundesministerium für Bildung und Forschung (BMBF)” (OSTEOPATH; 01EC1006B).

Last but not least, I would like to express my deepest gratitude to my family and friends for their unconditional support, care and love.